INVESTIGATION OF PVRIG AS A POTENTIAL TARGET OF LRBA

by

Ecem Gonca Ültanır

B.S., Chemical Engineering, Yıldız Technical University, 2020

Submitted to the Institute for Graduate Studies in
Science and Engineering in partial fulfillment of
the requirements for the degree of
Master of Science

Graduate Program in Molecular Biology and Genetics
Boğaziçi University

2023

ACKNOWLEDGEMENTS

I would like to express my sincere gratitude to my thesis supervisor, Prof. Batu Erman, for his invaluable support and guidance throughout my master's journey. I am deeply grateful for his trust in me from the very beginning. I am thankful to him for providing me with the opportunity to join his lab despite my lack of background in biology education. This step has undoubtedly been a significant milestone in both my career and my life. His curiosity and enthusiasm for science will always inspire me in my future work.

I would like to thank my jury members, Prof. Safa Barış and Assoc. Prof. Tolga Emre, for agreeing to be a part of my thesis committee and generously devoting their time to provide me with valuable feedback and suggestions.

I would like to express my special thanks to Dr. Pegah Zahedimaram, a former member of our laboratory. She was always available to answer my questions and was happy to share her knowledge with me. Without her diligent work on generating LRBA KO cell lines and conducting further characterizations, this project would not have been possible. I would also like to extend my gratitude to Büşra Şimşek, who patiently addressed my numerous questions. Having such professional and helpful people in the lab was truly invaluable.

I would like to thank all past and present members of the BE lab, including Dr. Pegah Zahedimaram, Dr. Görkem Odabaş, Dr. Sinan Öcal, Dr. Melike Gezen, Dr. Sarah Barakat, Büşra Şimşek, Alp Ertunga Eyüpoğlu, Gizem Çile, Ege Ezen, İzem Devecioğlu, Sude Ezen, Selen Balkan, Berkay Engin, Elif Karay, Mustafa Tuncay, Canberk Yeşilada. I consider myself fortunate to have had the opportunity to work in such a supportive and friendly environment thanks to their presence. I would like to express my special appreciation to Elif Karay for her dedicated work and direct help during the final stages of my project. I am also grateful to all members of the Sütlü lab, particularly Elif Çelik, who provided substantial help with my experiments. I deeply appreciate all her assistance. Furthermore, I am grateful for the friendships I formed during my two years of master's studies. I extend my special thanks to Sude Ezen, Gizem Çile, Ulduz Afshar, and Berfin Dağ for all the wonderful memories we shared.

I would like to extend my heartfelt thanks to my dearest Burak Halat, who has been a constant source of support throughout both the good and challenging times. His unwavering encouragement has made all the difficult moments much more manageable. He has never allowed me to doubt myself and has always inspired me to pursue the things I believed to be beyond my capabilities.

I express my deepest gratitude and thanks to each member of my family, particularly my mother, Olga Ültanır, and my father, Erkan Ültanır, for their endless support and love throughout my life. I am incredibly lucky to have them by my side.

Finally, I would like to thank The Scientific and Technological Research Council of Turkey (TÜBİTAK) 2210-A National Scholarship Program, and the TÜBİTAK 1004 project with the grant number 20AG007 for providing financial support during two years of my master's studies. Additionally, this study was supported by the TÜBİTAK with the grant number 318S202.

ABSTRACT

INVESTIGATION OF PVRIG AS A POTENTIAL TARGET OF LRBA

Identifying novel T-cell co-inhibitors and the mechanism of their regulation is of great importance for the development of novel immune checkpoint blockade therapies. LRBA is a key surface trafficking regulator of CTLA-4, which is a crucial T-cell co-inhibitory receptor. LRBA maintains immune homeostasis and prevents autoimmunity by directing internalized CTLA-4 back to the cell surface and preventing its lysosomal degradation. To date, the role of LRBA in the regulation of other T-cell co-receptors besides CTLA-4 have not been identified. In previous studies in our laboratory, a novel T-cell co-inhibitory receptor, PVRIG was found to be significantly downregulated on the surface of LRBA knockout Jurkat T-cells. In this thesis, we aimed to investigate this finding in more detail to find out whether LRBA regulates PVRIG through similar mechanisms as it regulates CTLA-4. To this end, we performed several co-immunoprecipitation experiments to investigate the physical interaction between endogenous PVRIG and LRBA proteins. In addition, we tried to understand whether LRBA could bind to PVRIG with its PH-BEACH domain, which is sufficient for CTLA-4 binding. We showed that the Flag-tagged PH-BEACH domain of LRBA co-immunoprecipitated with various constructs of PVRIG, including full length PVRIG, Tailless PVRIG, and TM-Tail PVRIG, all carrying c-Myc/His epitope tags. However, we could not fully confirm the specificity of these co-immunoprecipitation results. Therefore, there is a need for further investigation of the PVRIG and LRBA interaction using additional techniques. We also showed that PVRIG protein can undergo glycosylation, which may have implications on its overall function. This study adds valuable insights towards the regulation of PVRIG by LRBA.

ÖZET

LRBA'NIN POTANSİYEL BİR HEDEFİ OLARAK PVRIG'İN İNCELENMESİ

Yeni T hücresi ko-inhibitörlerinin tespiti ve hücre içi regülasyonlarına yönelik mekanizmaların belirlenmesi, yeni immün kontrol noktası engelleme terapilerinin geliştirilmesi açısından büyük önem taşımaktadır. LRBA, kritik bir T hücresi ko-inhibitör reseptörü olan CTLA-4'ün hücre yüzeyine trafiğinin düzenleyicisi olarak önemli bir rol oynamaktadır. LRBA, internalize olmuş CTLA-4'ü hücre yüzeyine geri yönlendirerek ve lizozomal degradasyonunu engelleyerek immün homeostazı sürdürmekte ve otoimmüniteyi önlemektedir. Bugüne kadar, LRBA'nın CTLA-4 dışında diğer T hücresi ko-reseptör hedefleri belirlenmemiştir. Laboratuvarımızdaki önceki çalışmalarda, PVRIG adlı yeni bir T hücresi ko-inhibitör reseptörünün, LRBA geni silinmiş Jurkat T hücresi yüzeyinde belirgin bir şekilde düşük seviyede olduğu tespit edilmiştir. Bu tez çalışmasında, LRBA'nın CTLA-4'ü düzenlediği mekanizmalar gibi, PVRIG'i de benzer şekilde düzenleyip düzenlemediğini daha ayrıntılı olarak araştırmayı amaçladık. Bu amaçla, endojen PVRIG ve LRBA proteinlerinin fiziksel etkileşimini incelemek için ko-immünopresipitasyon deneyleri gerçekleştirdik. Ayrıca, LRBA'nın CTLA-4 ile bağlantı kurabilen PH-BEACH bölgesiyle PVRIG'e bağlanıp bağlanamayacağını anlamaya çalıştık. LRBA'nın Flag etiketli PH-BEACH bölgesinin, c-Myc/His etiketli tam uzunluklu PVRIG, kuyruksuz PVRIG ve sadece kuyruklu PVRIG yapısıyla birlikte ko-immünopresipite edilebildiğini gösterdik. Ancak, ko-immünopresipitasyon sonuçlarının spesifikliğini tam olarak doğrulayamadık. PVRIG ve LRBA arasındaki bağlanmanın başka tekniklerle araştırılmasına ihtiyaç vardır. Ayrıca, PVRIG proteininin glikolizasyona uğrayabildiğini gösterdik. Bu, PVRIG'in hücre içindeki genel fonksiyonu üzerinde etkili bir faktör olabilir. Bu çalışma, PVRIG'in LRBA tarafından regülasyonuna yönelik değerli bilgiler sağlamaktadır.

TABLE OF CONTENTS

LIST OF FIGURES

LIST OF TABLES

LIST OF SYMBOLS

g	Gram
L	Liter
M	Molar
mA	Miliamper
ml	Mililiter
mM	Milimolar
ng	Nanogram
V	Volt
α	Greek letter alpha representing bacterial strain
β	Greek letter beta representing different protein isoforms
γ	Greek letter gamma representing different protein isoforms
θ	Greek letter theta representing different protein isoforms
κ	Greek letter kappa representing different protein subunits
µg	Microgram
µl	Microliter
µm	Micrometer

LIST OF ACRONYMS/ABBREVIATIONS

AKT	Protein Kinase B
AP-1	Activating Protein-1
AP-1	Clathring Adaptor Protein Complex-1
AP-2	Adaptor Protein Complex-2
AP-3	Adaptor Protein Complex-3
APC	Antigen Presenting Cell
APC	Allophycocyanin
APS	Ammonium Persulfate
BDCP	BEACH Domain-Containing Protein
BEACH	Beige and Chediak-Higashi
Cas	CRISPR-associated
CD3	Cluster of Differentiation 3
CD4	Cluster of Differentiation 4
CD8	Cluster of Differentiation 8
CD19	Cluster of Differentiation 19
CD28	Cluster of Differentiation 28
CD80	Cluster of Differentiation 80
CD86	Cluster of Differentiation 86
CD96	Cluster of Differentiation 96
CD112	Cluster of Differentiation 112
CD112R	CD112 Receptor
CD155	Cluster of Differentiation 155
CD226	Cluster of Differentiation 226
cDNA	Complementary Deoxyribonucleic Acid
CHS	Chediak-Higashi Syndrome
CLP	Common Lymphoid Progenitor
c-Myc	Cellular Myelocytomatosis Oncogene
CMV	Cytomegalovirus
CO_2	Carbon Dioxide
Co-IP	Co-Immunoprecipitation

CRISPR	Clustered Regularly Interspaced Short Palindromic Repeats
CTLA-4	Cytotoxic T-Lymphocyte Antigen 4
DMEM	Dulbecco's Modified Eagle Medium
DMSO	Dimethylsulfoxade
DNA	Deoxyribonucleic Acid
dNTP	Deoxyribonucleotide Triphosphate
DUF88	Domain of Unknown Function 1088
E. Coli	Escherichia Coli
EDTA	Ethylenediaminetetraacetic acid
EGF	Epidermal Growth Factor
EGFR	Epidermal Growth Factor Receptor
ER	Endoplasmic Reticulum
Fas	FS-7-Associated Surface Antigen
FasL	FS-7-Associated Surface Antigen Ligand
FBS	Fetal Bovine Serum
GFP	Green Fluorescent Protein
HBS	HEPES Buffered Saline
HCl	Hydrochloric acid
HEPES	4-(2-hydroxyethyl)-1-piperazineethanesulfonic Acid
His	Histidine
HRP	Horseradish Peroxidase
ICI	Immune Checkpoint Inhibitor
Ig	Immunoglobulin
IgV	Immunoglobulin Variable-like
IKKγ	Inhibitor of κB Kinase Gamma
IL-2	Interleukin-2
IP	Immunoprecipitation
IP3	1,4,5-inositol-triphosphate
ITAM	Immunoreceptor Tyrosine-Based Activation Motif
ITIM	Immunoreceptor Tyrosine-Based Inhibitory Motif
kDa	Kilodalton
KO	Knock-Out
LAT	Linker for Activation of T Cells

LB	Luria Broth
LeGO	Lentiviral Gene Ontology Vectors
LPS	Lipopolysaccharide
LRBA	Lipopolysaccharide-Responsive Beige-Like Anchor Protein
LYST	Lysosomal Trafficking Regulator
mAb	Monoclonal Antibody
MAPK	Mitogen Activated Protein Kinase
MFI	Mean Fluorescence Intensity
MHC	Major Histocompatibility Complex
mRNA	Messenger RNA
NaCl	Sodium Chloride
NBEA	Neurobeachin
NBEAL2	Neurobeachin- like 2
NFAT	Nuclear Factor of Activated T Cell
NF-κB	Nuclear Factor Kappa B
NK	Natural Killer
NKT	Natural Killer T cells
OD	Optical Density
PCR	Polymerase Chain Reaction
PD-1	Programmed Cell Death Protein 1
PD-L1	Programmed Cell Death Ligand 1
PE	Phycoerythrin
PI3K	Phosphatidylinositol 3-Kinase
PKCθ	Protein kinase C Theta
PLC-γ	Phosphoinositide Phospholipase C- Gamma
PNGase F	Peptide N-Glycosidase F
PP2A	Protein Phosphatase 2A
PVDF	Polyvinylidene Fluoride
PVRIG	Poliovirus Receptor-Related Immunoglobulin Domain
PVRL2	Poliovirus Receptor-Related 2
qPCR	Quantitaive Polymerase Chain Reaction
Rab11	Ras-Related Protein in Brain 11
RNA	Ribonucleic Acid

RNA-Seq	RNA Sequencing
rpm	Revolutions Per Minute
RPMI	Roswell Park Memorial Institute
RT-PCR	Reverse Transcription Polymerase Chain Reaction
SDS	Sodium Dodecyl Sulfate
SDS-PAGE	Sodium Dodecyl Sulfate Polyacrylamide Gel Electrophoresis
TBS	Tris Buffered Saline
TBST	Tris Buffered Saline with Tween-20
TCR	T Cell Receptor
TEMED	N,N,N',N'-tetramethylethylenediamine
TIGIT	T Cell Immunoreceptor With Ig and ITIM Domains
TM	Transmembrane
WT	Wild Type
Zap70	Zeta-Associated of 70 kD Tyrosine Kinase

1. INTRODUCTION

1.1. T-cells and T-cell Signaling

T-cells are crucial components of the adaptive immune system and are essential for mounting an immune response in an antigen-specific manner. Common lymphoid progenitors (CLPs) derive from hematopoietic stem cells in the bone marrow and migrate to the thymus to initiate T-cell lineage commitment and development. T-cells develop in the thymus from CLPs and undergo positive and negative selection to restrict reactivity to peptides presented in the context of MHC and to minimize self-reactivity. The T-cells that can escape the selection process migrate to peripheral lymphoid organs where they are activated by foreign antigens (Kumar et al., 2018). T-cell activation depends on the recognition of peptide-Major Histocompatibility Complex (pMHC) molecules on antigen presenting cells (APCs) by the T-cell Receptor (TCR). Therefore, the actual antigen for T-cells is not the antigen itself, but antigenic peptides presented on MHC Type I (MHC-I) or Type II (MHC-II) molecules (Shah et al., 2021). Each T-cell expressing a unique TCR complex recognizes unique pMHCs, which ensures the specificity of the T-cell response. CD4 and CD8 proteins are called co-receptors that aid TCR signaling by binding to invariant MHC sites away from the peptide-binding groove (Artyomov et al., 2010). T-cells are categorized into two major classes depending on their co-receptor expression; CD4+ T-helper cells (Th) and CD8+ cytotoxic T-cells (Tc) (Figure 1.1). CD4+ T-cells are restricted to recognize pMHC-II complexes whereas CD8+ T-cells are restricted to recognize pMHC-I complexes on APCs (Murphy & Weaver, 2017).

TCR:pMHC binding mediates the primary T-cell signaling that initiates a cascade of phosphorylation events starting with TCR complex subunit phosphorylation by the Lck tyrosine kinase. The TCR complex is phosphorylated on immunoreceptor tyrosine-based activation motifs (ITAMs) found on CD3 subunits. The Zap70 tyrosine kinase is recruited to the phosphorylated ITAM motifs and Lck further phosphorylates Zap70, resulting in its activation. Activated Zap70 phosphorylates the adaptor protein LAT, which in turn recruits additional adaptor proteins that mediate the assembly and activation of downstream molecules (Figure 1.2) (Courtney et al., 2018). Eventually, with various secondary

messengers and adaptor proteins, TCR:pMHC binding activates multiple signaling cascades. For instance, TCR:pMHC binding-mediated phospholipase C-γ (PLC-γ) phosphorylation leads to 1,4,5-inositol-triphosphate (IP3) activation, which results in Ca^{2+} entry into cytosol and triggering of Ca^{2+}-dependent calcineurin NFAT pathway (Yablonski et al., 2001). In addition, TCR:pMHC binding activates PKCθ which leads to the activation of IKKγ and the release of NF-κB from the inhibitory IκB complex (Yixia et al., 2014). NF-κB can then enter to the nucleus to regulate gene expression. Canonical PKCθ– IKKγ –NF-κB activation is essential for T-cell survival and activation. The NFAT, NF-κB, and AP-1 signaling pathways induce the transcriptional expression of various genes important in T-cell activation such as Interleukin-2 (IL-2). Another important signaling cascade initiated by TCR:pMHC engagement is RAS and MAPK pathways that control T-cell development, differentiation, and TCR-mediated signal (Shah et al., 2021).

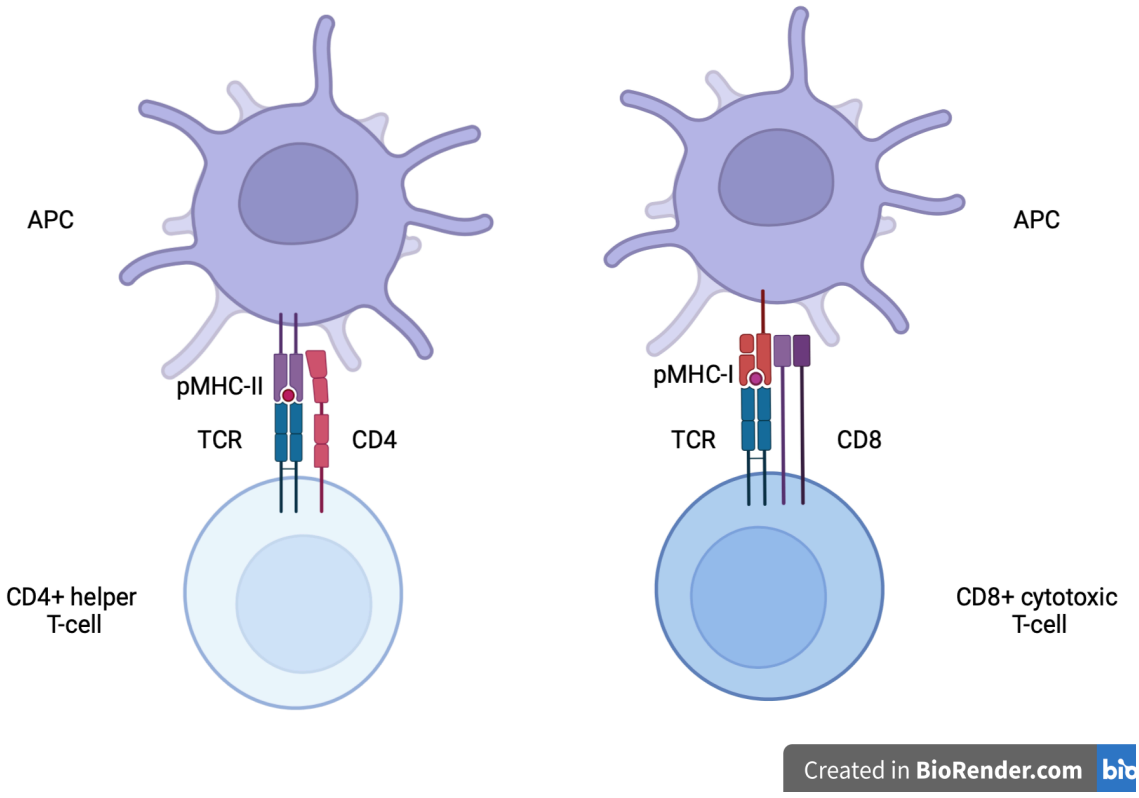

Figure 1.1. Schematic representation of CD4+ and CD8+ T-cells interacting with pMHC-II and pMHC-I complexes, respectively.

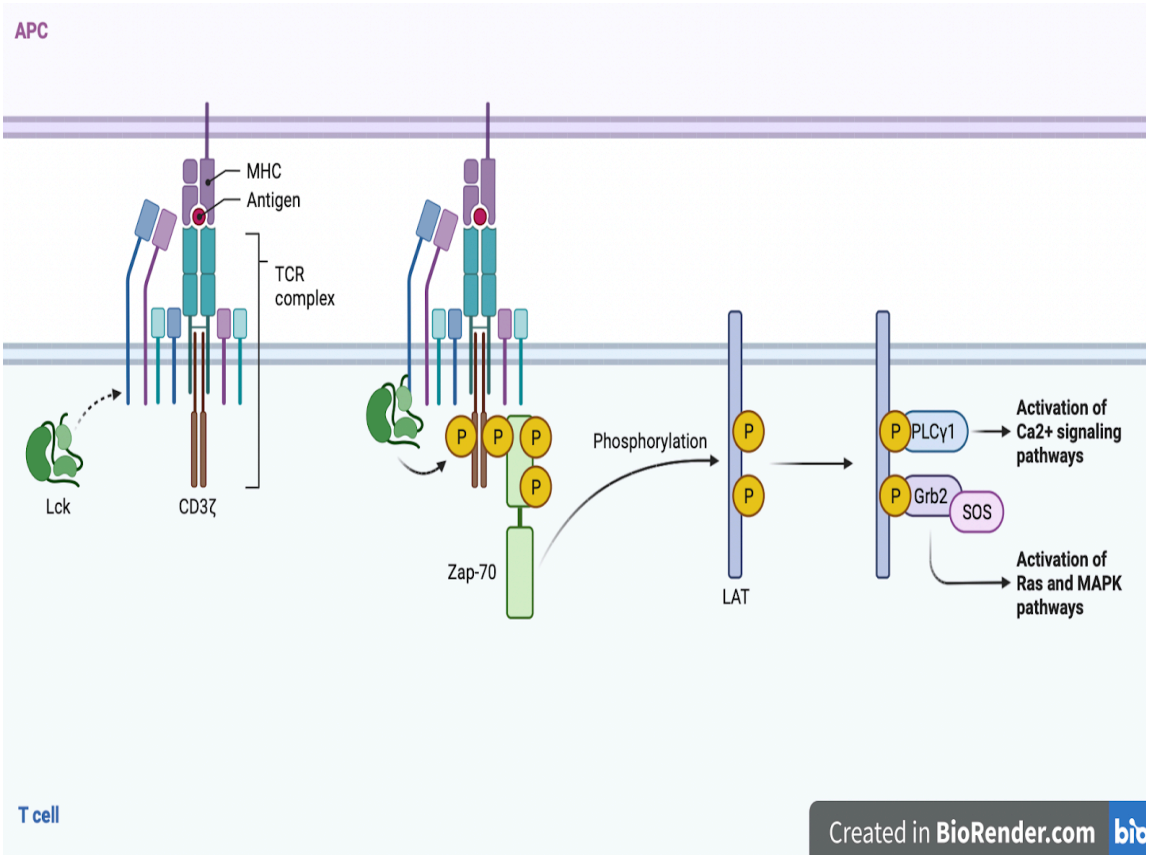

Figure 1.2. Overview of TCR downstream signaling.

1.2. T-cell Co-Signaling

pMHC recognition by TCR and co-receptors is called the primary signal that leads to T-cell activation. However, this primary signal alone is not sufficient for effective T-cell responses, and it needs to be stimulated by costimulatory receptor signaling, which was proposed as the two-signal model of T-cell activation (Lafferty and Cunningham, 1975). On the other hand, to control the T-cell activation response and the duration, there is a requirement for co-inhibitory signaling. The strength and the balance of co-stimulatory and co-inhibitory signaling determines the T-cell fate (Chen and Flies, 2013). There are various T-cell co-signaling pathways such as the B7-CD28-CTLA-4 axis, the PD-L1- PD-1 axis, and CD226-TIGIT-CD96 axis mediated by co-stimulatory or co-inhibitory receptors that belong to the Ig superfamily (Figure 1.3).

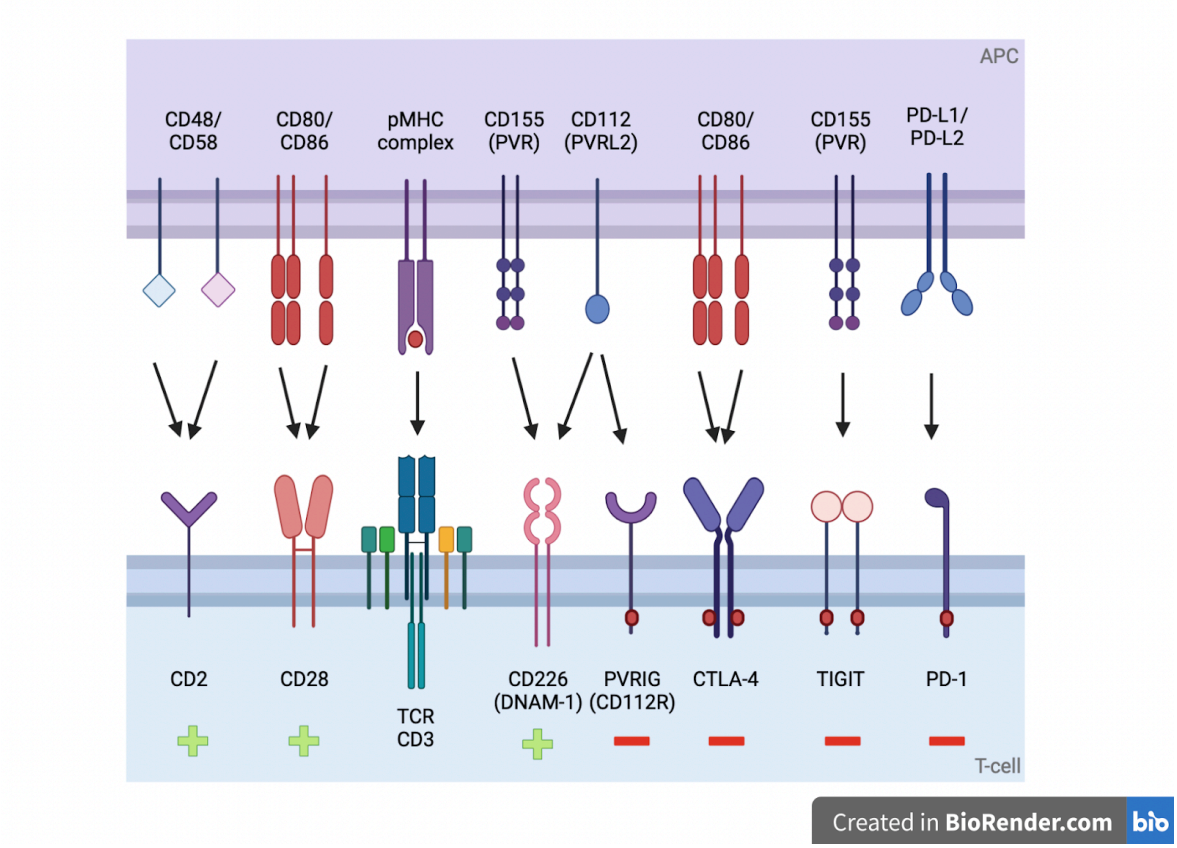

Figure 1.3. TCR co-signaling receptors and their ligands expressed on APCs are illustrated. Co-stimulatory receptors are indicated by a green plus sign while co-inhibitory receptors are indicated by a red minus sign.

Cytotoxic T-Lymphocyte Antigen 4 (CTLA-4) is a crucial T-lymphocyte co-inhibitory receptor and it is essential for maintaining immune homeostasis and preventing autoimmunity. CTLA-4 competes with the co-stimulatory receptor CD28 to bind their shared ligands CD80/CD86 (B7.1/B7.2) expressed on the surface of APCs (Krummel and Allison, 1995). CTLA-4 and its ligands' interaction leads to the inhibition of NFAT, NF-κB, and AP-1-mediated signaling pathways (Fraser et al., 1999). In addition to competitive binding, CTLA-4 can also decrease the CD80/CD86 expressed on APC surface via trans-endocytosis (trogocytosis) and thus reduces the ligand availability for CD28 (Qureshi et al., 2011; Zhao et al., 2022). As opposed to CD28, CTLA-4 does not mainly reside on the T-cell surface in resting cells. Instead, it is mostly found in intracellular compartments and its total expression as well as surface trafficking increases upon TCR stimulation. Even when expressed on the surface, it is rapidly internalized from the cell surface through endocytosis

(Iida et al., 2000; Rudd et al., 2009). Internalized CTLA-4 molecules can be either directed to lysosomal compartments for degradation or can be recycled back to the cell surface to maintain its co-inhibitory role. Since CTLA-4 has a higher affinity and avidity to CD80/CD86 than CD28, its surface expression regulation is highly critical in the outcome of T-cell response and fate (Pentcheva-Hoang et al., 2004).

The CD226-TIGIT-CD96 axis, on the other hand, is another signaling pathway that has been well characterized in the context of T-cell biology. T-cell immunoreceptor with Ig and ITIM Domains (TIGIT), and CD96 (TACTILE) are found at the core of this protein family and they compete with CD226 (DNAM-1) for binding to their shared ligand CD155. This regulatory signaling network resembles the CTLA-4/CD28 and CD80/CD86 signaling in terms of competitive ligand binding. In the CD226 axis, the shared ligand is CD155, while costimulatory CD226 and co-inhibitory TIGIT are the competing receptors. Identification of Poliovirus receptor-related Immunoglobulin domain (PVRIG) has added more complexity to this signaling axis. PVRIG (CD112R) competes with the co-stimulatory receptor CD226 for binding to CD112 which is another ligand found in the same axis (Conner et al., 2022).

PD-1 and the engagement of its ligands PD-L1/PD-L2 at the T-cell surface also negatively affects TCR signaling by inhibiting the induction of genes expressing cytokines and survival proteins by the inhibition of the PI3K/Akt pathway (Parry et al., 2005). Antagonizing T-cell co-inhibitory receptor-mediated immune suppression has been the central target of cancer immunotherapy (Figure 1.4). Targeting the immune checkpoint inhibitors (ICIs) including CTLA-4 and PD-1 through monoclonal antibodies (mAb), alone or in combination, have become a standard in the treatment of various types of cancers such as metastatic melanoma and metastatic non-small-cell lung cancer (Rotte, 2019). Drugs inhibiting PD-1 (Nivolumab), PD-L1 (Atezolizumab) and CTLA-4 (Ipilimumab) have been approved by the FDA and are actively used in the clinic for cancer immunotherapy (Bagchi et al., 2021). However, not all cancer patients can benefit from checkpoint blockade therapy, as most develop resistance or have no therapy response at all (Zaretsky et al., 2016). Tumor mutational burden and the tumor microenvironment molecular characteristics are associated with the effectiveness of ICI therapy. The identification of novel T-cell checkpoint co-receptors and blocking antibodies to further extend the use and effectiveness of ICIs within broader cancer types, is an active area of research. The CD226-TIGIT-CD96 axis is subject

to investigation as a novel cancer immunotherapy target (Alteber et al., 2021; Zeng et al., 2021; Conner et al., 2022). PVRIG, which functions as a co-inhibitory receptor akin to CTLA-4 and PD-1 could be the target of novel ICIs. In mice, PVRIG deficiency led to reduced tumor growth *in vivo* and increased CD8+ T-cell responses (Murter et al., 2019). In human tumor-infiltrating lymphocytes (TILs), PVRIG blockade alone or in combination with TIGIT or PD-1 blockade was able to enhance the production of cytokines and the cytotoxicity of CD8+ effector T-cells. On the gene expression level, higher PVRIG expressing T-cells were observed to have higher TIGIT and PD-1 expression as well. In line with this observation, triple blockade of PVRIG, TIGIT, and PD-1 have resulted in the highest rise in T-cell function (Whelan et al., 2019).

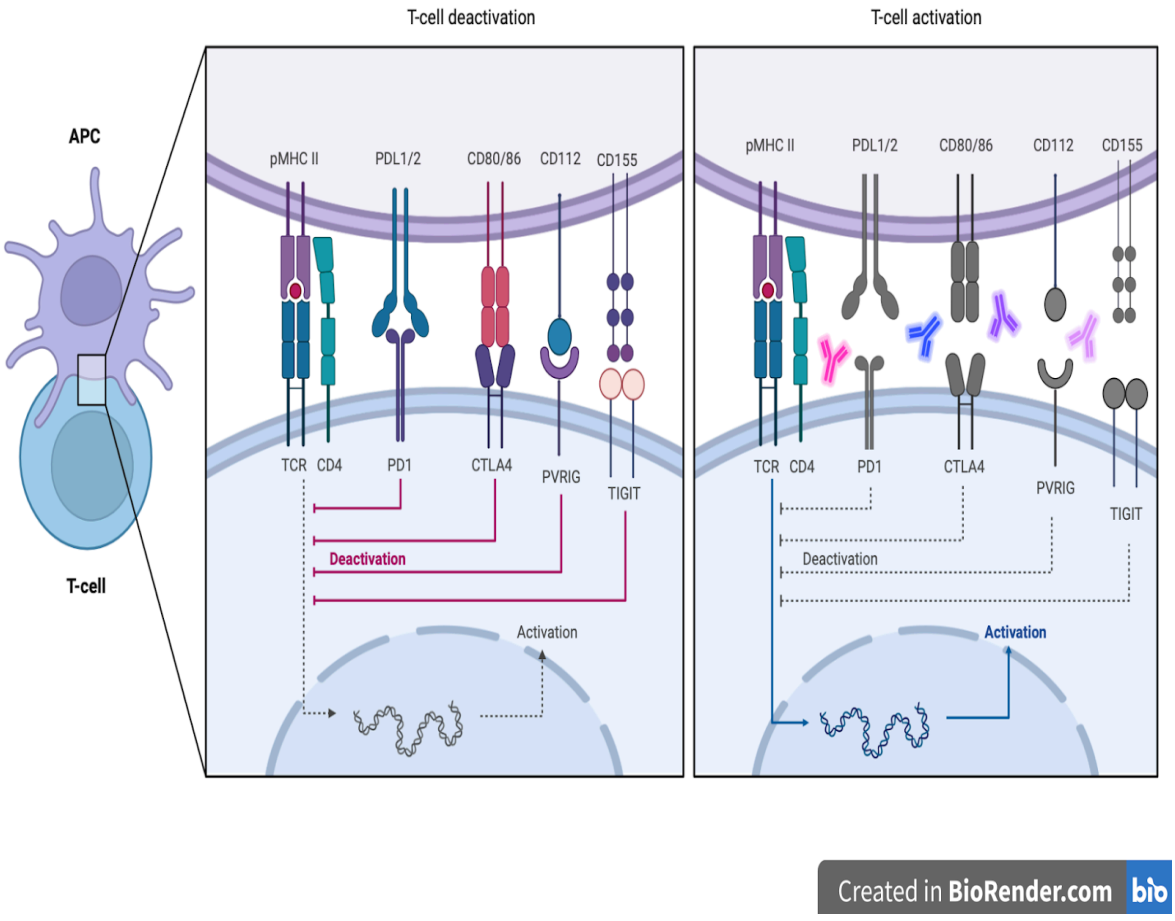

Figure 1.4. A schematic representation of T-cell activation through ICI blockade by blocking antibodies.

1.3. PVRIG

1.3.1. The PVRIG Gene

The PVRIG gene was discovered with the search to identify genes that are preferentially expressed in human T-cells and code for single extracellular immunoglobulin variable-like (IgV) domain-containing transmembrane proteins (Zhu et al., 2016). PVRIG was also named as CD112R in the same study where CD112 was found as the ligand of PVRIG. So far, CD112 is the only known ligand of PVRIG.

The PVRIG gene is primarily expressed in human Natural Killer cells (NK) and T-lymphocytes. PVRIG-expressing T-lymphocytes are mostly CD8+ effector/memory cells. Low numbers of naive T-cells (CD45RA+CCR7+) also express PVRIG, but it is undetectable in CD4+ helper T-cells from the peripheral blood. The activation of CD8+ and CD4+ T-cells further increases the PVRIG expression both at the gene and protein levels (Zhu et al., 2016). In mice, on the other hand, NK cells and NKT cells highly express PVRIG transcripts whereas it is almost undetectable in CD8+ and CD4+ T-cells. Upon activation of mouse CD8+ and CD4+ T-cells, PVRIG expression was only upregulated in activated mouse CD8+ T-cells (Murter et al., 2019).

1.3.2. The PVRIG Protein

In humans, the PVRIG gene encodes a single-pass transmembrane protein with a molecular mass of 37 kDa, having one extracellular IgV domain, one transmembrane domain, and an intracellular domain (hereafter referred to as the “tail”). The human PVRIG tail sequence has a ~65.3% homology with that of mice (Zeng et al., 2021). To determine if PVRIG protein exists in disulfide bonded multimers, Zhu et al. (2016) treated cell lysates to reducing and nonreducing conditions and observed PVRIG at the same size and thus concluded that PVRIG is expressed in cell membranes as a monomer (Zhu et al., 2016).

The PVRIG tail has two tyrosine residues, at position 233 and 293. Y233 is found within an immunoreceptor tyrosine-based inhibitory (ITIM)-like motif (VPYA) and this motif can be phosphorylated. PVRIG can interact with phosphatases like SHIP (Src homology region 2 containing inositol 5’-polyphosphatase 1), SHP-1 (Src homology region

2-containing phosphatase-1), and SHP-2 (Src homology region 2-containing phosphatase-2) shown by co-immunoprecipitation experiments where these interactions further increase upon pervanadate treatment (Zhu et al., 2016). As pervanadate increases phosphorylation of cytoplasmic tails by inhibiting phosphatase activity, it is thought that the interaction of PVRIG with these phosphatases is mediated by the phosphorylation of its tail tyrosines.

By competing with the co-stimulatory receptor CD226 to bind CD112, PVRIG inhibits the NFAT pathway-mediated T-cell activation and emerges as a novel T-cell co-inhibitory receptor (Zhu et al., 2016). In NK cells, PVRIG interaction with CD112 on target cells also leads to suppression of NK cell-mediated-cytotoxicity (Xu et al., 2017). PVRIG can bind to CD112 with higher affinity than CD226 does, as determined by surface plasmon resonance experiments (Zhu et al., 2016). The higher affinity interaction between the PVRIG-CD112 when compared to that between CD226-CD112 is conserved in mice (Murter et al., 2019).

1.4. LRBA

1.4.1. The LRBA Gene

Lipopolysaccharide-responsive beige-like anchor protein (LRBA) deficiency is a rare autosomal recessive disease, first described in 2012 in five children having distinct homozygous *LRBA* mutations that abolishes LRBA protein expression (Lopez-Herrera et al., 2012). Due to diverse autoimmune manifestations, LRBA deficiency is considered to be a primary immunodeficiency disorder (Gámez-Díaz, 2018). Mutations in the LRBA gene that causes LRBA protein loss is associated with a broad range of immune-related dysregulations. In LRBA deficient patients, recurrent infections, lymphoproliferation, and autoimmunity have been recorded (Jaramillo and Vargas, 2018). A decrease in surface and intracellular CTLA-4 protein levels in CD4+ T-cells and autophagy defects in B cells are crucial outcomes of LRBA deficiency (Lopez-Herrera et al., 2012; Lo et al., 2015). LRBA is an important player of immune homeostasis and its implications on the immune system functionality needs to be studied from diverse aspects.

The *LRBA* gene was first identified by a gene-trapping strategy where the aim was to trap lipopolysaccharide (LPS)-responsive genes. LPS is a bacterial cell wall antigen and a potent inducer of innate immune signaling and maturation in monocytes, dendritic cells, and

B cells. LPS stimulates inflammatory cytokine production and antigen presentation so that these activated immune cells further activate Th lymphocytes that mount an immune response towards bacterial pathogens. *LRBA* (named as "*lba*" in the corresponding study) was found to be included among several trapped novel LPS-responsive genes and its expression was shown to increase up to 4-fold in macrophages and B cells upon LPS stimuli (Wang et al., 2001).

The LRBA gene is located on human chromosome 4q31.3 with a length of 750839 base pairs and it has 58 exons. The human *LRBA* encodes for two protein transcripts that differ in exon 39, and are translated into 2851 and 2863 amino acid-containing protein isoforms. The mRNA expression of the LRBA gene has been observed by RT-PCR and qPCR in various tissues including mainly lymph nodes, bone marrow, spleen, kidney, pancreas, fetal liver, as well as in diverse cancer tissues like breast, prostate, colorectal, renal, pancreas, and lung cancers (Wang et al., 2004). However, its expression is not confined to only immune system cells, which shows its role in basic cellular mechanisms in addition to its immune regulatory role.

1.4.2. The LRBA Protein

LRBA encodes for a large protein product with ~319 kDa of molecular mass (Jaramillo and Vargas, 2018). LRBA protein consists of several domains, although the function of each domain is not fully known yet. Among them, the Beige and Chediak-Higashi (BEACH) domain is the most well-studied domain. It is well-conserved among the nine human proteins that are members of BEACH domain-containing proteins (BDCPs) (Figure 1.5). BEACH domain is thought to be involved in vesicle trafficking and it is mostly located towards the C-terminal part of the protein. In these proteins, before the BEACH domain, the Pleckstrin homology (PH) domain is found, and the WD40 domain (tryptophan and aspartic acid repeats) comes right after the BEACH domain. Whereas BDCPs mostly considered as scaffolding proteins, WD40 domain-containing proteins have been associated in various functions such as autophagy, apoptosis, signal transduction and vesicle trafficking (Cullinane et al., 2013). PH domains, on the other hand, can bind to phosphoinositides which facilitates their association with biological membranes. Proteins with various functions have

the PH domain, including kinases, cytoskeletal proteins, membrane transport regulators, and intracellular signaling adaptors (Lemmon, 1999).

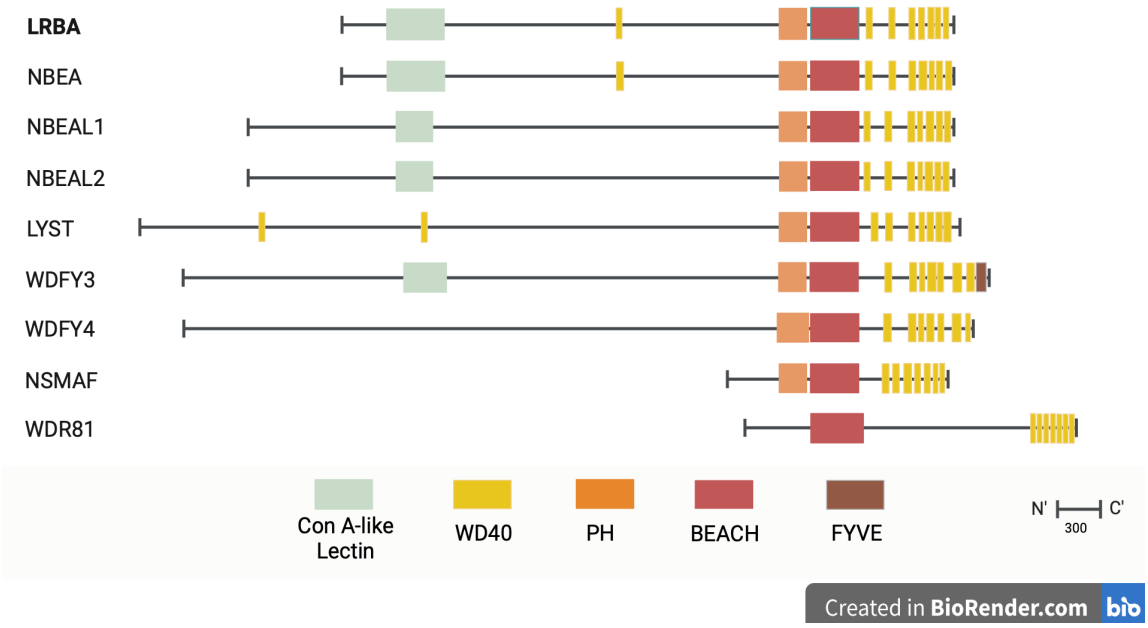

Figure 1.5. Protein domain alignment of nine human BDCPs.

In addition to LRBA, mutations in genes coding for BDCPs have been also linked to diverse clinical outcomes. For instance, LYST is the first BDCP identified in humans and it is known to be essential for the cytotoxic granule sorting. It contains a PH-domain, BEACH-domain and WD repeats like most of the BDCPs (Cullinane et al., 2013). Biallelic mutations in *LYST* result in Chediak-Higashi syndrome (CHS) which is an immunodeficiency disorder. CHS is characterized by recurrent infections, hypopigmentation of hair, skin, and eyes, and abnormal NK and neutrophil function (Westbroek et al., 2007). Interestingly, in one study, intracellular trafficking and thus cell surface expression of CTLA-4 was found to be impaired in T-cells of CHS patients (Barrat et al., 1999).

On the other hand, another well-studied protein in the BDCP family is Neurobeachin (NBEA) which also has a C-terminal PH-domain followed by BEACH and WD domains. NBEA has a ConA-like lectin domain as well as a central Domain of Unknown Function 1088 (DUF88) similar to LRBA (Cullinane et al., 2013). The PH and BEACH domains of both LRBA and NBEA were crystallized and their structures were computationaly predicted.

It was found that they have significant structural homology (Jogl et al., 2002; Gebauer et al., 2004), which may be an indication of a similar function for these two proteins through their PH-BEACH domains. *NBEA* mutations was implicated in autism in humans, and platelets of autistic patients with *NBEA* mutations were shown to have dense granules with abnormal morphology (Cullinane et al., 2013).

Another BDCP protein family member Neurobeachin-like 2 (NBEAL2) also has Con-A like lectin domain and PH-BEACH-WD40 domains. Loss of functions in NBEAL2 gene leads to grey platelet syndrome (GPS) characterized by bleeding disorders (Cullinane et al., 2013). Some portion of GPS patients develop autoimmunity as well (Rensing-Ehl et al., 2015). In a recently published study, NBEAL2 and CTLA-4 were shown to be interacting shown by co-immunoprecipitation experiments. Moreover, low levels of CTLA-4 were observed in NBEAL2 deficient patient derived effector T-cells, but not in regulatory T-cells, providing an evident for the existence of the NBEAL2-dependent CTLA-4 regulation mechanism in conventional T-cells (Delage et al., 2023).

GFP fused BEACH-WD domain of LRBA was associated with the ER, plasma membrane, endocytic vesicles, trans-golgi complex and lysosomes upon LPS stimuli as determined by confocal and electron microscopy analysis in murine macrophages (Wang et al., 2001). According to the computational predictions, human LRBA is located in various compartments inside the cell including cytosol, plasma membrane, ER, and Golgi apparatus. In addition, using an ImageStream (imaging flow cytometer), LRBA was shown to be localized within recycling endosomes and trans-golgi complexes in human T-cells, suggesting its role for vesicle trafficking (Lo et al., 2015). It was also shown that LRBA is required to deliver CTLA-4 to Rab11+ recycling endosomes and thus maintaining CTLA-4 surface expression on T lymphocytes (Janman et al., 2021).

1.4.3. Function of the LRBA Protein

The overall clinical manifestations of LRBA deficiency parallels those of CTLA-4 insufficiency which stems from autosomal heterozygous *CTLA-4* mutations (Schubert et al., 2014). The common characteristics of these two syndromes include hypogammaglobulinemia, autoantibody-mediated cytopenias, and organ-specific

autoimmunity (Lo et al., 2016). As a molecular consequence, in both syndromes, there is a decrease in CTLA-4 protein levels. Unrestrained immune response regulation due to low CTLA-4 levels leads to autoimmunity and lymphoproliferation (Verma et al., 2017). Indeed, the relationship between LRBA and CTLA-4 was first formulated due to clinical observations where LRBA-deficient patients showed significant improvement of their lymphoproliferative phenotype upon Abatacept treatment (Lo et al., 2015). Abatacept is a CTLA-4-Immunoglobulin Fc fusion protein drug that was originally developed to treat CTLA-4 deficiency. It is proposed to function by competitively binding to CD80/CD86 ligands of the T-cell co-stimulatory molecule CD28 (Herrero-Beaumont et al., 2012). LRBA-deficient patients have decreased total CTLA-4 protein levels in their T-cells compared to healthy controls, although CTLA-4 mRNA levels are not affected. These results revealed that LRBA post-translationally regulates CTLA-4 expression, and the molecular mechanism of this regulation was further identified (Lo et al., 2015).

LRBA colocalizes with CTLA-4 and Rab11 (a recycling endosome marker) on recycling endosomes and is required for the recycling of internalized CTLA-4 back to the cell surface (Janman et al., 2021). In addition, LRBA and CTLA-4 can be co-immunoprecipitated, making it likely that they physically interact. In *in vitro* studies, the PH-BEACH domain of LRBA was alone capable of binding CTLA-4. On the other hand, the Y201VKM motif on the CTLA-4 tail is required and sufficient for LRBA binding (Lo et al., 2015). The Y201VKM motif of CTLA-4 is an ITIM-motif and it is important for the regulation of T-cell signaling by the binding of phosphatases like SHP-2 (Guntermann and Alexander, 2002). Whether the interaction of LRBA and SHP-2 on the same motif are mutually exclusive is not known. Neither is it known whether LRBA requires any post-translational modifications of this motif for this interaction.

Although the main function of LRBA is thought to be the regulation of CTLA-4 protein trafficking, there are other proteins whose vesicular trafficking is associated with LRBA. One of such proteins is the Epidermal Growth Factor Receptor (EGFR) (Jaramillo and Vargas, 2018). EGFR is a tyrosine kinase receptor expressed in various tissue types and it interacts with EGF and TGF-β. Ligand interactions cause receptor dimerization and trans-auto-phosphorylation which leads to cell growth, proliferation, differentiation, and inhibition of apoptosis. Disrupted regulation of the EGFR receptor localization leads to enhanced

EGFR signaling which enables cancer development. The EGFR expression is regulated by clathrin-mediated endocytosis and it is either directed to lysosomes or back to the cell surface (Sigismund et al., 2008), similar to CTLA-4. Despite the fact that whether there is a physical interaction between LRBA and EGFR is still not known, it was shown that EGFR expression and phosphorylation decreases in dominant-negative LRBA mutants, highlighting LRBA as a potential regulator of EGFR and a potential molecular target for cancer therapy (Wang et al., 2004).

Another protein whose trafficking may be dependent on LRBA protein is the death receptor Fas ligand FasL, which facilitates apoptosis upon Fas binding (Waring and Müllbacher, 1999; Jaramillo and Vargas, 2018). Internalization of FasL occurs upon its interaction with Fas, and it is crucial for apoptosis triggering. The alteration of FasL amounts on the cell membrane in LRBA-deficient patients is not known to date. However, the increase in serum FasL and a decrease in apoptosis mediated by Fas was observed in LRBA-deficient patients (Revel-Vilk et al., 2015), suggesting that it is possible for LRBA to also regulate FasL in a similar way to CTLA-4.

1.5. Our Laboratory's Previous Studies on Possible LRBA Targets

In previous work in our laboratory, WT and LRBA knock-out (KO) Jurkat T-cells were surface protein biotinylated, streptavidin immunoprecipitated and analyzed by mass spectrometry to identify proteins that have altered surface expression upon LRBA loss (Zahedimaram, 2022). The main logic behind this study was to identify novel LRBA targets and to gain a better understanding of the roles of LRBA besides CTLA-4 trafficking, mainly on CD4+ T-cells. Among other proteins, Poliovirus Receptor-Related Immunoglobulin Domain (PVRIG) was found to be significantly reduced on the surface of an LRBA KO Jurkat single cell clone (Figure 1.6). This was the most interesting immunologically relevant potential target of LRBA. PVRIG resembles CTLA-4 in the context of its co-inhibitory function in T-cell signaling as well as the presence of an ITIM-motif on its tail where LRBA binding may be possible.

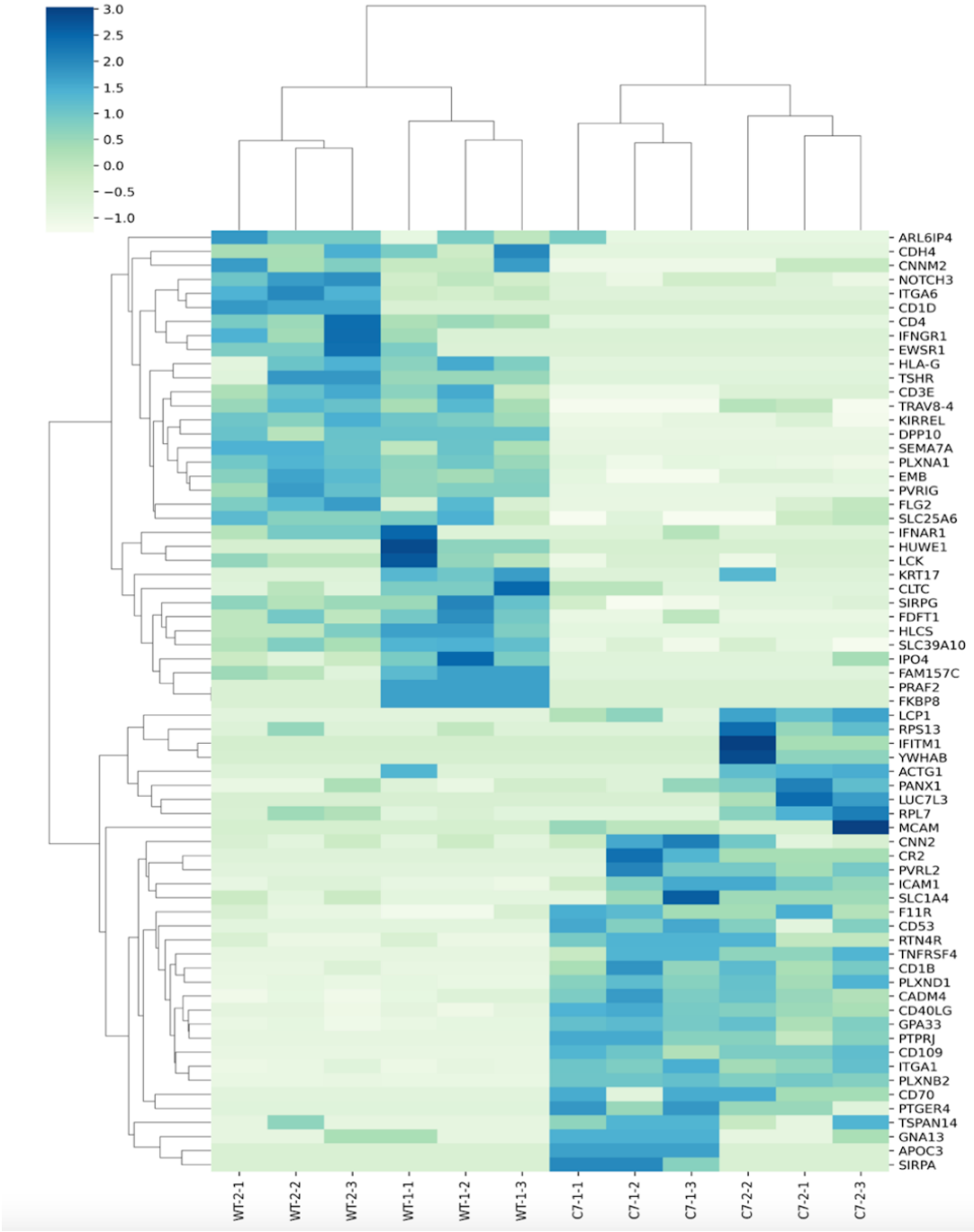

Figure 1.6. Heat map plot showing proteins whose surface expression was significantly altered between WT and LRBA KO Jurkat samples (Zahedimaram, 2022).

2. AIM OF THE STUDY

LRBA has an essential role in immune homeostasis by regulating the post-translational expression of CTLA-4, a crucial T-cell co-inhibitory receptor. CTLA-4 has a dynamic surface expression where it is rapidly internalized from the T-cell surface by endocytosis. LRBA is required to prevent lysosomal degradation of internalized CTLA-4 and to recycle it back to the cell surface, thus maintaining a balanced immune response. In LRBA deficient patients, CTLA-4 protein levels dramatically decrease in T-cells and lead to autoimmunity. However, other potential targets of LRBA in T-cells besides CTLA-4 have not yet been characterized.

In previous work in our laboratory, the alternative targets of LRBA were investigated by surface protein biotinylation, streptavidin immunoprecipitation, followed by mass spectrometry analysis in WT and LRBA KO Jurkat T-cells. PVRIG protein, a recently identified T-cell co-inhibitory receptor, was found to be significantly downregulated on the LRBA KO Jurkat T-cell surface. Up to date, there is no study that examined the functional relationship between LRBA and PVRIG in T-cells.

In this study, we wanted to investigate the mechanisms of the relationship between LRBA and PVRIG proteins and the possible mechanisms for PVRIG downregulation in the absence of LRBA protein.

This study aims to;

- Validate the surface and intracellular downregulation of PVRIG in the absence of LRBA in T-cells,

- Identify whether LRBA and PVRIG physically interact by co-immunoprecipitation experiments.

3. MATERIALS

3.1. Chemicals

Chemicals used in this study are listed in Appendix A section.

3.2. Equipment

Equipment used in this study are listed in Appendix B section.

3.3. Buffers and Solutions

Tris-Boric Acid-EDTA (TBE) Buffer: To prepare 5X TBE stock buffer, 54 g Tris-Base, 27.5 g Boric Acid, and 20 ml 0.5M EDTA (pH 8) was mixed in 1 L ddH_2O. To prepare 0.5X TBE solution, 1:10 dilution from 5X TBE was prepared with ddH_2O.

Agarose Gel: For 1% (w/v) agarose gel preparation, 1 g of agarose powder was dissolved in 100 ml 0.5X TBE by heating, then cooled for a while and 0.01% (v/v) ethidium bromide was added.

Calcium Chloride ($CaCl_2$) Solution for Competent Cell Preparation: Final concentrations of 60 mM $CaCl_2$, 15% (v/v) glycerol, and 10 mM PIPES (pH 7) was mixed in ddH_2O.

Calcium Chloride ($CaCl_2$) Solution for Transfection: To prepare 10 ml 2M $CaCl_2$ solution, 2.22 g $CaCl_2$ was dissolved in 10 ml ddH_2O.

HBS Solution (2X): 1.5 mM Na_2HPO_4, 50 mM HEPES, and 280 mM NaCl were mixed in 100 ml ddH_2O after the pH was adjusted to a value between 7.05 and 7.1. Final solution was filtered with a 0.22 μm filter and stored at -20°C.

Chloroquine Diphosphate (25 mM): To prepare 1 ml 25 mM chloroquine diphosphate solution, 0.013 g of chloroquine diphosphate was dissolved in 1 ml ddH_2O, filtered with a 0.22 μm filter, and stored at -20°C.

IP Lysis Buffer: Final concentrations of 1% Triton-X-100, 50 mM Tris (pH 7.4), 150 mM NaCl, and 2 mM EDTA were mixed and completed with ddH_2O up to desired buffer amount. The solution was filtered with a 0.22 μm filter and cooled down on ice. 25X protease inhibitor stock solution was added to the filtered solution with a final 1X concentration.

Triton-X-100 Lysis Buffer: For 10 ml Triton-X-100 lysis buffer, 0.5 ml 20% Triton-X-100, 0.5 ml 1M Tris-HCl (pH 7.4), 0.3 ml 5M NaCl, 0.04 ml 0.5M EDTA (pH 8), and Roche complete mini EDTA-free protease inhibitor tablet was added together and final volume was adjusted to 10 ml with ddH_2O.

Tris-Base (0.5M) Buffer: To prepare 100 ml 0.5M Tris-Base (pH 6.8), 6 gr Tris-Base was dissolved in 80 ml ddH_2O, pH was adjusted to 6.8 by using 6M HCl, and volume was completed to 100 ml with ddH_2O.

Tris-Base (1.5M) Buffer: To prepare 250 ml 1.5M Tris-Base (pH 8.8), 45.5 g Tris-Base was dissolved in 150 ml ddH_2O, pH was adjusted to 8.8 by using HCl, and final volume was completed to 250 ml with ddH_2O.

Tris-Acetate (1.5M) Buffer: To prepare 100 ml 1.5M Tris-Acetate (pH 7), 18 gr Tris-Base was dissolved in 80 ml ddH_2O, pH was adjusted to 7 by using acetic acid, and volume was completed to 100 ml with ddH_2O.

Tris-Acetate Acrylamide Solutions: For 8 ml separating 3% Tris-Acetate Acrylamide solution, 0.8 ml 30% Acrylamide, 2 ml Tris-Acetate (1.5M) buffer (pH 7), 80 μl 10% SDS, 80 μl 10% APS, 8 μl TEMED and 5 ml ddH_2O were mixed. For 8 ml separating 8% Tris-Acetate Acrylamide solution, 2.13 ml 30% Acrylamide and 3.7 ml ddH_2O were mixed with the same amount of the rest of the materials.

Tris-Glycine Acrylamide Solutions: For 8 ml separating 10% Tris-Glycine Acrylamide solution, 2.67 ml 30% Acrylamide, 2 ml Tris-Base (1.5M) buffer (pH 8.8), 80 µl 10% SDS, 80 µl 10% APS, 8 µl TEMED and 3.2 ml ddH_2O were mixed. For 5 ml stacking 6% Tris-Glycine Acrylamide solution, 1 ml 30% Acrylamide, 1.25 ml Tris-Base (0.5M) buffer (pH 6.8), 50 µl 10% SDS, 50 µl 10% APS, 5 µl TEMED and 2.6 ml ddH_2O were mixed.

Tricine Running Buffer: To prepare 1 L 1X Tricine running buffer, 8.95 gr Tricine, 6.06 gr Tris-Base, and 1 gr SDS were added together and dissolved in 1 L ddH_2O.

Tris-Glycine Running Buffer: To prepare 1 L 10X Tris-Glycine running buffer (pH 8.3), 30.3 gr Tris-Base, 144 gr Glycine, and 10 gr SDS was dissolved in 1 L ddH_2O.

Wet Transfer Buffer: To prepare 1 L 1X transfer buffer, 100 ml 10X Tris-Glycine running buffer, 100 ml methanol, 3.75 ml 10% SDS was added together and final volume was adjusted to 1 L with ddH_2O.

TBS and TBS-T Buffers: To prepare 1 L 10X TBS, 24 g Tris-Base and 88 g NaCl was combined and dissolved in 800 ml ddH_2O, and pH was adjusted to 7.6 by using HCl. Final volume was adjusted to 1 L by using ddH_2O. The 10X TBS solution was diluted in 1:10 ratio in ddH_2O to obtain a 1X TBS solution. To prepare 1X TBS-T solution, Tween-20 was added to 1X TBS solution in a final 0.1% concentration.

3.4. Growth Media

Luria Broth (LB): 20 g LB powder was dissolved in 1 L ddH_2O and autoclaved at 121°C for 15 minutes. 100 µg/ml final concentration of ampicillin was added to the LB medium for ampicillin selection.

LB-Agar: 20 g LB powder and 15 gr bacterial agar powder was dissolved in 1 L ddH_2O and autoclaved at 121°C for 15 minutes. Ampicillin was added in final concentration of 100 µg/ml after LB-Agar was cooled down a little, and then poured into petri dishes. Sterile LB-Agar plates were kept at 4°C after solidification.

Complete DMEM: HEK293T cells were maintained in DMEM with 10% (v/v) heat-inactivated fetal bovine serum, 2 mM L-Glutamine, 25 mM HEPES, and 1% PenStrep (100 U/ml Penicilium and 100 μg/ml Streptomycin).

Complete RPMI: Jurkat cells were maintained in RPMI 1640 with 10% heat-inactivated fetal bovine serum, 2 mM L-Glutamine, 1 mM Sodium Pyruvate, 0.1 mM MEM Non-essential amino-acid solution, 25 mM HEPES, and 1% PenStrep (100 U/ml Penicilium and 100 μg/ml Streptomycin).

Freezing medium: 6% DMSO (v/v) in heat-inactivated fetal bovine serum was used for cell freezing.

3.5. Enzymes

Enzymes used in this study are listed in Table 3.1.

Table 3.1. Enzymes used in this study.

Enzyme	**Company**
EcoRI-HF	New England Biolabs, USA
NotI	New England Biolabs, USA
NotI-HF	New England Biolabs, USA
HindIII-HF	New England Biolabs, USA
SalI-HF	New England Biolabs, USA
NcoI	New England Biolabs, USA
PvuII-HF	New England Biolabs, USA
Q5 High-Fidelity DNA Polymerase	New England Biolabs, USA
T4 DNA Ligase	New England Biolabs, USA
Taq DNA Polymerase	New England Biolabs, USA
PNGase F, Recombinant	New England Biolabs, USA

3.6. Antibodies

Antibodies used in this study are listed in Table 3.2.

Table 3.2. Antibodies used in this study.

Antibody	Company	Catalog Number	Usage Application & Dilutions
PVRIG (E9X9B) Rabbit mAb	Cell Signaling Technology	29599S	Western Blotting (1:2500) & Immunoprecipitation
β-Actin (D6A8) Rabbit mAb	Cell Signaling Technology	8457	Western Blotting (1:1000)
Anti-LRBA antibody produced in rabbit	Sigma-Aldrich	HPA023597	Western Blotting (1:2500)
Purified anti-His Tag Antibody	Biolegend	652502	Western Blotting (1:1000)
Purified anti-Vinculin Clone:W18245A Isotype: Rat IgG2a, κ	Biolegend	938402	Western Blotting (1:500)
Monoclonal ANTI-FLAG® M2-Peroxidase (HRP) antibody produced in mouse	Sigma-Aldrich	A8592	Western Blotting (1:1000)
c-Myc Monoclonal Antibody 9E10	Biolegend	626802	Western Blotting (1:1000)
Anti-rabbit IgG, HRP-linked Antibody	Cell Signaling Technology	7074S	Western Blotting (1:2500)
HRP Goat anti-rat IgG (minimal x-reactivity) Clone: Poly4054 Isotype: Goat Polyclonal IgG	Biolegend	405405	Western Blotting (1:2500)

Table 3.2. Antibodies used in this study (cont).

Antibody	Company	Catalog Number	Usage Application & Dilutions
PE human CD112R (PVRIG)	Biolegend	301503	Flow Cytometry (1:10)
Anti-Human CD112 APC	Biolegend	337411	Flow Cytometry (1:40)

3.7. Commercial Kits

Commercial kits used in this study are listed in Table 3.3.

Table 3.3. Commercial kits used in this study.

Commercial Kits	Company
Dynabeads® Protein A	Life Technologies, USA
Nucleo Spin® Gel and PCR Clean-up Kit	Macherey-Nagel, USA
QIAGEN® Plasmid Midi Kit	QIAGEN, Germany
Pierce™ Anti-c-Myc Magnetic Beads	Thermo Scientific, USA

3.8. Bacterial Strains

Escherichia coli (E. coli) DH5α strain was used for plasmid amplifications.

3.9. Mammalian Cell Lines

HEK293T: A derivative of human embryonic kidney 293 (HEK293) cell line that expresses mutant version of the SV40 large T antigen.

Jurkat: An immortalized human T-lymphocyte cell line that was originally obtained from a peripheral blood of a boy patient with acute T-cell leukemia.

3.10. Plasmids and Oligonucleotides

Plasmids and oligonucleotides used in this study are given in Table 3.4. and Table 3.5.

Table 3.4. Plasmids used in this study.

Plasmid Name	Purpose of Use	Source
p3X Flag CMV 7.1	Mammalian expression vector for expressing N-terminal Flag-tagged proteins	Sigma-Aldrich #E7533
pCI-neo Flag-PH-BEACH	Mammalian expression vector for expressing N-terminal Flag-tagged PH-BEACH domain of LRBA	Gift from Bernice Lo et al.
pcDNA Myc/His 3.1 (-) A	Mammalian expression vector for expressing C-terminal Myc- and 6xHis-tagged proteins	Invitrogen #V855-20
PVRIG Myc/His	Mammalian expression vector for expressing C-terminal Myc- and 6xHis-tagged PVRIG protein	Lab construct
Tailless PVRIG Myc/His	Mammalian expression vector for expressing C-terminal Myc- and 6xHis-tagged Tailless PVRIG	Lab construct
TM-Tail PVRIG Myc/His	Mammalian expression vector for expressing C-terminal Myc- and 6xHis-tagged TM-Tail PVRIG	Lab construct
pLeGO-iT2p	Lentiviral construct for IRES-dTomato expression	Gift from Prof. Boris Fehse
pLeGO-iT2p-PVRIG	Lentiviral construct for PVRIG-IRES-dTomato expression	Lab construct

Table 3.5. Oligonucleotides used in this study.

Oligo Name	Purpose of Use	Sequence (5' to 3')
PVRIG-EcoRI-Fwd	PCR for PVRIG gene from Jurkat cDNA with forward EcoRI cut site.	ATACGAATTCATGAGAACA GAGGCACAGGTGCCGG
PVRIG-NotI-Rev	PCR for PVRIG gene from Jurkat cDNA with reverse NotI cut site.	TAGCGGCCGCTCATCGA ACTCCTAAGGGTCCTTCCATG
PVRIG-NotI-Fwd	PCR for PVRIG gene from Jurkat cDNA with forward NotI cut site.	TGCGGCCGCATGAGAA CAGAGGCACAGGTGCCG
PVRIG-EcoRI-Rev	PCR for PVRIG gene from Jurkat cDNA with reverse EcoRI cut site.	ACGCGAATTCGTGATCGAA CTCCTAAGGGTCCTTCCATGGC
Tailless-PVRIG-EcoRI-Rev	PCR for Tailless PVRIG from PVRIG Myc/His plasmid with reverse EcoRI cut site.	AATTAGAATTCGTCGGCGCAGC AGATGAAGGAGGTAGACACAGC
TM-Tail-PVRIG-NotI-Fwd	PCR for PVRIG's transmembrane (TM) and tail domains from PVRIG Myc/His plasmid with forward NotI cut site.	ATGCGGCCGCATGGA CCTGGCCGGGATCTT
WD40-HindIII-Fwd	PCR for LRBA's WD40 domain from Jurkat cDNA with forward HindIII cut site.	TATAAGCTTGACCAAAGT ATTCAAGTGCATTCCCAGTGC
WD40-SalI-Rev	PCR for LRBA's WD40 domain from Jurkat cDNA with reverse SalI cut site.	TATGTCGACTTATTCATGAT GCCACCGGTTAAAGTCGTTGTA

4. METHODS

4.1. Bacterial Cell Culture

Bacterial culture growth: The *Escherichia coli (E. coli)* DH5α strain was grown overnight in LB medium at 37°C while shaking at 220 rpm. Glass beads were used to spread the bacteria on LB Agar-containing petri dishes and incubated at 37°C without shaking with the petri dishes placed upside down. A single colony was picked from plates after 16 hours. According to the application purpose, growth media was prepared with or without selective antibiotics. For long-term storage of bacterial cells, a 10% final concentration of glycerol (v/v) was added to 1 ml cryo-vial tubes containing an overnight grown bacterial culture, and stored at -80°C. For bacterial cultures used for preparing plasmid DNA, a bacterial colony was first grown in 3 ml of selective medium in a glass tube with vigourous shaking at 220 rpm, 37°C for 16 hours and was transferred to 100 ml of the same selective medium in an Erlenmeyer flask and continued to be cultured overnight.

Competent cell preparation: One vial of *E. coli* cell stock (200 µl) was added to 40 ml LB in a 250 ml flask, incubated at 37°C overnight while shaking at 220 rpm. At the end of the incubation period, 4 ml of grown bacteria culture was added into 400 ml LB in a 2 L flask and incubated at 37°C, shaking at 220 rpm. OD was measured every 20 minutes. To measure growth by OD, two cuvettes were used for spectroscopic measurement with 2 ml of grown culture or LB alone as a blank. When OD value reached 0.35-0.375, cells were immediately put on ice and aliquoted into eight 50 ml-falcons. Falcons were kept on ice for 10 minutes, then centrifuged at 3000 rpm for 10 minutes at 4°C. Cell pellets in each falcon were resuspended in 10 ml ice-cold $CaCl_2$ solution, centrifuged at 2500 rpm for 5 minutes at 4°C. Each pellet was resuspended in 10 ml ice-cold $CaCl_2$ solution one more time and kept on ice for 30 minutes. During 30 minutes, 100 eppendorf tubes (1.5 ml) were placed on ice. At the end of the incubation time, the falcon tubes were centrifuged at 2500 rpm for 5 minutes at 4°C, supernatants discarded, and pellets were resuspended in 2 ml ice-cold $CaCl_2$. The contents of all 8 falcon tubes were combined in one falcon tube (16 ml in total), and aliquoted into the ice-cold 1.5 ml eppendorf tubes waiting on ice (each 200 µl), capped and immersed into liquid nitrogen for flash freezing. All eppendorfs were taken from the liquid

nitrogen and stored at -80°C for further use. During competent cell preparation, all growth media was prepared without antibiotics. The transformation efficiency of competent cells was calculated by transforming different concentrations of pUC19 plasmid DNA. Transformation efficiency of prepared competent cells varied between 10^7-10^8 cfu per μg of pUC19 plasmid DNA transformed.

Transformation of competent bacteria: 200 μl DH5α competent cells thawed on ice. Ligation products containing 100 μg plasmid DNA was added to competent cells and kept on ice for 30 minutes followed by heat shocking at 42°C for 90 seconds and transferred on ice for 3 minutes. Subsequently, 800 μl of LB media without antibiotics was added and cells were incubated at 37°C with 220 rpm shaking for 1 hour. The cells were centrifuged at 13,000 rpm for 30 seconds and 900 μl of the supernatant was discarded. Cells were resuspended in the remaining 100 μl LB and spread on LB Agar plates by using glass beads. Plates were incubated at 37°C overnight.

Plasmid DNA isolation: Plasmid DNA was isolated using either the alkaline lysis protocol from *Molecular Cloning: A Laboratory Manual* (Sambrook et al., 2001) or the Qiagen Mini-Midiprep Kits according to the manufacturer's instructions. A NanoDrop spectrophotometer was used to measure the concentration and purity of isolated DNA.

4.2. Mammalian Cell Culture

Maintenance of cell lines: Complete DMEM with 10% FBS (v/v) was used for culturing HEK293T cells in sterile tissue culture flasks. Cells were kept in an incubator at 37°C and 5% CO_2. The cells were split in a 1:10 ratio every 2 days by using complete DMEM medium. Complete RPMI 1640 with 10% FBS (v/v) was used for culturing Jurkat T-cells in sterile tissue culture flasks and kept in an incubator at 37°C and with 5% CO_2. Cells were seeded with a density of 400.000-500.000 cells/ml and were split in a 1:4 to 1:5 ratio in complete RPMI medium every 2-3 days.

Cell Freezing: Cells were counted and the desired cell density per vial was adjusted ($5x10^6$ cells per vial for Jurkat cells, $3.5x10^6$ cells per vial for HEK293T cells). Cells were centrifuged at 200g for 5 minutes and the cell pellet was resuspended in 0.5 ml FBS for each

vial. The cell suspension was incubated at 4°C for 20 minutes. During incubation, FBS with 12% DMSO (v/v) was prepared. At the end of incubation time, 0.5 ml FBS with 12% DMSO for each vial was added onto cells, making the final DMSO concentration 6% (v/v). Cells were aliquoted in 1 ml into cryotubes and stored in -80°C for at least 24 hours and then transferred to a liquid nitrogen tank for long-term storage.

Cell Thawing: The cryotubes were transferred to room temperature from -80°C or a liquid nitrogen tank. For every vial to be thawed, 9 ml of complete medium was placed in 15 ml-falcon tubes. After the cells were thawed, they were slowly added onto the 9 ml complete medium and centrifuged at 200g for 5 minutes. Supernatants were discarded and the cell pellet was resuspended in 5 ml complete medium and placed into a sterile tissue culture flask and kept in an incubator.

Transfection: $3.5x10^6$ HEK293T cells were seeded to 10cm tissue culture treated plates in a total of 10 ml complete DMEM, 16 hours before the transfection. When cell confluency reached 70%, 12 μg of DNA in up to 450 μl ddH_2O was mixed with 50 μl 2M $CaCl_2$. The mixture was added onto 500 μl 2X HBS solution in 50-ml falcon tubes drop by drop while making bubbles with a serological pipette. The total mixture was incubated at room temperature for up to 20 minutes. Meanwhile, 10 μl 25mM chloroquine was added dropwise onto the medium of the transfection plates, corresponding to a 1:1000 dilution. The incubated DNA mixture was then distributed onto cells in a dropwise manner and the medium was changed with fresh DMEM 8 hours after the transfection.

4.3. Cloning of PVRIG and LRBA Domains

In order to construct PVRIG c-Myc/His plasmids, the pcDNA 3.1 Myc/His (-) A backbone was used. Full length PVRIG insert was amplified from Jurkat cDNA. Tailless PVRIG and TM-Tail PVRIG domains were amplified by using the established full length PVRIG Myc/His plasmid. All designed forward primers have NotI cut site and all reverse primers have EcoRI cut site.

pcDNA PVRIG-Myc/His Cloning: PCR for amplifying full length PVRIG gene was performed as shown in Table 4.1 and Table 4.2.

Table 4.1. PCR of PVRIG cDNA from Jurkat T-cell cDNA.

Jurkat cDNA (1:20 dilution)	1 µl
NEB 10X Standard Taq Reaction Buffer	5 µl
10 mM dNTPs	1 µl
10 µM Forward Primer	1 µl
10 µM Reverse Primer	1 µl
NEB Taq DNA Polymerase	0.25 µl
ddH_2O	Up to 50 µl
Total volume	50 µl

Table 4.2. Reaction conditions for PVRIG cDNA PCR.

Step	**Temperature**	**Time**
Initial Denaturation	95°C	30 seconds
35 Cycles	95°C	30 seconds
	68°C	60 seconds
	68°C	1 minute
Final Extension	68°C	5 minutes

The PCR product was run on a 1% agarose gel prepared with 0.5X TBE buffer for 1 hour at 100 V. A small amount of PCR product (1-2 µl) was used for visualization, and the remaining PCR product was directly extracted from the gel without visualization for reducing the UV exposure time. For the DNA isolation from the gel, NucleoSpin Gel and PCR Clean-up kit was used according to the manufacturer's protocol. Isolated DNA concentration was determined by a NanoDrop spectrophotometer. Gel isolated PCR products were digested with NotI and EcoRI enzymes for 3 hours at 37°C (Table 4.3) and cleaned up by using Nucleospin Gel and PCR Clean-up kit.

The pcDNA 3.1 Myc/His (-) A vector backbone was digested with NotI and EcoRI enzymes for 3 hours at 37°C (Table 4.4) and the digested plasmid was run on a 1% agarose gel for 1 hour at 100 V followed by gel extraction by using NucleoSpin Gel and PCR Clean-up kit.

Table 4.3. Digestion of PVRIG PCR product.

PCR product	1000 ng
NEB2.1 10X Buffer	5 µl
EcoRI-HF	0.3 µl
NotI	0.8 µl
ddH_2O	Up to 50 µl
Total	50 µl

Table 4.4. Digestion of pcDNA 3.1 Myc/His (-) A backbone plasmid.

pcDNA 3.1 Myc/His (-) A plasmid	6 µg
NEB2.1 10X Buffer	5 µl
EcoRI-HF	0.6 µl
NotI	0.8 µl
ddH_2O	Up to 50 µl
Total	50 µl

Digested vector concentration was determined by the NanoDrop spectrophotometer. The ligation was performed at 25°C for 10 minutes according to the Table 4.5.

Table 4.5. Ligation of backbone vector and insert.

Digested PVRIG insert	125 ng
Digested vector backbone	100 ng
NEB T4 DNA Ligase	1 µl
NEB 10X T4 DNA Ligase Buffer	2 µl
ddH_2O	Up to 20 µl
Total volume	20 µl

Ten µl of the ligation product and control sample was transformed into 200 µl of competent DH5α *E. coli* and plated onto petri dishes containing antibiotic selective LB. After overnight incubation, colonies were picked from transformation plates and mini-prep culture was started by incubating each colony with 3 ml of LB and 1:1000 (v/v) appropriate

antibiotic at 37°C overnight. After overnight incubation, plasmid DNA (mini-prep) was isolated and digested with diagnostic restriction enzymes (Table 4.6.). Cloning confirmation was done by running diagnostic digestion samples on an agarose gel and analysing the resultant band sizes.

Table 4.6. Colony DNA digestion for cloning confirmation.

	Uncut Colony DNA	Cut Colony DNA
DNA	1000 ng	1000 ng
NEB 2.1 10X Buffer	2 µl	2 µl
EcoRI-HF	-	0.3 µl
NotI	-	0.3 µl
ddH_2O	Up to 20 µl	Up to 20 µl
Total volume	20 µl	20 µl

pcDNA TM-Tail and Tailless PVRIG-Myc/His Clonings: PCR for amplifying TM-Tail PVRIG and Tailless PVRIG was performed as shown in Table 4.7. PCR reaction conditions for TM-Tail PVRIG and Tailless PVRIG are given in Table 4.8 and 4.9, respectively.

Table 4.7. PCR of TM-Tail PVRIG and Tailless PVRIG from PVRIG Myc/His plasmid.

PVRIG Myc/His plasmid	1 ng
5X Q5 Reaction Buffer	10 µl
10 mM dNTPs	1 µl
10 µM Forward Primer	2.5 µl
10 µM Reverse Primer	2.5 µl
NEB Q5 High-Fidelity DNA Polymerase	0.5 µl
ddH_2O	Up to 50 µl
Total volume	50 µl

Table 4.8. Reaction conditions for TM-Tail PVRIG PCR.

Step	Temperature	Time
Initial Denaturation	98°C	30 seconds
35 Cycles	98°C	10 seconds
	72°C	30 seconds
	72°C	15 seconds
Final Extension	72°C	5 minutes

Table 4.9. Reaction conditions for Tailless PVRIG PCR.

Step	Temperature	Time
Initial Denaturation	98°C	30 seconds
35 Cycles	98°C	10 seconds
	72°C	30 seconds
	72°C	25 seconds
Final Extension	72°C	5 minutes

The digested vector backbone (Table 4.4) was used in the cloning of both constructs. Ligation was performed at 25°C for 10 minutes by using 3:1 insert to vector DNA mass ratio. Cloning confirmation was performed accordingly to Table 4.6.

pLeGO-iT2p-PVRIG Cloning: To construct the pLeGO-iT2p-PVRIG plasmid, the pLeGO-iT2p backbone was used. Full length PVRIG insert was amplified from Jurkat T-cell cDNA with PVRIG-EcoRI-Fwd and PVRIG-NotI-Rev primers. PCR was performed by using the same amounts of materials as shown in Table 4.1 with the only exception as using 1:40 dilution of Jurkat cDNA instead of 1:20. PCR reaction conditions are given in Table 4.10. PCR product digestion was performed as it was shown in Table 4.3.

Digestion of pLeGO-iT2p vector backbone was performed as shown in Table 4.11. Digested vector was extracted from agorose gel by using NucleoSpin Gel and PCR Clean-up kit and concentration was determined by using a NanoDrop spectrophotometer. Ligation was performed at 25°C for 10 minutes by using 3:1 insert to vector DNA mass ratio.

Table 4.10. Reaction conditions for PVRIG PCR.

Step	Temperature	Time
Initial Denaturation	95°C	30 seconds
35 Cycles	95°C	30 seconds
	67°C	1 minute
	68°C	1 minute
Final Extension	68°C	5 minutes

Table 4.11. Digestion of pLeGO-iT2p backbone plasmid.

pLeGO-iT2p	5 µg
NEB2.1 10X Buffer	5 µl
EcoRI-HF	0.5 µl
NotI	0.6 µl
ddH_2O	Up to 50 µl
Total	50 µl

CMV p3X Flag-WD40 Cloning: To construct Flag-WD40 plasmid, the p3X Flag CMV 7.1 vector backbone was used. WD40 domain of LRBA was amplified from Jurkat cDNA with WD40-HindIII-Fwd and WD40-SalI-Rev primers as shown in Table 4.12 and Table 4.13.

Table 4.12. PCR of WD40 domain of LRBA from Jurkat cDNA.

Jurkat cDNA (1:20 dilution)	1 µl
5X Q5 Reaction Buffer	10 µl
10 mM dNTPs	1 µl
10 µM Forward Primer	2.5 µl
10 µM Reverse Primer	2.5 µl
NEB Q5 High-Fidelity DNA Polymerase	0.5 µl
ddH_2O	Up to 50 µl
Total volume	50 µl

Table 4.13. Reaction conditions for WD40 PCR.

Step	Temperature	Time
Initial Denaturation	98°C	30 seconds
35 Cycles	98°C	10 seconds
	72°C	30 seconds
	72°C	25 seconds
Final Extension	72°C	5 minutes

p3X Flag CMV 7.1 vector digestion was performed as shown in Table 4.14. Digested vector was extracted from agorose gel by using NucleoSpin Gel and PCR Clean-up kit and concentration was determined by using NanoDrop spectrophotometer. Ligation was performed at 25°C for 10 minutes by using 3:1 insert to vector DNA mass ratio.

Table 4.14. Digestion p3X Flag CMV 7.1 backbone plasmid.

p3X Flag CMV 7.1	6 µg
NEB 10X CutSmart Buffer	5 µl
HindIII-HF	0.5 µl
SalI-HF	0.5 µl
ddH_2O	Up to 50 µl
Total	50 µl

4.3. Flow Cytometry

Surface Staining: The cells were counted and $1x10^6$ cells were washed with 1X PBS for 2 times. Cells were then incubated with appropriate amount of antibody for 30 minutes on ice. Antibody dilutions were prepared in 1X PBS according to desired antibody dilution. Following the incubation, stained cells were washed with PBS for 3 times and resuspended in fresh PBS for flow cytometry analysis. As controls, unstained cells were used.

Intracellular Staining: The cells were counted and $1x10^6$ cells were washed with 1X PBS for 2 times. The cells were fixed with a 4% PFA solution for 20 minutes on ice. Cells were washed with a 1X permeabilization buffer and incubated with the proper amount of

antibody for 30 minutes on ice. Antibody dilutions were prepared in a 1X permeabilization buffer according to desired antibody dilution. Stained cells were washed with 1X permeabilization buffer for 3 times and resuspended in 1X PBS for flow cytometry analysis. Due to a lack of isotype control antibodies, unstained cells were used as controls.

Flow cytometry data were collected using a Beckton Dickenson FACS Calibur or Accuri C6 flow cytometer and analysed using FlowJo software (Tree Star, Inc, V.10).

4.4. Western Blotting and Co-Immunoprecipitation

Cell Lysis: For western blotting, $6x10^6$ Jurkat T-cells were counted using a hematocytometer under an inverted microscope and washed 2 times with 1X PBS. Cells were resuspended in 30 µl Triton-X-100 Lysis Buffer per $1x10^6$ cells and incubated for 30 minutes on ice. Cells were then centrifuged for 10 minutes at 14,000 rpm, 4°C. Supernatants were collected and either directly used or aliquoted into 30 µl for long-term storage at -80°C. The cell lysate was mixed with 1X Laemmli Buffer and boiled at 95°C for 10 minutes before loading onto poly acrylamide gels.

SDS-PAGE Gel Preparation, Wet Transfer, and Visualization: For LRBA blotting, a 3-8% Tris-Acetate gradient gel was prepared. Firstly, 1 ml of 8% Tris Acetate Acrylamide solution was poured into the glass spacer. Subsequently, 4 ml of 3% and 3 ml of 8% Tris Acetate Acrylamide solution was pipetted into a 10 ml serological pipet and a single air bubble was gently sucked into the pipet to mix the solutions to form a gradient. The mixed gradient solution was gently poured on top of the 1 ml 8% Tris Acetate Acrylamide solution in the glass spacer. The gel solution was layered on top with isopropanol. After setting of the poly acrylamide gel for 30 minutes, the isopropanol was discarded. 5 ml of 3% Tris Base Acrylamide solution stacking gel pipetted on top, and the well comb was placed. Gels were either used the on the same day or after 1-2 days upon being kept at 4°C wrapped in wet towels for hydrations. Acrylamide Gel electrophoresis was performed by using a 1X Tricine buffer at 100 V constant voltage for ~2 hours. After running, wet transfer was performed by using 0.45 µm PVDF membranes upon membrane activation with methanol for 1 minute. Transfer was performed with constant 250 mA for 3 hours in the cold room (4°C) with ice-cold 1X Tris Glycine transfer buffer.

For standard Acrylamide Gel electrophoresis, 10% separating and 4% or 6% stacking Tris Glycine Acrylamide gels were prepared. Electrophoresis was performed by using a 1X Tris Glycine running buffer at constant 100 V for 1.5-2 hours. After running, wet transfer was performed by using 0.45 μm PVDF membranes upon membrane activation with methanol for 1 minute. Transfer was performed with constant 250 mA for 1.5 hours in the cold room (4°C) with ice-cold 1X Tris Glycine transfer buffer. For all blottings, followed by wet-transfer, membranes were blocked for 1 hour by incubating with 5% skim milk in TBS-T (0.1% Tween) at room temperature. Membranes were then washed for 10 minutes 3 times with 1X TBS-T and incubated with the appropriate primary antibodies with desired dilutions prepared in 5% skim milk-containing 1X TBS-T solution at 4°C overnight. Membranes were washed with 1X TBS-T 3 times each for 10 minutes, and incubation with horseradish peroxidase (HRP)-conjugated secondary antibody dilutions prepared in 5% skim milk-containing 1X TBS-T solution was performed at room temperature for 1 hour. Membranes were washed and visualized using ECL with Syngene G:BOX Chemi Xrq.

PNGase F Treatment: $6x10^6$ Jurkat T-cells were lysed with 90 μl Triton-X-100 Lysis Buffer. 9 μl of cell lysate was mixed with 1 μl 10X Glycoprotein Denaturing Buffer and heated for 10 minutes at 100°C. Mixture was immediately chilled on ice and centrifuged for 10 seconds. 2 μl of 10X Glycobuffer 2, 2 μl of 10% NP-40, and 1 μl of undiluted or diluted PNGase F was added to the mixture. Total volume was completed up to 20 μl with ddH_2O, and the mixture was incubated at 37°C for 1 hour. 5 μl of 1X Laemmli buffer was added to the mixture before loading sample on poly acrylamide gel. PNGase F dilutions were prepared in 1X Glycobuffer 2.

Co-Immunoprecipitation: For co-immunoprecipitation with Pierce Anti-c-Myc Magnetic Beads and western blot analysis, $10x10^6$ HEK293T cells were lysed with 300 μl IP lysis buffer for 1 hour on ice. Lysed cells were centrifuged for 10 minutes at 14,000 rpm, 4°C, and supernatant was collected. Some amount of lysate was kept for input control and the remaining lysate was used in co-immunoprecipitation which was performed according to manufacturer's instructions. For co-immunoprecipitation of endogenous PVRIG from WT Jurkat T-cells or transfected non tagged PVRIG from HEK293T cells, $10x10^6$ cells were lysed with IP lysis buffer. Some amount of lysate was kept for input control and the remaining lysate was used in co-immunoprecipitation. Dynabeads Protein A was conjugated

with anti-hPVRIG antibody and then incubated with cell lysates according to the manufacturer's instructions.

4.5. Statistical Analysis

For PVRIG western blot quantification, the one-way ANOVA test was used in Microsoft Excel (version 16.66.1) by choosing a $p<0,05$ significance value. Graphs were prepared by using GraphPad Prism (GraphPad Software Inc. La Jolla, CA, USA, version 9.0.0).

4.6. RNA-Seq Data Analysis for WT and LRBA KO Jurkat Cells

RNA Sequencing was performed by Refgen Biyoteknoloji by using Illumina NovaSeq 6000. RNA-Seq counts were aligned to the reference human genome (GRCh38/hg38) by using the HISAT2 tool (HISAT 2.2.1 release 7/24/2020) (Kim et al., 2019), which is performed by Ege Ezen. The read counts were subjected to differential gene expression (DEG) analysis by using DESeq2 tool (release 3.17) (Love et al., 2014) in R programming language by filtering log2 fold change>1 and P adjusted value <0,05. Hierarchical heatmap figures were made by using Pheatmap library (version 1.0.12) in R, and PCA analysis was visualized by using ggplot package (release 3.4.2) (Wickham, 2009) in R. For enrichment analysis of DEGs, the PANTHER (release 17.0) (Mi et al., 2019) web tool was utilized.

5. RESULTS

5.1. Cloning of PVRIG and LRBA Domains

To heterologously express the PVRIG protein in cells that normally do not express PVRIG, and to overexpress PH-BEACH and WD40 domains of LRBA, we generated eukaryotic expression constructs. We constructed various plasmids by molecular cloning to investigate whether there is a physical interaction between the PVRIG and LRBA proteins by co-immunoprecipitation experiments. All the cloning experiments were confirmed by the colony plasmid DNA restriction digestion followed by agarose gel electrophoresis. Firstly, the same enzymes used for the cloning were used for digestion as an initial confirmation, followed by additional digestion reactions with various enzymes depending on the insert and the vector backbone. We also wanted to construct eukaryotic expression plasmids that express full length LRBA or only the PH-BEACH-WD40 domains of LRBA for using them in co-IP experiments, but the clonings were not successful (data not shown).

5.1.1. Cloning of the Full Length PVRIG Gene

5.1.1.1. Cloning of PVRIG Gene Into pLeGO-iT2p Plasmid. Full length PVRIG gene was amplified from Jurkat T-cell line by using PVRIG-EcoRI-Fwd and PVRIG-NotI-Rev primers, and cloned into the pLeGO-iT2p plasmid as described in the methods section. EcoRI and NotI enzymes were used for the diagnostic digestion of plasmid DNA isolated from 11 colonies (Figure 5.1). Glycerol stocks were prepared from two colonies that contained the insert. The presence of two bands of 988 and 9178 base pairs in EcoRI-NotI digested plasmid DNA confirmed the correct cloning of the PVRIG cDNA into the pLeGO-iT2p.

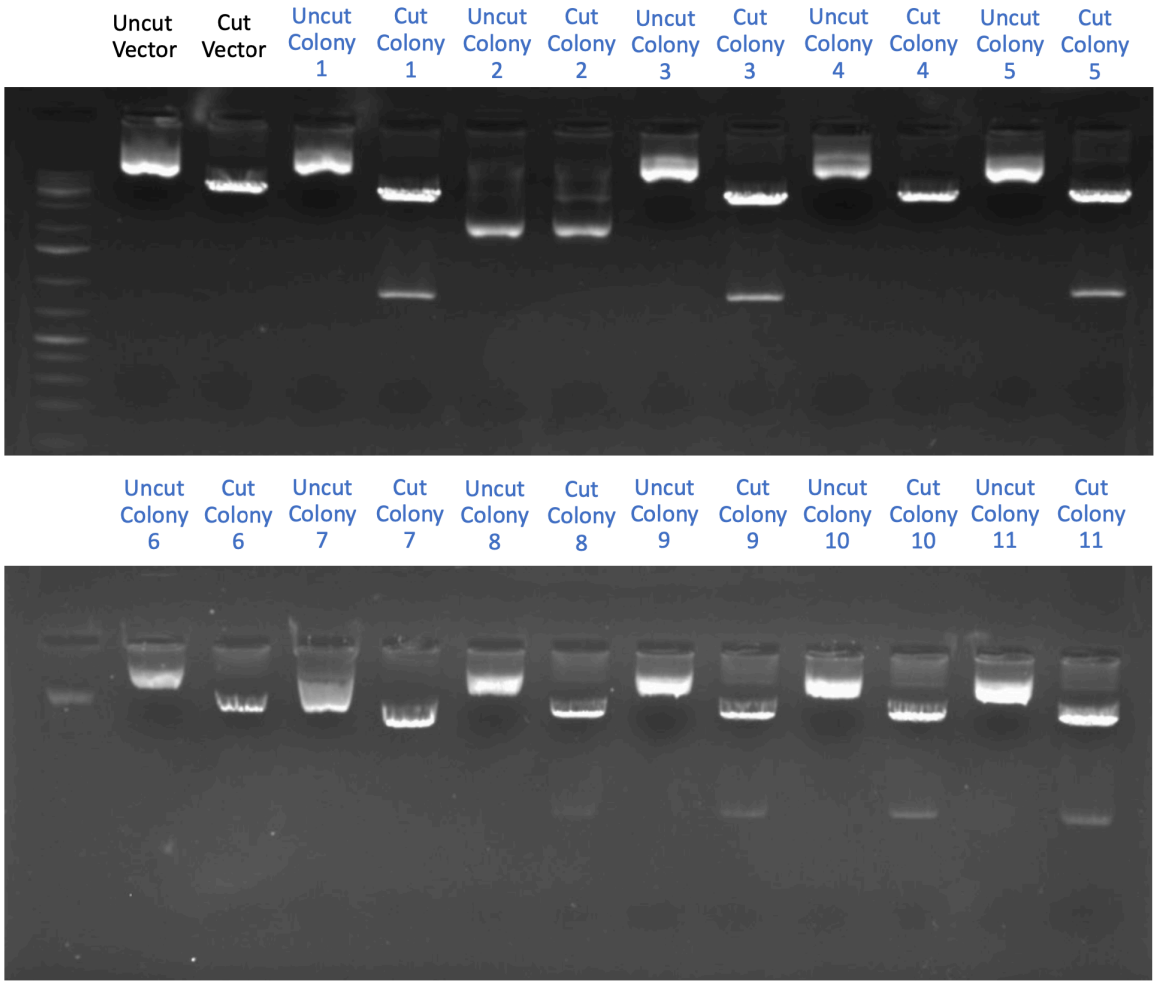

Figure 5.1. Gel image of the restriction digestion of empty vector (pLeGO-iT2p) and mini-prep colonies for the pLeGO-iT2p-PVRIG cloning with EcoRI and NotI enzymes.

5.1.1.2. Cloning of PVRIG Gene into pcDNA 3.1 Myc/His (-) A Plasmid. The full length PVRIG gene was amplified from Jurkat T-cell line by using PVRIG-NotI-Fwd and PVRIG-EcoRI-Rev primers, and cloned into the pcDNA 3.1 Myc/His (-) A plasmid as described in the methods section. NotI and EcoRI enzymes were used for the diagnostic digestion of plasmid DNA isolated from nine colonies (Figure 5.2). Glycerol stock was prepared from two colonies that contained the insert. One of the colonies was also used for midi-prep DNA isolation and further digested with additional restriction enzymes for confirmation (Figure 5.3). The presence of two bands of 989 and 5495 base pairs in EcoRI-NotI digested and three bands of 678, 1069, 1096, and 3641 base pairs in PvuII digested plasmid DNA confirmed the correct cloning of the PVRIG cDNA into the pcDNA 3.1 Myc/His (-) A plasmid. In the

case of PvuII digestion, the almost identical sizes of 1069 and 1096 base pair bands appear as a single band.

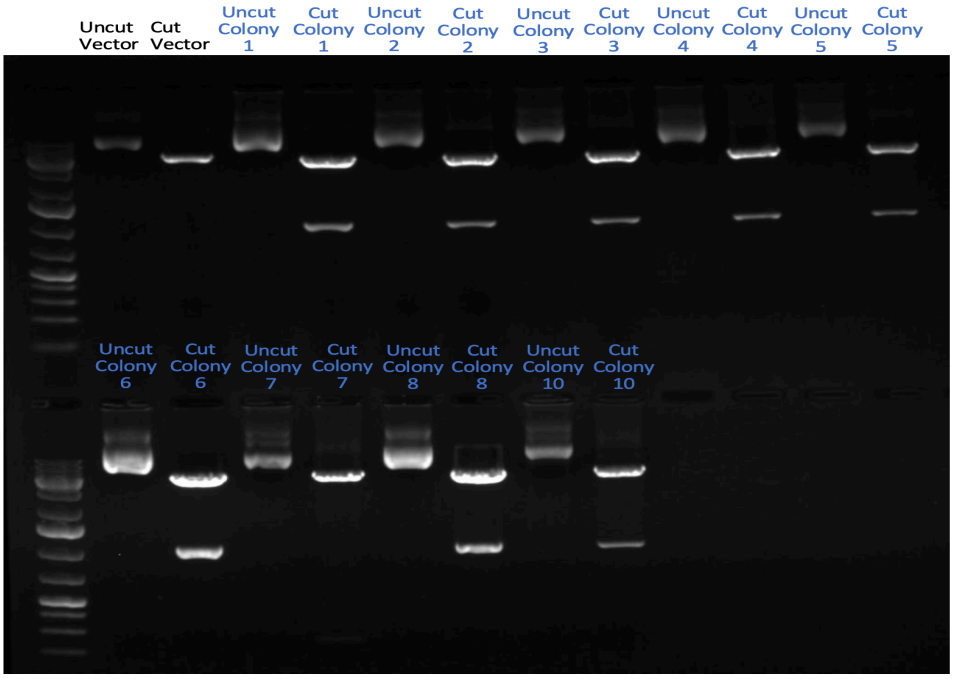

Figure 5.2. Gel image of the restriction digestion of empty vector and mini-prep colonies for the PVRIG Myc/His cloning with EcoRI and NotI enzymes.

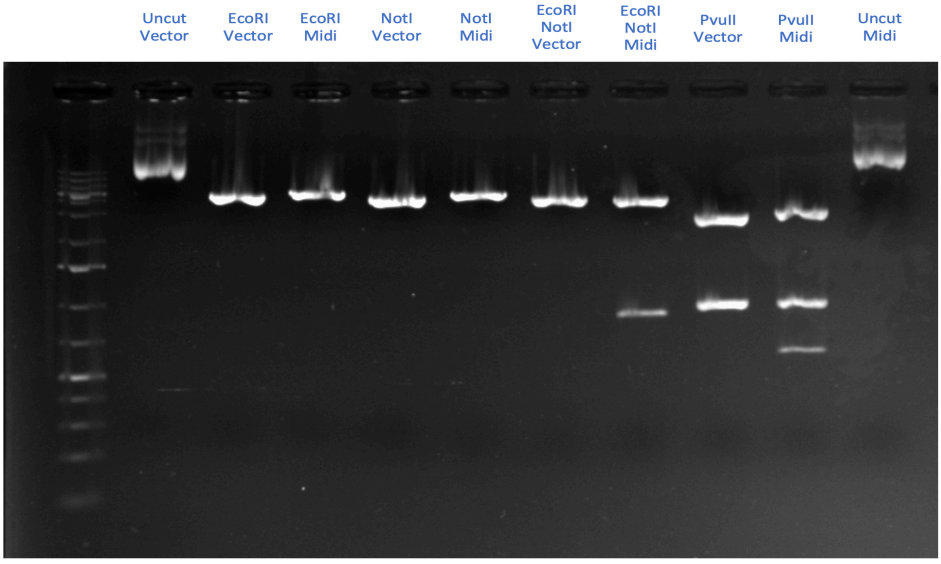

Figure 5.3. Gel image of the restriction digestion of an empty vector backbone (Vector) and midi-prep of PVRIG Myc/His cloning (Midi) with indicated enzymes.

5.1.1.3. Cloning of a Tailless PVRIG into pcDNA 3.1 Myc/His (-) A Plasmid. Primers were designed to amplify the PVRIG gene without its cytoplasmic tail, hereafter named "Tailless PVRIG". Constructed PVRIG Myc/His plasmid was used as a template for the PCR, and PVRIG-NotI-Fwd and Tailless-PVRIG-EcoRI-Rev primers were used for amplification. The PCR product was digested with NotI and EcoRI enzymes and cloned into the pcDNA 3.1 Myc/His (-) A plasmid. The same restriction enzymes were used for the diagnostic digestion of plasmid DNA from eleven colonies (Figure 5.4). Glycerol stock was prepared from two colonies that contained the insert. The presence of two bands of 593 and 5495 base pairs in EcoRI-NotI digested plasmid DNA confirmed the correct cloning of the Tailless PVRIG into the pcDNA 3.1 Myc/His (-) A plasmid.

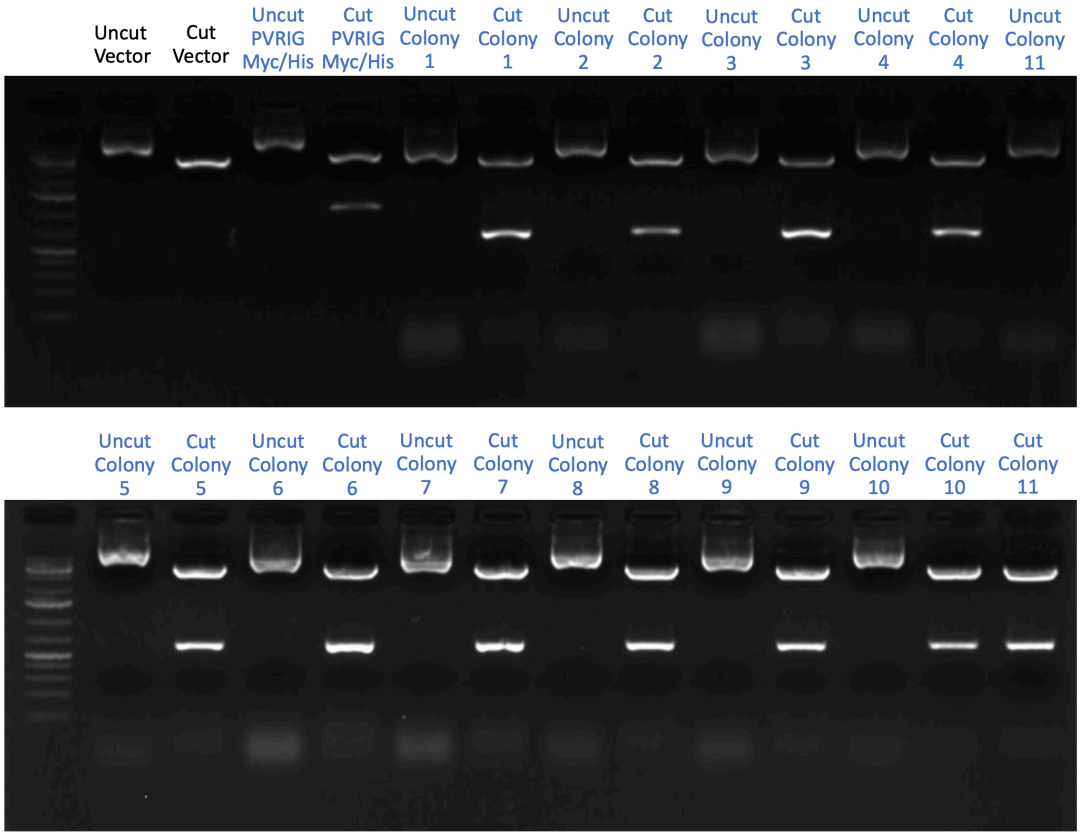

Figure 5.4. Gel image of the restriction digestion of empty vector backbone (Vector), PVRIG Myc/His cloning, and the Tailless PVRIG Myc/His cloning with EcoRI and NotI enzymes.

5.1.1.4. Cloning of a TM-Tail PVRIG into pcDNA 3.1 Myc/His (-) A Plasmid. Primers were designed to amplify PVRIG gene starting from its transmembrane (TM) domain until the end of its cytoplasmic tail, hereafter named "TM-Tail PVRIG". Constructed PVRIG Myc/His plasmid was used as a template for the PCR, and TM-Tail-PVRIG-NotI-Fwd and PVRIG-EcoRI-Rev primers were used for amplification. The PCR product was digested with NotI and EcoRI enzymes and cloned into the pcDNA 3.1 Myc/His (-) A plasmid. The same restriction enzymes were used for the diagnostic digestion of plasmid DNA from four colonies (Figure 5.5). Glycerol stock was prepared from two colonies that contained the insert. The presence of two bands of 482 and 5495 base pairs in EcoRI-NotI digested plasmid DNA confirmed the correct cloning of the TM-Tail PVRIG into the pcDNA 3.1 Myc/His(-) A plasmid.

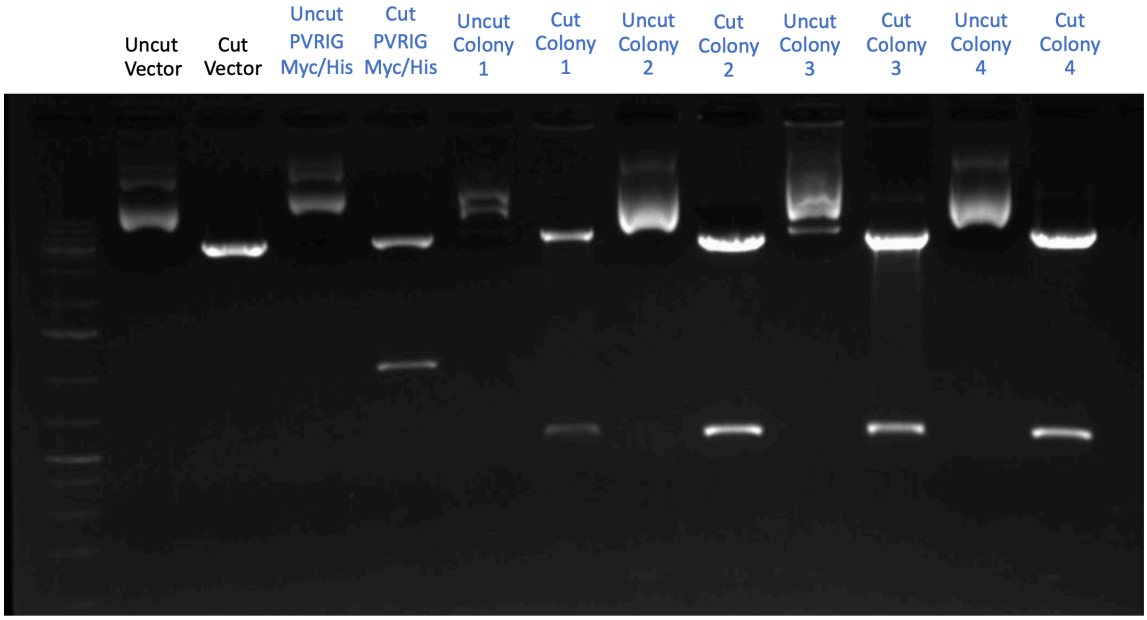

Figure 5.5. Gel image of the restriction digestion of empty vector backbone (Vector), PVRIG Myc/His cloning, and the TM-Tail PVRIG Myc/His cloning with EcoRI and NotI enzymes.

The schematic representation of all constructed Myc/His tagged PVRIG plasmids are given in Figure 5.6.

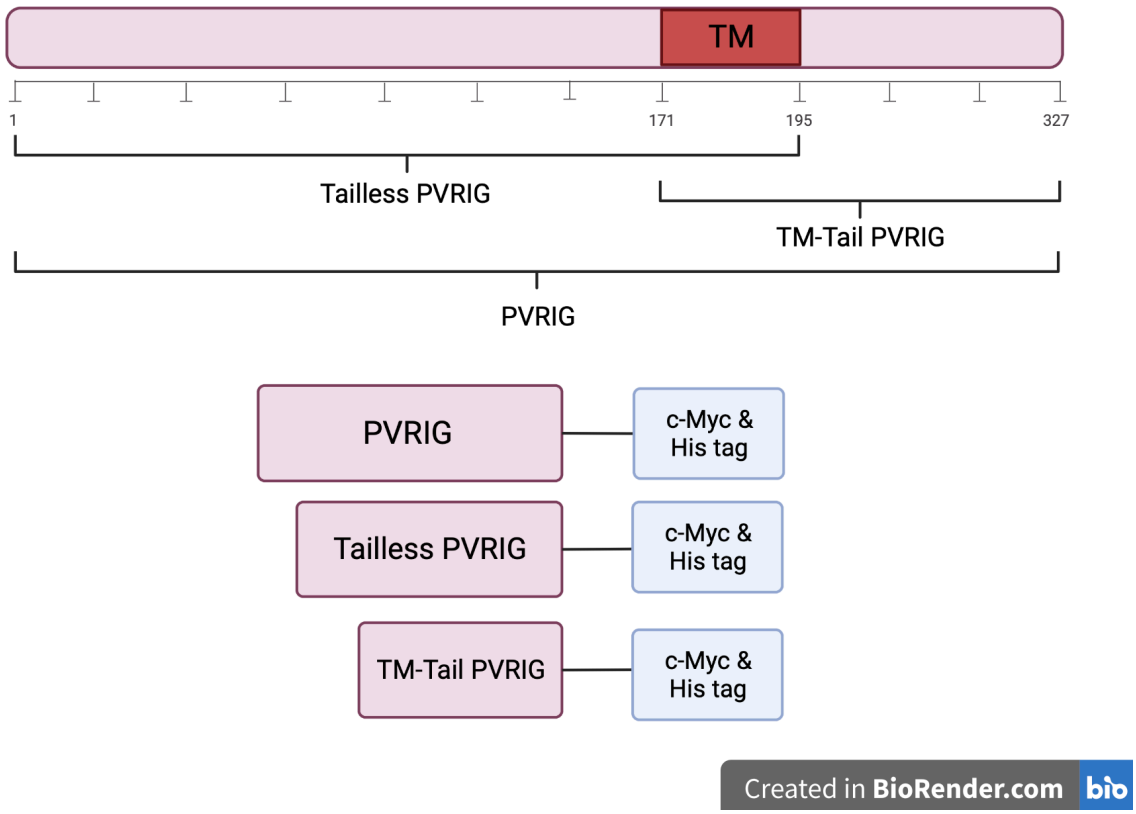

Figure 5.6. Schematic representation of the constructs for full length PVRIG and PVRIG domains fused with c-Myc/His epitope tags. Bar with numbers indicate amino acid positions.

5.1.2. Cloning of WD40 Into the p3x Flag CMV 7.1 Vector

The WD40 domain of LRBA was amplified by PCR from Jurkat T-cell line by using the WD40-HindIII-Fwd and WD40-SalI-Rev primers, and cloned into p3x Flag CMV 7.1 plasmid as described in the methods section. The PCR product was digested with HindIII and SalI enzymes and cloned into the p3x Flag CMV 7.1 plasmid. The same enzymes were used for the diagnostic digestion of plasmid DNA from 15 colonies (Figure 5.7). Glycerol stock was prepared from two colonies that contained the insert. The presence of two bands of 813 and 4672 base pairs in HindIII-SalI digested plasmid DNA confirmed the correct cloning of the WD40 domain of LRBA into the p3x Flag CMV 7.1 plasmid. pCI-neo-Flag-PH-Beach plasmid was kindly gifted from Bernice Lo et al.

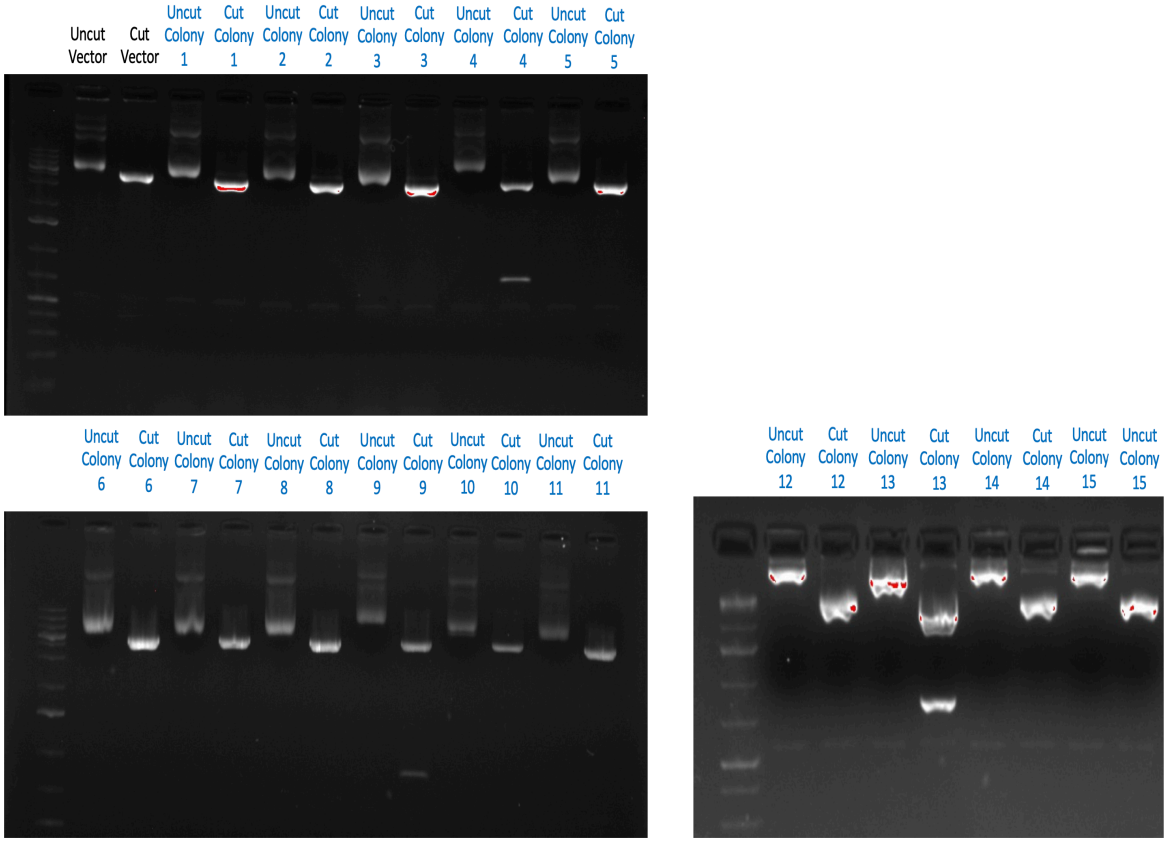

Figure 5.7. Gel image of the restriction digestion of empty vector and mini-prep colonies for the WD40-p3xFLAGCMV7.1 cloning with HindIII and SalI enzymes.

The plasmids created in this section were used to transfect HEK293T cells to identify the potential physical interaction between the PH-BEACH or WD40 domains of LRBA protein and the full length, Tailless, or TM-Tail PVRIG constructs by co-immunoprecipitation experiments in section 5.5.

5.2. Reconfirmation of the Absence of LRBA Protein in LRBA KO Jurkat T-Cells

In previous studies in our lab, LRBA KO Jurkat T-cells were established by using CRISPR/Cas9 technology, and knock-out efficiency was investigated (Zahedimaram, 2022). In this study, we reconfirmed that these cell lines indeed lost LRBA expression. LRBA protein levels were examined in pools of WT and LRBA KO Jurkat T-cells as well as three single cell clones, C7, C8, and C14 by western blotting. As expected, the Jurkat LRBA KO pool cell line has a dramatic reduction of LRBA protein expression. Similarly, LRBA protein

expression was almost undetectable in the three single cell clones shown by western blotting (Figure 5.8).

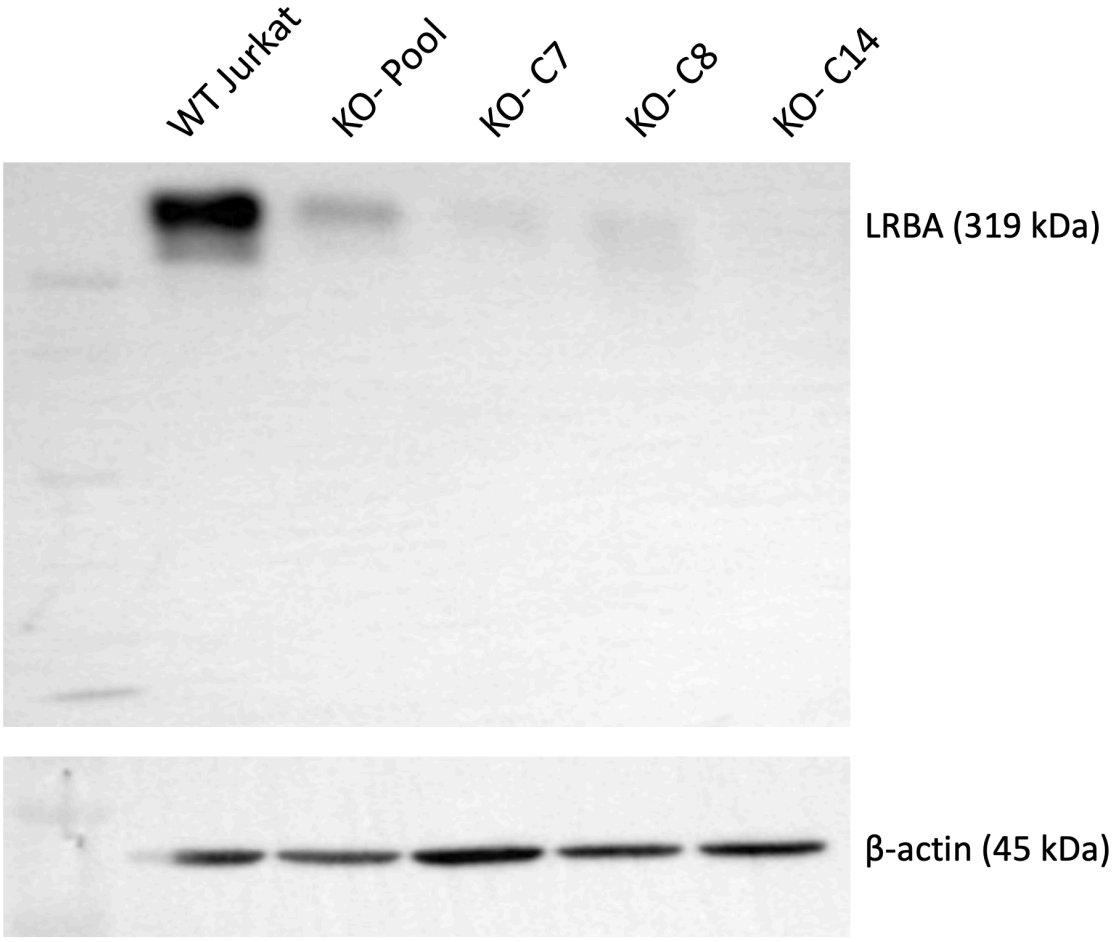

Figure 5.8. Western blotting analysis of LRBA protein levels in WT and LRBA KO Jurkat T-cells. β-actin blotting was used as loading control.

5.3. Investigation of PVRIG Protein Downregulation in LRBA KO Jurkat T-Cells

In previous studies in our lab, PVRIG protein was found to be significantly downregulated on the surface of the LRBA KO C7 Jurkat T-cell clone, compared to WT Jurkat T-cells. This study identified multiple proteins whose surface expression was altered in LRBA KO cells by surface protein biotinylation, streptavidin immunoprecipitation followed by mass spectrometry analysis (Figure 1.6) (Zahedimaram, 2022). Because the mass spectrometry experiment compared a pool of WT cells to a single cell cloned LRBA

KO clone (C7), it was possible that clone-specific expression differences were responsible for the change in PVRIG expression. It is possible that the process of single cell cloning may induce some gene and protein expression differences that are not solely dependent on the expression of LRBA. To causally link the absence of LRBA expression to alterations in PVRIG surface protein expression, we examined pools of LRBA KO cells that express a CRISPR/Cas9 construct that was not subjected to single cell cloning (hereafter named KO Pool), and two other single cell clones (C8 and C14) in addition to C7. We investigated surface and total PVRIG protein downregulation in LRBA KO Jurkat T-cells by flow cytometry (Figure 5.9 and 5.10), and western blotting experiments (Figure 5.11 and 5.12). To quantify expression differences obtained by flow cytometry, we calculated PVRIG surface protein expression using the following Percent Expression formula: (KO stained MFI- KO unstained MFI)/(WT stained MFI- WT unstained MFI)*100. PVRIG surface expression was found to be decreased in pools of LRBA KO Jurkat T-cells as well as single cells clones C7 and C8. Therefore, the expression of surface PVRIG was mildly reduced in the absence of LRBA protein in Jurkat T-cells (Table 5.1). To determine if the decrease in surface PVRIG expression levels was due to changes in steady state protein expression levels, we performed intracellular staining by fixation and permeabilization of cells followed by flow cytometry (Figure 5.10). This method allows for the staining of both surface and intracellular proteins thus is a good measure of total protein expression level in the cells. Total PVRIG expression differences were quantified with the same Percent Expression formula and the total expression of PVRIG was found to be decreased in pools of LRBA KO Jurkat T-cells as well as all three single cell clones (Table 5.1).

Table 5.1 Percent expression of PVRIG protein in LRBA KO Jurkat T-cell lines.

Percent Expression of PVRIG Protein	WT	KO Pool	C7	C8	C14
Surface	100	85,4	83,2	73,1	119,7
Intracellular	100	73,3	76,6	52,7	84,6

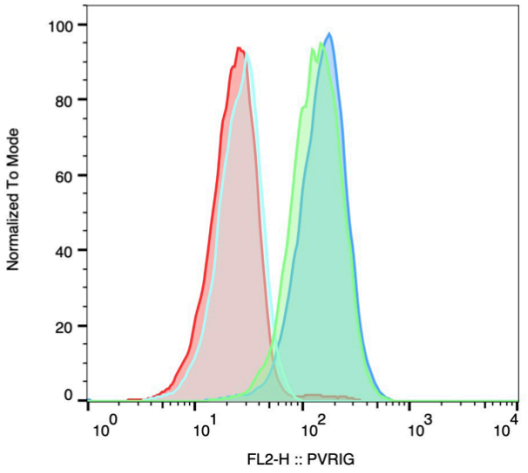

Sample Name	Subset Name	Geometric Mean : FL2-H
Pool Surface PVRIG.016	Jurkat	134
Pool Unstained.009	Jurkat	25.7
WT PVRIG Surface.004	Jurkat	150
WT Unstained 4.006	Jurkat	23.2

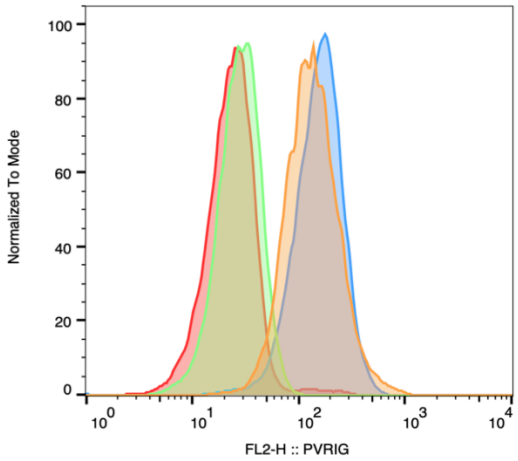

Sample Name	Subset Name	Geometric Mean : FL2-H
C7 Surface PVRIG-2.013	Jurkat	133
C7 Unstained.007	Jurkat	27.5
WT PVRIG Surface.004	Jurkat	150
WT Unstained 4.006	Jurkat	23.2

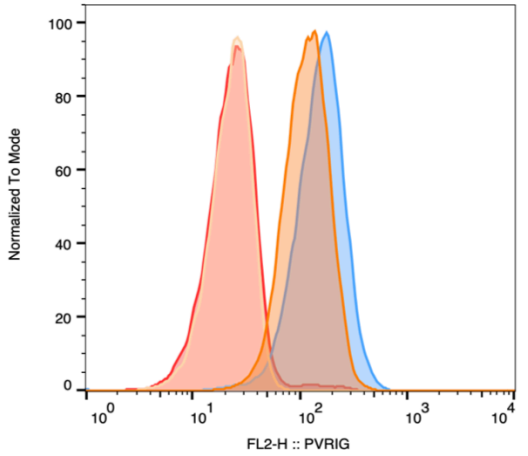

Sample Name	Subset Name	Geometric Mean : FL2-H
C8 Surface PVRIG.014	Jurkat	115
C8 Unstained.008	Jurkat	22.3
WT PVRIG Surface.004	Jurkat	150
WT Unstained 4.006	Jurkat	23.2

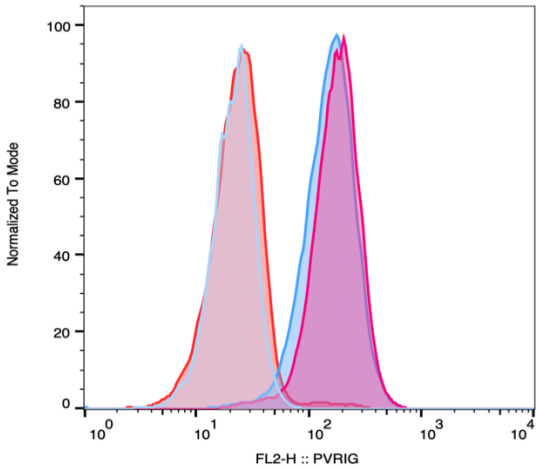

Sample Name	Subset Name	Geometric Mean : FL2-H
C14 Unstained.010	Jurkat	21.1
C14 Surface PVRIG.015	Jurkat	173
WT PVRIG Surface.004	Jurkat	150
WT Unstained 4.006	Jurkat	23.2

Figure 5.9. Cell surface PVRIG staining of WT and LRBA KO Jurkat T-cells. All cells were stained with PE conjugated anti-human CD112R (PVRIG) antibody. Unstained cells were used as controls.

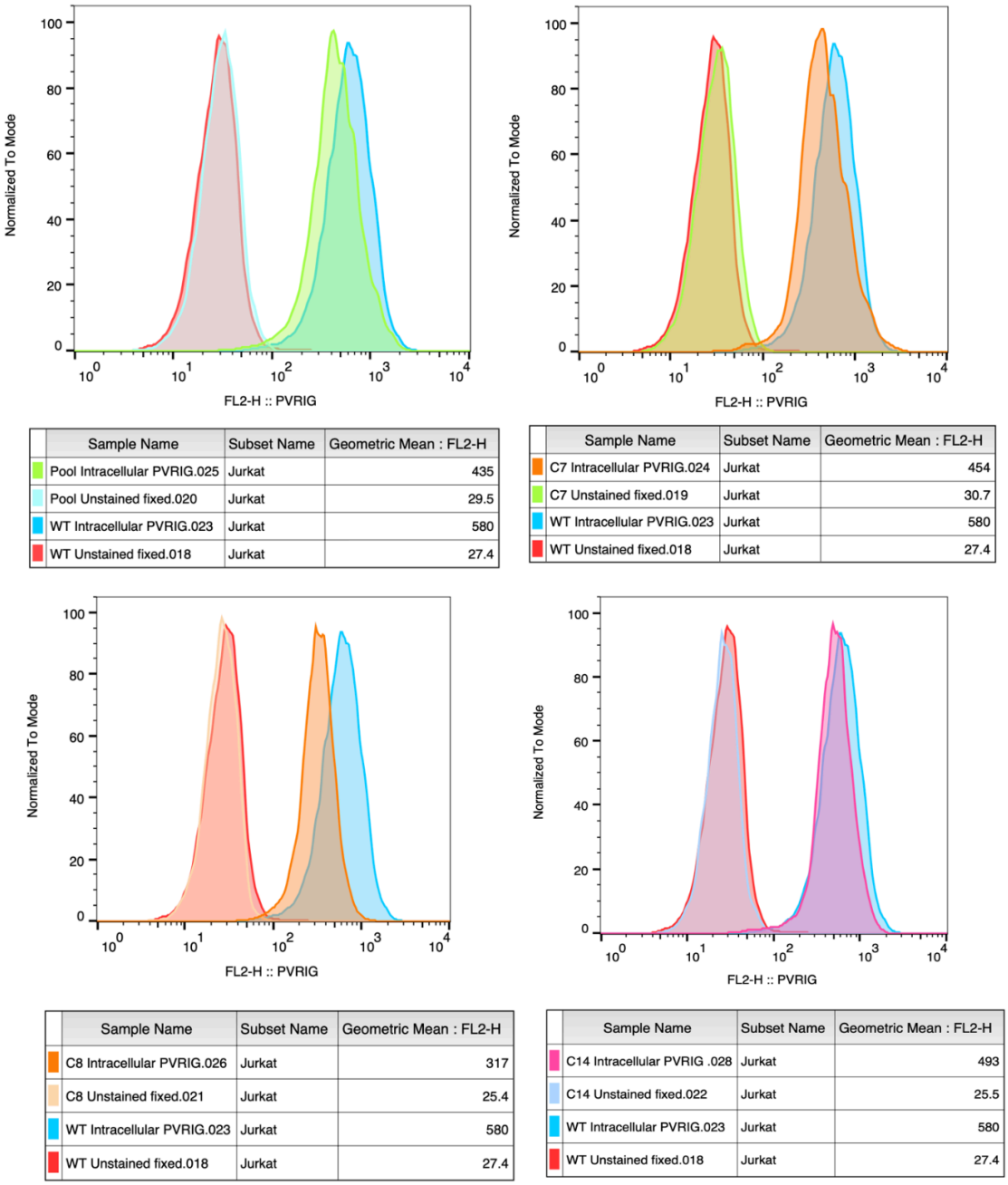

Sample Name	Subset Name	Geometric Mean : FL2-H
Pool Intracellular PVRIG.025	Jurkat	435
Pool Unstained fixed.020	Jurkat	29.5
WT Intracellular PVRIG.023	Jurkat	580
WT Unstained fixed.018	Jurkat	27.4

Sample Name	Subset Name	Geometric Mean : FL2-H
C7 Intracellular PVRIG.024	Jurkat	454
C7 Unstained fixed.019	Jurkat	30.7
WT Intracellular PVRIG.023	Jurkat	580
WT Unstained fixed.018	Jurkat	27.4

Sample Name	Subset Name	Geometric Mean : FL2-H
C8 Intracellular PVRIG.026	Jurkat	317
C8 Unstained fixed.021	Jurkat	25.4
WT Intracellular PVRIG.023	Jurkat	580
WT Unstained fixed.018	Jurkat	27.4

Sample Name	Subset Name	Geometric Mean : FL2-H
C14 Intracellular PVRIG .028	Jurkat	493
C14 Unstained fixed.022	Jurkat	25.5
WT Intracellular PVRIG.023	Jurkat	580
WT Unstained fixed.018	Jurkat	27.4

Figure 5.10. Total PVRIG staining in WT and LRBA KO Jurkat T-cells. All cells were fixed, permeabilized, and stained with PE conjugated anti-human CD112R (PVRIG) antibody. Unstained cells were used as controls.

To confirm the decrease in surface and total PVRIG protein expression levels found by flow cytometry, we performed western blotting with an antibody that detects PVRIG protein. We found that PVRIG specific bands migrated at 37 kDa as expected, but we also

observed larger bands which are likely due to post-translational modification of the PVRIG protein (Figure 5.11).

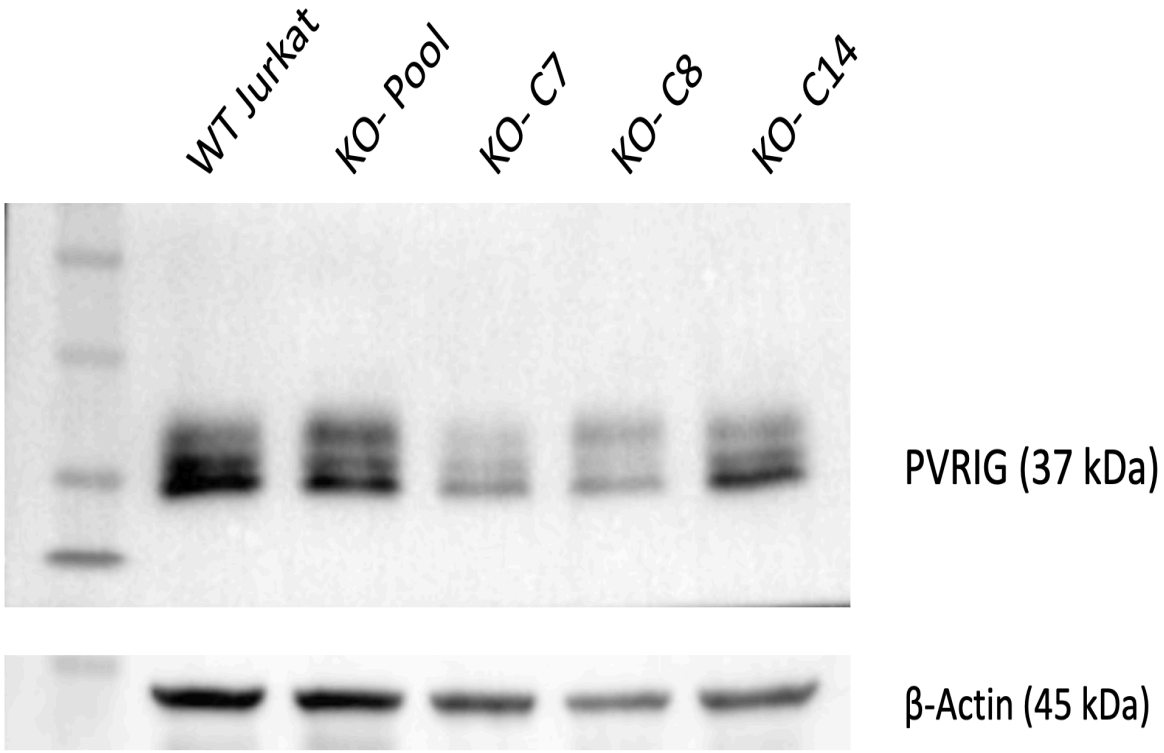

Figure 5.11. Western blot analysis of PVRIG protein levels in WT and LRBA KO Jurkat cells. β-actin blotting was used as loading control. Representative image of three independent experiments.

Quantification of the total band intensity of the PVRIG bands indicated that there was a statistically significant change in the normalized PVRIG levels in the single cell clones C7 and C8. On the other hand, the KO pool and single cell clone C14 did not have a statistically significant change in PVRIG band intensity (Figure 5.12).

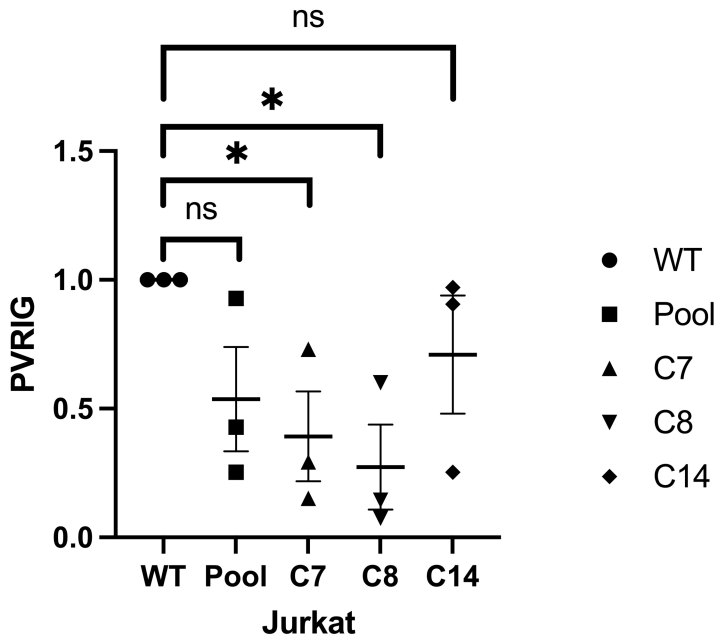

Figure 5.12. Western blotting quantification of PVRIG protein levels in WT, LRBA KO Pool and single cell clones C7, C8, and C14 Jurkat. *p<0,05 (One-way ANOVA was used for statistical data analysis).

5.4. Investigation of the Post-Translational Glycosylation Pattern of the PVRIG Protein

In order to find out the glycosylation state of the PVRIG protein, cell lysates from WT Jurkat T-cell line were treated with varying dilutions of PNGase F enzyme and PVRIG western blotting was performed (Figure 5.13). β-actin blotting was used as a loading control. When compared with untreated samples, the PVRIG band in treated samples appear to have slightly higher mobility indicating a smaller size. Therefore, we whink this experiment demonstrates that PVRIG proteins expressed in Jurkat T-cells are post-translationally modified by glycosylation. Also we note that the three bands observed in untreated samples (Figure 5.11) are absent in samples prepared for PNGase F treatment. This does not seem to be dependent on the presence of PNGase F enzyme as smears are observed in all samples with varying concentrations of PNGase F enzyme.

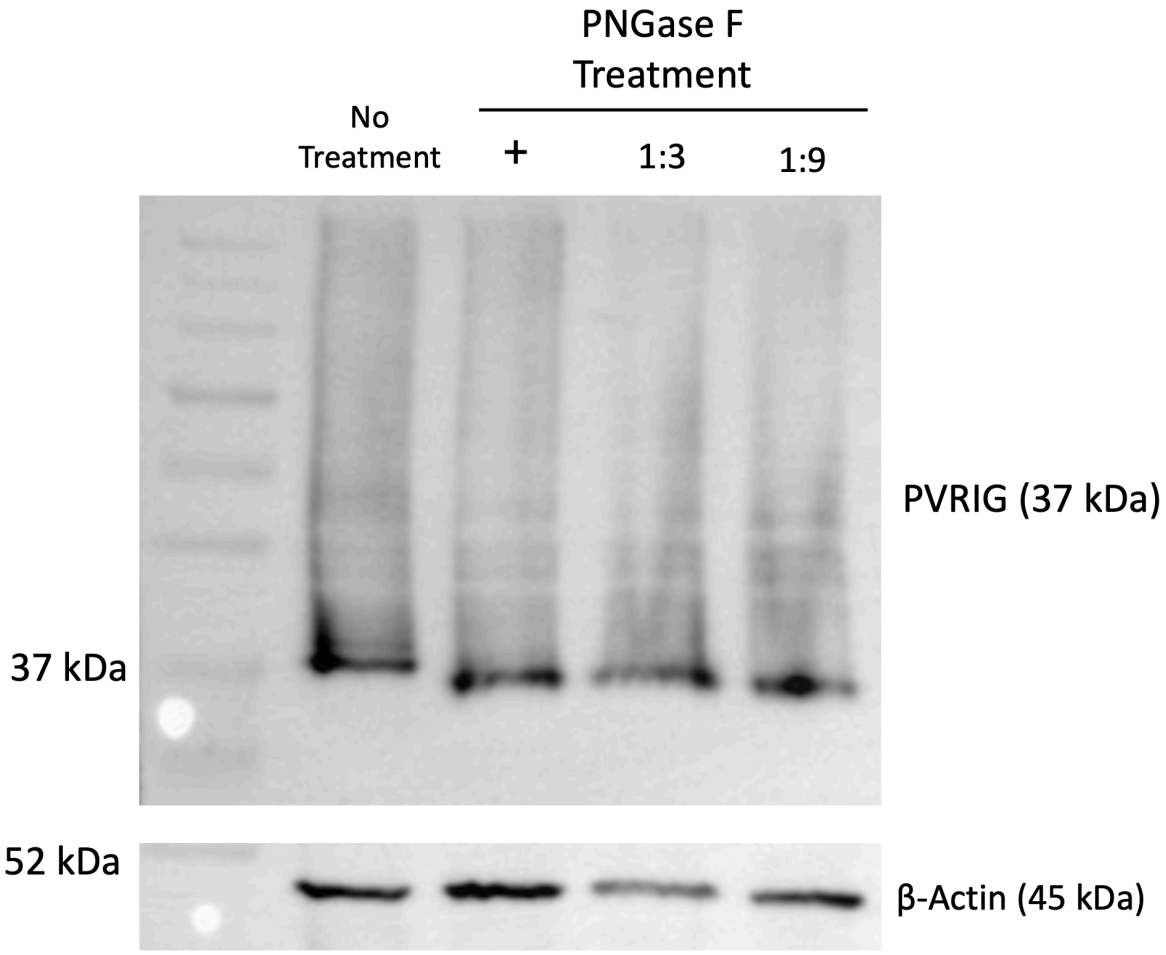

Figure 5.13. PVRIG western blotting of untreated and PNGase F treated Jurkat T-cell lysates. β-actin blotting was used as loading and treatment control.

5.5. Investigation of the Interaction Between PVRIG and LRBA

To investigate whether PVRIG and LRBA interact with each other physically, we performed a series of co-immunoprecipitation experiments with various plasmid constructs in cotransfected HEK293T cells as well as with endogenous PVRIG protein from Jurkat T-cells. Firstly, in co-transfected HEK293T cells, Flag-PH-BEACH, but not Flag-WD40, was found to be co-immunoprecipitate with PVRIG-c-Myc/His as shown by anti-c-Myc immunoprecipitation followed by anti-Flag tag blotting (Figure 5.14 and 5.15).

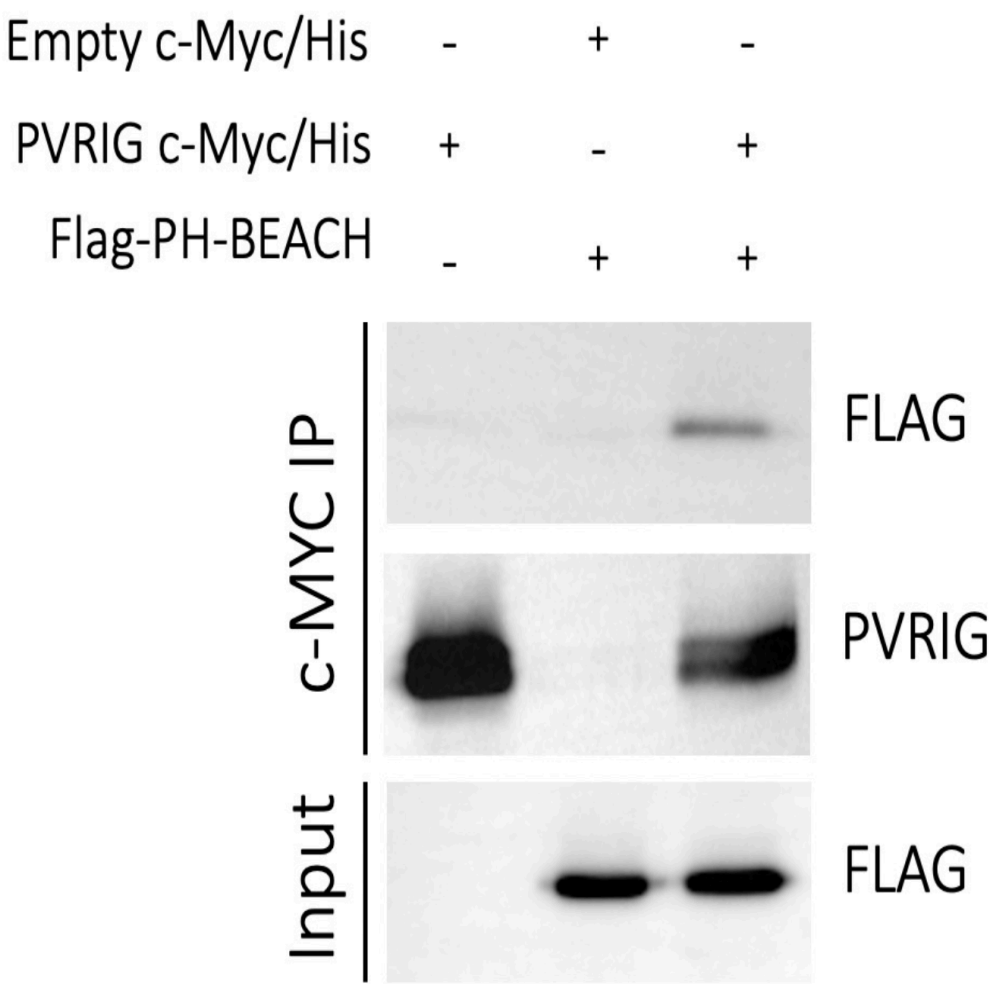

Figure 5.14. Co-IP experiment of cotransfected HEK293T cells with Empty c-Myc/His or PVRIG c-Myc/His plasmids together with Flag-PH-BEACH plasmid. IP was performed with anti-c-Myc beads. Western blotting was done by loading both IP and whole cell lysate (input) on a gel and blotting with anti-PVRIG and anti-FLAG.

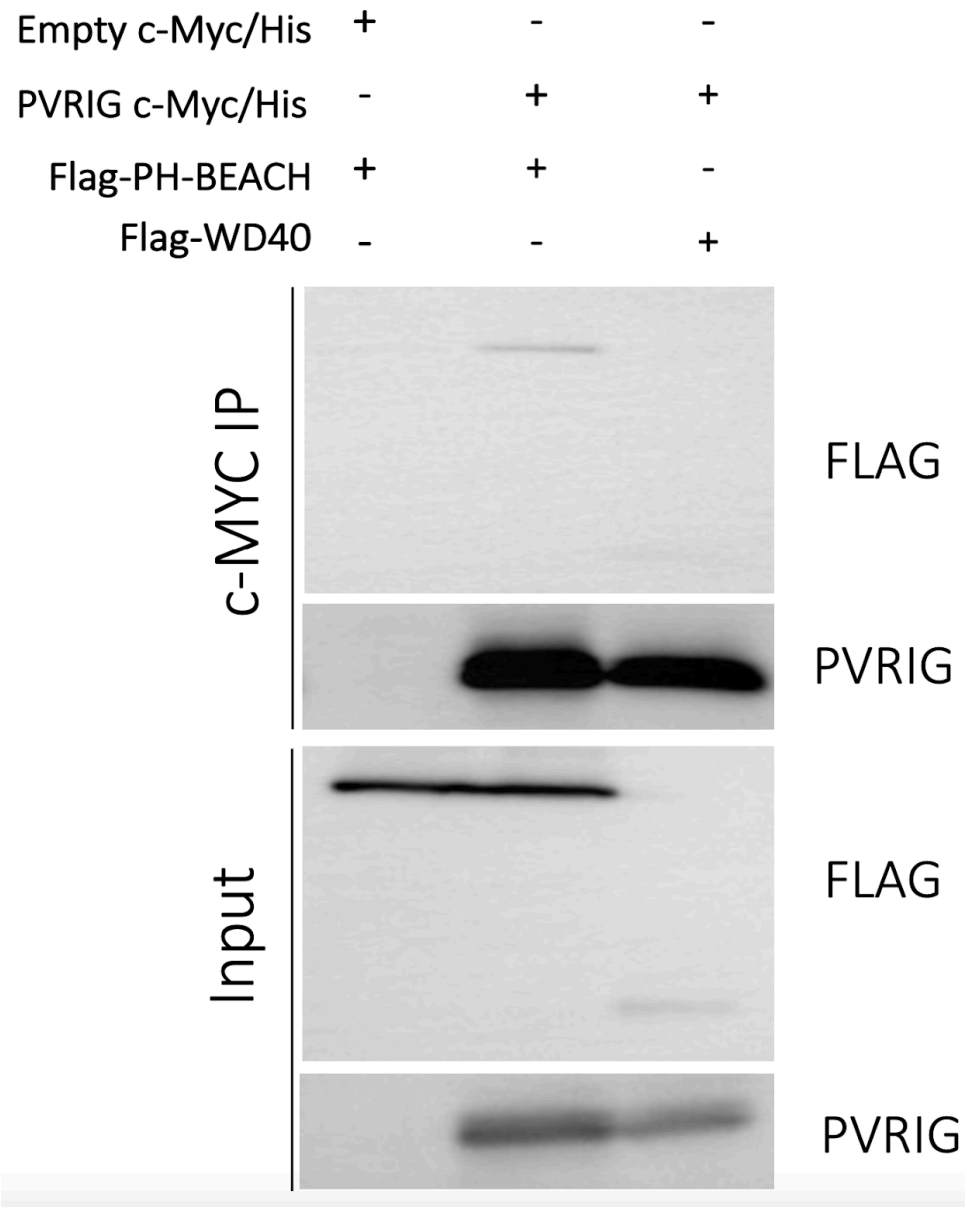

Figure 5.15. Co-IP experiment of cotransfected HEK293T cells with Empty c-Myc/His or PVRIG c-Myc/His plasmids together with Flag-PH-BEACH or Flag-WD40 plasmids. IP was performed with anti-c-Myc beads. Western blotting was done by loading both IP and whole cell lysate (input) on a gel and blotting with anti-PVRIG and anti-FLAG.

We also performed anti-c-Myc IP followed by anti-Flag blotting by using HEK293T cells that were co-transfected with Tailless or TM-Tail PVRIG constructs with Flag-PH-Beach plasmid. Similarly, Flag-PH-Beach could be co-immunoprecipitated in these conditions as well (Figure 5.16).

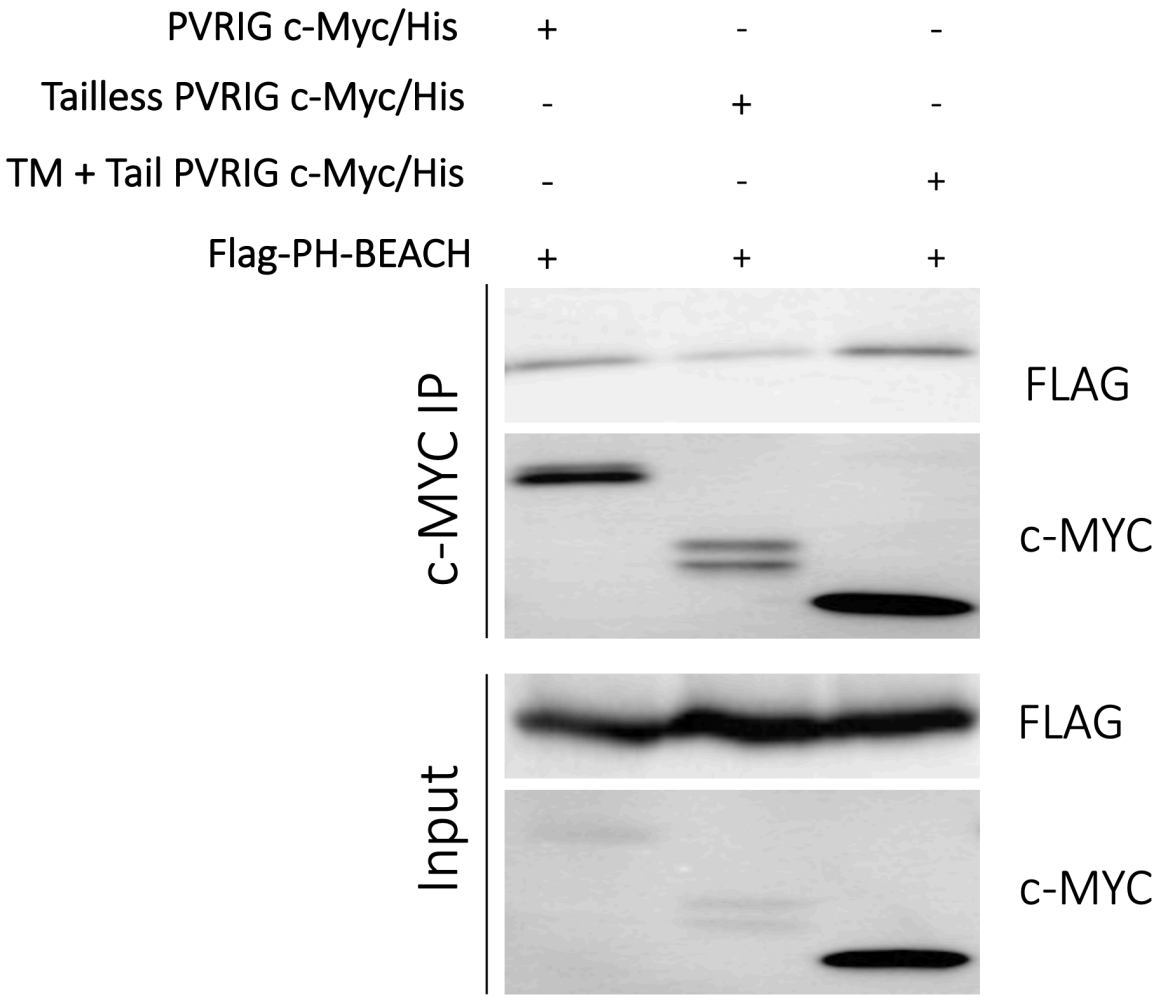

Figure 5.16. Co-IP experiment of cotransfected HEK293T cells with PVRIG c-Myc/His or Tailless PVRIG c-Myc/His or TM-Tail PVRIG c-Myc/His plasmids together with Flag-PH-BEACH plasmid. IP was performed with anti-c-Myc beads. Western blotting was done by loading both IP and whole cell lysate (input) on a gel and blotting with anti-c-Myc and anti-FLAG.

To investigate if the observed Flag band is co-immunoprecipitated due to possible nonspecific interaction between c-Myc/His tag and Flag tag, we used CD19-c-Myc/His and Flag-PH-BEACH co-transfected HEK293T cells to immunoprecipitate c-Myc tagged proteins and check for Flag tag blot (Figure 5.17). Flag-PH-BEACH could also be co-immunoprecipitated by using a CD19-c-Myc/His construct.

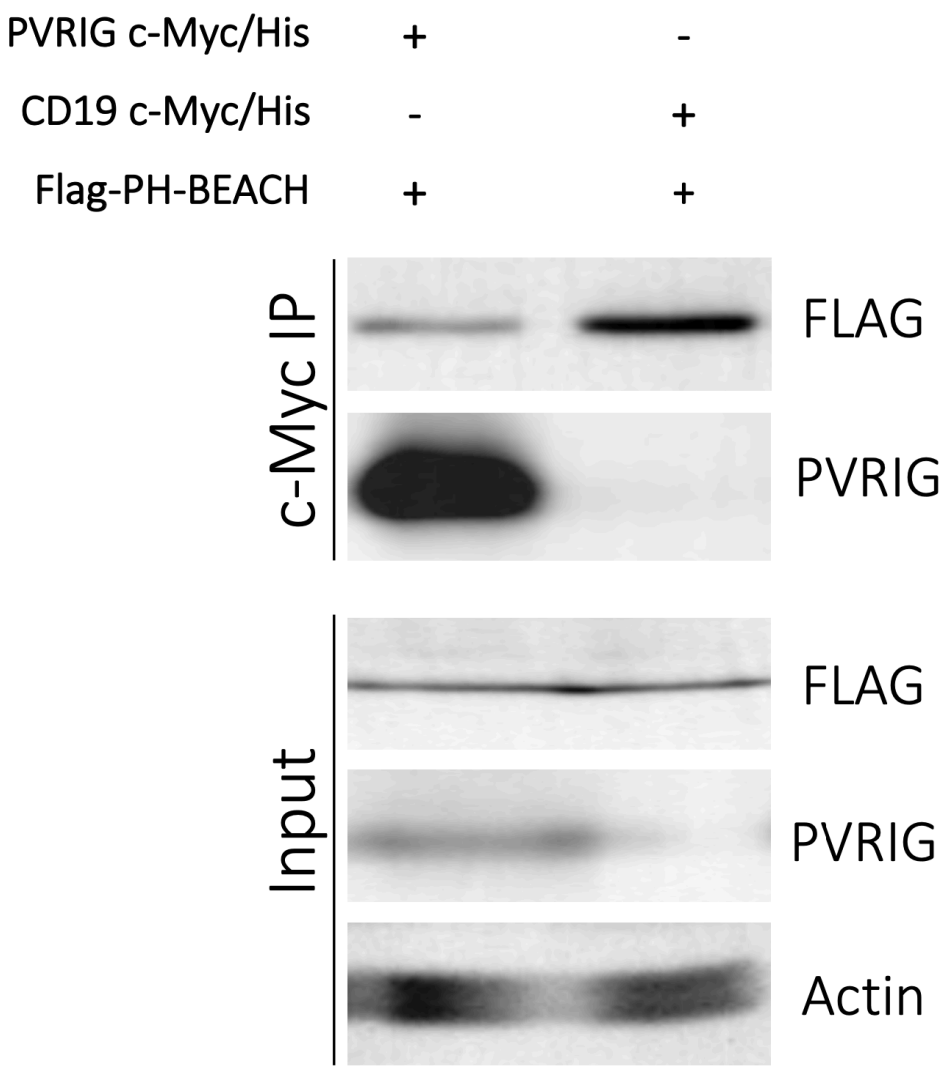

Figure 5.17. Co-IP experiment of cotransfected HEK293T cells with PVRIG c-Myc/His or CD19 c-Myc/His plasmids together with Flag-PH-BEACH plasmid. IP was performed with anti-c-Myc beads. Western blotting was done by loading both IP and whole cell lysate (input) on a gel and blotting with anti-Flag, anti-PVRIG, and anti-Actin.

Experiment on Figure 5.17 was repeated with increasing washing steps during co-immunoprecipitation from three to eight times to investigate the Flag-PH-BEACH co-immunopecipitation with PVRIG-c-Myc/His and CD19-c-Myc/His. Flag-PH-BEACH could still be co-immunoprecipitated upon increased wash steps with both PVRIG-c-Myc/His and CD19-c-Myc/His (Figure 5.18).

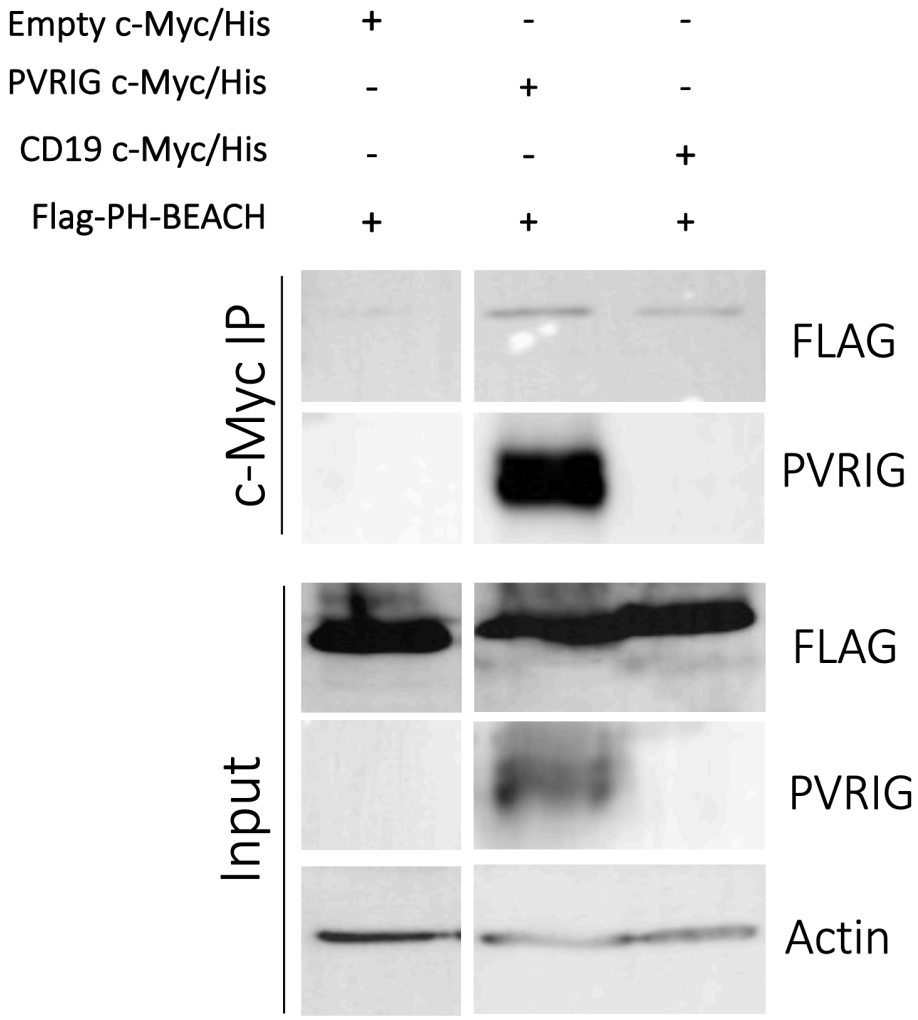

Figure 5.18. Co-IP experiment of cotransfected HEK293T cells with Empty-c-Myc/His, PVRIG c-Myc/His or CD19 c-Myc/His plasmids together with Flag-PH-BEACH plasmid. IP was performed with anti-c-Myc beads with increased wash steps. Western blotting was done by loading both IP and whole cell lysate (input) on a gel and blotting with anti-Flag, anti-PVRIG, and anti-Actin.

To further check for co-IP specificity, non-tagged PVRIG and Flag-PH-BEACH expressing cotransfected HEK293T cells were used to pull-down PVRIG protein and check for Flag tag co-immunoprecipitation (Figure 5.19).

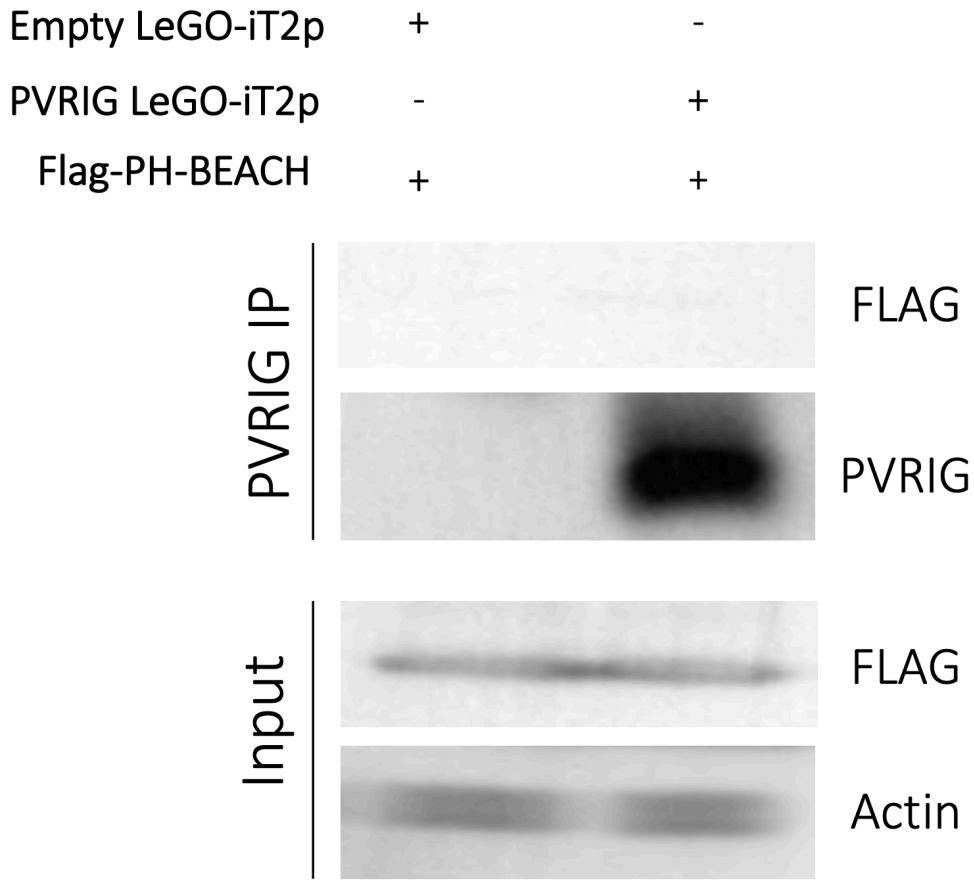

Figure 5.19. Co-IP experiment of cotransfected HEK293T cells with Empty pLeGO-iT2p or PVRIG-pLeGO-iT2p plasmids together with Flag-PH-BEACH plasmid. IP was performed with Protein A beads conjugated with anti-hPVRIG antibody. Western blotting was performed by loading both IP and whole cell lysate (input) on a gel and blotting with anti-Flag, anti-PVRIG, and anti-Actin antibodies.

We also wanted to investigate the interaction between endogenous PVRIG and LRBA proteins by using WT Jurkat T-cells. To this end, we pulled-down PVRIG protein and performed LRBA western blotting. However, since there was no LRBA band in the co-IP lane, we couldn't detect the endogenous interaction of PVRIG and LRBA proteins in WT Jurkat T-cells by co-immunoprecipitation (Figure 5.20).

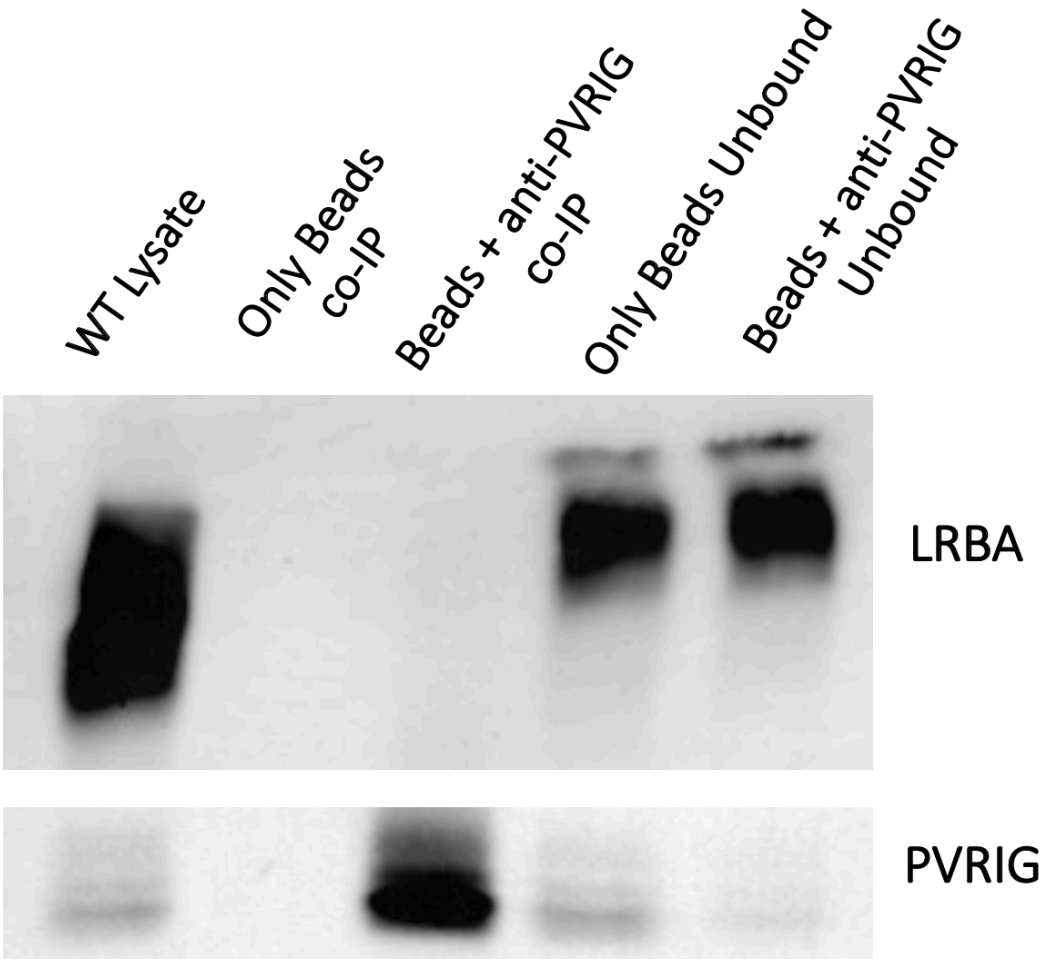

Figure 5.20. Co-IP experiment of WT Jurkat cells. IP was performed with Protein A beads conjugated with anti-hPVRIG antibody. Western blotting was done by loading both IP and whole cell lysate samples on a gel and blotting with anti-PVRIG and anti-LRBA.

5.6. Investigation of CD112 Levels in LRBA KO Jurkat Cells

In previous work in our lab, CD112, the ligand for PVRIG, was found to be significantly upregulated on the LRBA KO C7 Jurkat T-cell surface when compared to WT Jurkat T-cells in the same surface protein biotinylation and mass spectrometry experiment that identified the downregulation of PVRIG (Figure 1.6). It was not clear if the downregulation of one receptor and the upregulation of its ligand was causally related. To further investigate this result, we checked the CD112 protein upregulation in LRBA KO Jurkat T-cell surface by using flow cytometry (Figure 5.21). In accordance with the mass

spectrometry results, CD112 was found to be higher in the C7 Jurkat T-cell clone surface when compared to WT Jurkat T-cell. We found that this difference was not evident for the pool of LRBA KO Jurkat T-cells or two other single cell clones (C8 and C14). These findings indicate that the higher expression of CD112 on the C7 Jurkat T-cell clone was likely due to an epigenetic or mutational change in gene expression during the single cell selection process that this clone went through. Moreover, because the other two LRBA KO clones expressed normal levels of CD112 while they have decreased PVRIG levels indicates that the change in CD112 expression on the C7 Jurkat T-cell clone was independent of PVRIG and LRBA expression levels.

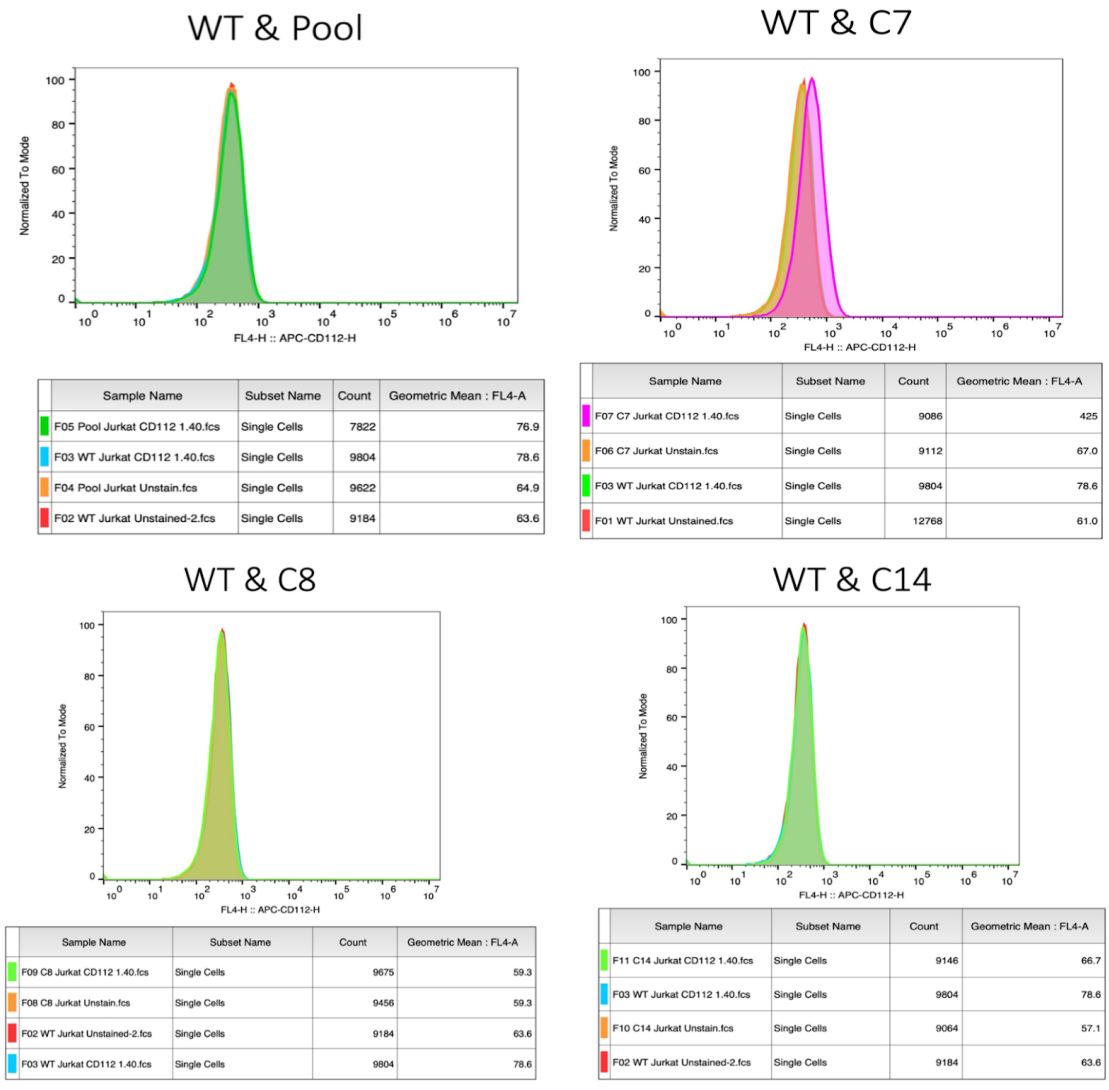

Sample Name	Subset Name	Count	Geometric Mean : FL4-A
F05 Pool Jurkat CD112 1.40.fcs	Single Cells	7822	76.9
F03 WT Jurkat CD112 1.40.fcs	Single Cells	9804	78.6
F04 Pool Jurkat Unstain.fcs	Single Cells	9622	64.9
F02 WT Jurkat Unstained-2.fcs	Single Cells	9184	63.6

Sample Name	Subset Name	Count	Geometric Mean : FL4-A
F07 C7 Jurkat CD112 1.40.fcs	Single Cells	9086	425
F06 C7 Jurkat Unstain.fcs	Single Cells	9112	67.0
F03 WT Jurkat CD112 1.40.fcs	Single Cells	9804	78.6
F01 WT Jurkat Unstained.fcs	Single Cells	12768	61.0

Sample Name	Subset Name	Count	Geometric Mean : FL4-A
F09 C8 Jurkat CD112 1.40.fcs	Single Cells	9675	59.3
F08 C8 Jurkat Unstain.fcs	Single Cells	9456	59.3
F02 WT Jurkat Unstained-2.fcs	Single Cells	9184	63.6
F03 WT Jurkat CD112 1.40.fcs	Single Cells	9804	78.6

Sample Name	Subset Name	Count	Geometric Mean : FL4-A
F11 C14 Jurkat CD112 1.40.fcs	Single Cells	9146	66.7
F03 WT Jurkat CD112 1.40.fcs	Single Cells	9804	78.6
F10 C14 Jurkat Unstain.fcs	Single Cells	9064	57.1
F02 WT Jurkat Unstained-2.fcs	Single Cells	9184	63.6

Figure 5.21. Cell surface CD112 staining of WT and LRBA KO Jurkat cells. All cells were stained with an APC anti-human CD112 antibody. Unstained cells were used as controls.

5.7. RNA-Seq Data Analysis of WT and LRBA KO Jurkat T-Cells

To investigate the changes in the transcriptional profile of Jurkat T-cells upon LRBA protein loss, we used purified whole cell RNA from WT and LRBA KO Jurkat T-cells for RNA-Seq analysis. The original LRBA targeting construct that generated the cells analyzed by surface mass spectrometry was a lentiviral construct that expressed the CRISPR/Cas9 which targeted the endogenous LRBA gene. Because lentiviral delivery of CRISPR/Cas9 enzymes integrates these elements into the genome which continuously expressed, we wanted to take another approach by transiently expressing the CRISPR/Cas9 enzymes targeting the LRBA gene. The CRISPR/Cas9 plasmid had a puromycin resistance gene, hence the puromycin antibiotic was used to select the KO cells, and cells that were not selected with puromycin were used as a wild-type control in the RNA-Seq analysis. Sample preparation and KO confirmation was previously done in our lab. These experiments confirmed by flow cytometry and western blotting that LRBA expression was downregulated in Jurkat T-cells selected from a transient CRISPR/Cas9 expression and that unselected cells retained LRBA expression (Zahedimaram, 2022). For this thesis, we have used the raw RNA-Seq .fastq files and .bam files that were aligned to reference human genome (GRCh38/hg38). Firstly, to see the variance of the WT and LRBA KO samples, hierarchical heatmap analysis and principal component analysis (PCA) was used (Figure 5.22a and b). Then, differential gene expression (DEG) was identified in WT and LRBA KO samples (Figure 5.23a), and gene ontology enrichment analysis was performed for identified DEGs (Figure 5.23b). The purpose of DEG enrichment analysis was to identify the altered molecular functions, biological processes, and protein classes in LRBA deficient Jurkat T-cells. By understanding these altered pathways, we may interpret the observed experimental results in this cell line more reasonably and comprehensively. We found out that molecular functions like transcriptional regulator activity and molecular transducer activity, biological processes like immune system process and signaling, and protein classes like membrane traffic protein, scaffold/adaptor protein, and intercellular signal molecule were affected in LRBA KO Jurkat T-cells. However, our enrichment results were not statistically significant, thus the enriched pathways may not be directly related with the absence of LRBA protein, pointing out a requirement for the experimental replication of RNA-Seq by using our WT and LRBA KO Jurkat T-cells as a part of future work.

(a)

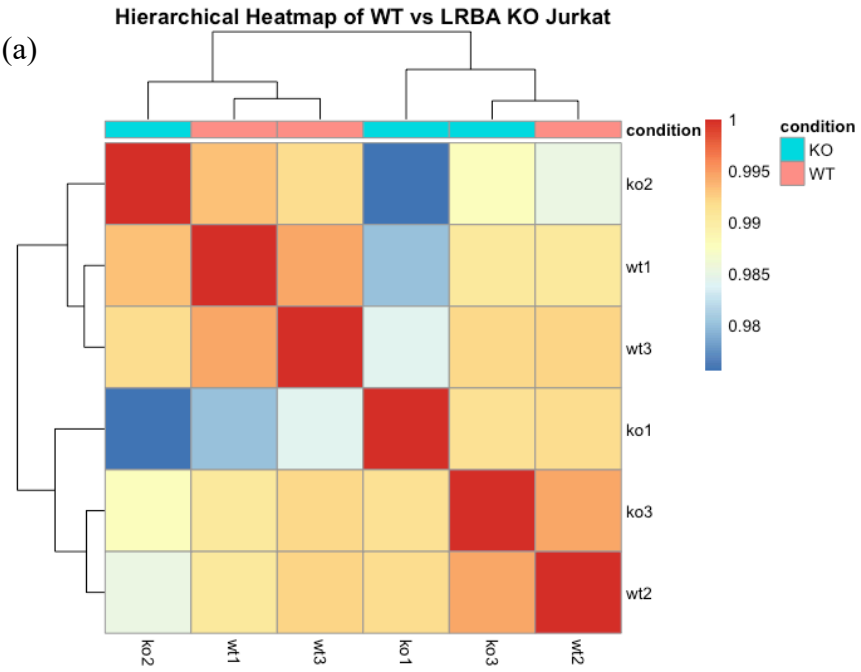

(b)

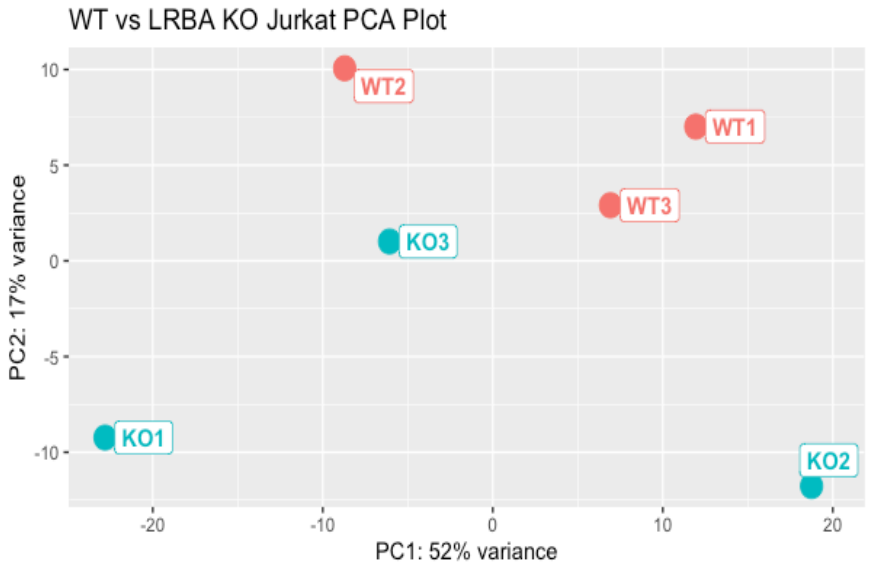

Figure 5.22. RNA-Seq sample clustering, (a) Hierarchical heatmap and (b) Principal Component Analysis (PCA) of WT and LRBA KO Jurkat samples.

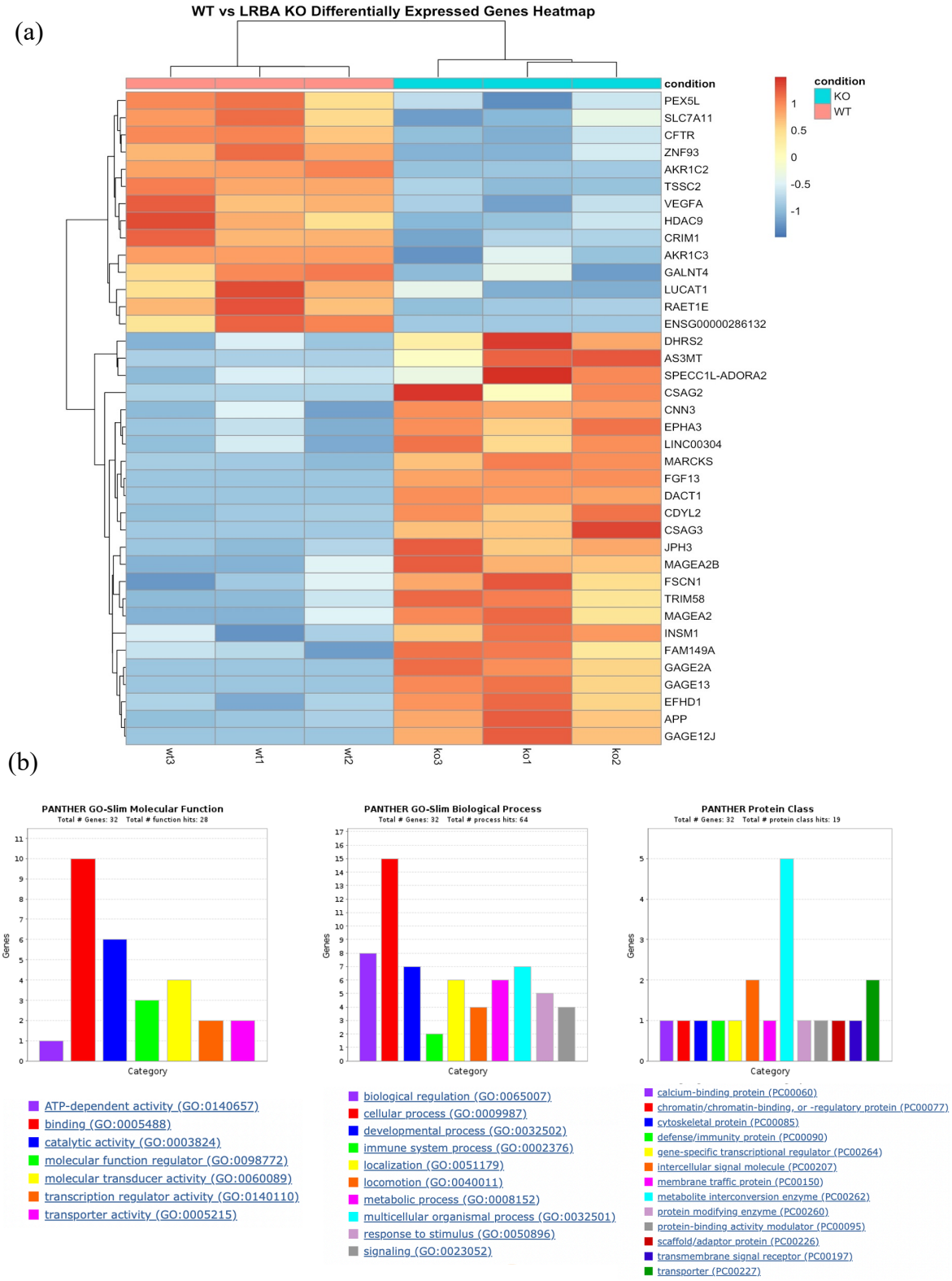

Figure 5.23. Differential Gene Expression (DEG) analysis of WT and LRBA KO Jurkat T-cells, (a) Heatmap of DEGs, (b) Enrichment analysis of DEGs for molecular function, biological process, and protein class.

6. DISCUSSION

LRBA deficiency leads to various immune deficiency outcomes similar to CTLA-4 insufficiency (Hou et al., 2017). In the absence of LRBA, T-cells have a dramatic decrease in total CTLA-4 protein compared to healthy controls. Treatment with the CTLA-4-Ig fusion drug shows great improvement in LRBA-deficient patients (Lo et al., 2015), which inspired researchers to investigate the molecular mechanisms underlying the association between LRBA and CTLA-4. LRBA acts as a critical regulator of CTLA-4 surface trafficking, thus maintaining a regulated immune response by controlling CTLA-4 post-translational expression (Lo et al., 2015). CTLA-4, an essential T-cell co-inhibitory receptor, plays a role in preventing excessive T-cell signaling and autoimmunity. It exerts its inhibitory role by binding to its ligands CD80/CD86 on APCs and mediating inhibitory signaling. In addition, CTLA-4 reduces the availability of ligands for the co-stimulatory receptor CD28 through a cell-extrinsic mechanism, as both receptors share the same ligands (Rudd et al., 2009; Qureshi et al., 2011).

LRBA belongs to the Beach Domain-Containing Proteins (BDCPs) family, which consists of nine human protein members. Most BDCPs are large proteins with a molecular mass exceeding 300 kDa, and they are thought to act as scaffolding proteins owing to their large size and their involvement in various cellular mechanisms (Cullinane et al., 2013). The BEACH domain is well-conserved among human BDCPs and it is linked to vesicle trafficking and membrane dynamics (Gebauer et al., 2004). Indeed, LRBA has been shown to interact with CTLA-4 through its PH-BEACH domain, which is alone sufficient for CTLA-4 binding, as demonstrated by co-IP experiments. In addition to the PH-BEACH domain, the ConA-like domain of LRBA can also bind to CTLA-4. On the other hand, the Y201VKM motif found on the CTLA-4 tail is essential to mediate the LRBA-CTLA-4 interaction. Mutation of the Y201V residue in CTLA-4 tail disrupts LRBA binding, highlighting the specific requirement of the Y201VKM motif for LRBA interaction (Lo et al., 2015).

The Y201VKM motif of CTLA-4 is an ITIM motif, where phosphatases like SHP-2 and PP2A can bind to phosphorylated Y201VKM and negatively regulate TCR-mediated

signaling (Chuang et al., 1999; Chuang et al., 2000). This motif also serves as a binding site for clathrin adaptor proteins AP-1 and AP-2 (Schneider et al., 1999). Nonphosphorylated Y201VKM motif is required for AP-2 binding and internalization of CTLA-4 from the T-cell surface by endocytosis (Shiratori et al., 1997). Binding of AP-1 to the same motif, on the other hand, directs intracellular CTLA-4 to lysosomal compartments for degradation (Schneider et al., 1999). Knockdown of AP-1, but not AP-2 or AP-3, partially rescues CTLA-4 loss in LRBA knockdown cells (Lo et al., 2015), suggesting that LRBA prevents CTLA-4's lysosomal degradation by competing with AP-1 for binding to the Y201VKM motif. Through these complex mechanisms, CTLA-4 surface expression and intracellular localization are tightly regulated. Despite the increase in CTLA-4 levels and surface expression upon T-cell activation, it is dynamically internalized from the cell surface by endocytosis and recycled back to the cell surface mediated by LRBA binding.

Considering LRBA's large size and intracellular localization, it is likely to have other binding partners apart from CTLA-4. However, it is currently unknown whether LRBA regulates any other co-signaling receptor's post-translational expression and intracellular localization in T-cells. To address this question, LRBA KO Jurkat T-cell models were established by Dr. Zahedimaram (2022) in our lab. She also identified proteins that have altered surface expression upon LRBA loss by using surface protein biotinylation, streptavidin immunoprecipitation, and mass spectrometry analysis. Among the potential LRBA targets, a recently identified T-cell co-inhibitory receptor PVRIG was found to be significantly reduced on the surface of LRBA KO single cell clone C7 Jurkat (Zahedimaram, 2022), which was the most immunologically relevant finding for us.

In this thesis, our aim was to investigate whether LRBA regulates PVRIG in a similar manner to CTLA-4. PVRIG acts as a co-inhibitory receptor in T and NK cells, and contains an ITIM-like motif on its tail, where LRBA binding may be possible. The molecular mechanisms for PVRIG intracellular trafficking and surface expression regulation have not been fully examined up to date. It is currently not known whether PVRIG is internalized from the cell surface by endocytosis and if it has a recycling mechanism. However, studies have shown that PVRIG, but not TIGIT, undergoes rapid internalization from the surface of activated CD8+ T-cells, which draws attention for the presence of regulatory mechanisms similar to CTLA-4 (Whelan et al., 2019). Based on the resemblance between PVRIG and

CTLA-4, we hypothesized that LRBA may be directly binding to the ITIM-like motif of PVRIG and regulates its surface expression in CD4+ T-cells, which could enlighten the downregulated surface levels of PVRIG in LRBA KO Jurkat T-cells.

To begin, we generated various PVRIG constructs, either alone or fused with c-Myc/His epitope tags, through molecular cloning for use in co-IP experiments. These included full length PVRIG, Tailless PVRIG, and TM-Tail PVRIG (Figures 5.1-5.6). In addition, we constructed a Flag tagged WD40 domain of LRBA (Figure 5.7). The Flag-tagged PH-BEACH construct was kindly gifted from Bernice Lo et al.

We wanted to confirm the absence of LRBA protein in LRBA KO Jurkat T-cells for using them in subsequent experiments, which were established by Dr. Zahedimaram (2022). As expected, the KO pool showed a dramatic reduction in LRBA protein compared to WT cells, while it was almost completely absent in the three different KO single cells clones C7, C8, and C14 (Figure 5.8). Next, we investigated PVRIG protein levels using flow cytometry and western blotting techniques to experimentally validate the downregulation of PVRIG in LRBA KO cells observed in the mass spectrometry data analysis (Zahedimaram, 2022). We aimed to determine whether the downregulation of PVRIG could be observed in both the KO pool and other KO single cell clones. In addition, since the surface protein biotinylation followed by mass spectrometry approach only captured surface alterations, we wanted to investigate if alteration in PVRIG expression was only confined to cell surface. PVRIG was found to be decreased on the cell surface of KO pool, and single cell clones C7 and C8, but not on C14, compared to WT (Figure 5.9). Total PVRIG staining confirmed the downregulation of PVRIG in all LRBA KO Jurkat T-cells compared to WT cells, indicating that PVRIG downregulation was not limited to cell surface (Figure 5.10). We also performed PVRIG western blotting (Figure 5.11) and analyzed the statistical significance (Figure 5.12) by using one-way ANOVA test with a significance threshold of $p<0,05$. The downregulation of PVRIG in C7 and C8 was found to be significant whereas it was not significant in KO pool and C14.

To investigate the potential physical interaction between PVRIG and LRBA proteins, we used our constructed plasmids for the co-IP experiments by cotransfecting HEK293T cells. Initially, we found out that Flag-PH-BEACH could be co-immunoprecipitated with

PVRIG-c-Myc/His by using anti-c-Myc beads (Figure 5.14). The same co-IP strategy was utilized with the Flag-WD40 construct, however it did not co-immunoprecipitate with PVRIG-c-Myc/His, unlike Flag-PH-BEACH (Figure 5.15). Still, it is worth noting that the lower expression of Flag-WD40 might have affected the efficiency of co-IP.

Based on the initial findings suggesting an interaction between PVRIG and the PH-BEACH domain of LRBA, we aimed to determine if PH-BEACH binds to the ITIM motif of PVRIG's tail, similar to its binding with CTLA-4. To this end, we used Tailless PVRIG and TM-Tail PVRIG plasmids in the same co-IP strategy. Surprisingly, FLAG-PH-BEACH could be co-immunoprecipitated with both Tailless PVRIG and TM-Tail PVRIG (Figure 5.16). These results made us doubtful regarding the specificity of the PH-BEACH binding with PVRIG. It was also possible to observe an unspecific binding of c-Myc/His and Flag epitope tags. To check this possibility, we used CD19-c-Myc/His construct as a negative control in subsequent co-IP experiments. In contrast to our expectations, FLAG-PH-BEACH could be co-immunoprecipitated with CD19-c-Myc/His (Figure 5.17). The same experiment was repeated with increased wash steps with the hope of getting rid of any unspecific co-IP bands. However, Flag-PH-BEACH still co-immunoprecipitated with both PVRIG and CD19 constructs even with increased wash steps (Figure 5.18). To further check for the specificity, we immunoprecipitated non-tagged PVRIG protein using anti-hPVRIG-conjugated Protein A beads and checked for Flag blot from cotransfected HEK293T cells (Figure 5.19). We were unable to observe a Flag blot co-immunoprecipitated with PVRIG protein. Subsequently, we performed LRBA blotting after immunoprecipitating endogenous PVRIG protein from WT Jurkat T-cells, but endogenous LRBA could not be co-immunoprecipitated with endogenous PVRIG (Figure 5.20).

Based on the various co-IP experiments, we couldn't reach to a conclusive idea regarding the physical interaction between LRBA and PVRIG. It is possible that LRBA-mediated alterations in PVRIG may not occur through a direct physical interaction. Another possibility is that we were unable to capture PVRIG and LRBA interaction by co-IP experiments because of their weak, transient, or context-dependent nature of interaction. Further investigation on PVRIG and LRBA interaction using alternative techniques such as proximity-based assays or co-localization studies should be employed. Furthermore, we demonstrated that PVRIG protein can undergo glycosylation (Figure 5.13), which might be

influencing its interaction with binding partners, intracellular trafficking, and overall cellular function.

Another interesting finding from the mass spectrometry analysis was the upregulation of PVRIG's ligand, CD112 (PVRL2), on the surface of LRBA KO C7 single cell clone (Figure 1.6) while PVRIG was found to be downregulated. To be able to causally link the downregulation of one receptor and the upregulation of its ligand in LRBA-dependent manner, we performed cell surface CD112 staining of WT and LRBA KO Jurkat T-cells (Figure 5.21). In line with the mass spectrometry results, CD112 was found to be increased on the surface of LRBA KO C7 cell clone, but no change was detected in other KO cell lines. This increase in CD112 may be a specific phenotype of the C7 single cell clone rather than being directly related to the absence of LRBA.

Finally, to gain better insights on the effects of LRBA loss and altered pathways in LRBA deficiency, we performed RNA-Seq data analysis on WT and LRBA KO Jurkat T-cells. Hierarchical clustering and PCA analysis showed that WT and KO samples were clustered within each other (Figure 5.22), which was not a preferential outcome for differential gene expression (DEG) analysis. DEG analysis identified 38 genes (Figure 5.23a), and PANTHER Protein Class enrichment revealed various protein classes such as scaffolding protein, membrane traffic molecule, and calcium-binding protein that were affected in LRBA KO samples (Figure 5.23b). However, no significant pathway enrichment was observed for neither molecular function, biological process, or protein class. Due to sample clustering results, it is necessary to repeat the sample preparation and RNA-sequencing to obtain more conclusive results. Moreover, it is possible that the loss of LRBA may not globally affect the transcriptional profile within the cell, which could explain the interclustering of WT and KO Jurkat samples.

Overall, in this study, we demonstrated the decreased surface and total levels of PVRIG in LRBA KO Jurkat T-cells. Although the direct physical interaction between LRBA and PVRIG could not be fully confirmed through co-immunoprecipitation experiments, further examination of this interaction using alternative techniques such as proximity-based techniques is required. We also showed that PVRIG protein can undergo glycosylation, which might be an affecting factor for its overall functionality within the cell. Future

investigations should focus on studying the surface dynamics of PVRIG, including its internalization and surface retention mechanisms. In addition, since PVRIG is also a co-inhibitory receptor for NK cells, alterations of PVRIG expression in WT and LRBA KO NK cells should be investigated. Lastly, exploring the impact of other BDCP proteins on the regulation of both CTLA-4 and PVRIG could expand the therapeutic options that can be developed for immunodeficiency disorders.

REFERENCES

Alteber, Z., M. F. Kotturi, S. Whelan, S. Ganguly, E. Weyl, D. M. Pardoll, J. G. Hunter, and E. Ophir, 2021, "Therapeutic Targeting of Checkpoint Receptors within the DNAM1 Axis", *Cancer Discovery*, Vol. 11, No. 5, pp. 1040–1051.

Artyomov, M. N., M. Lis, S. Devadas, M. M. Davis, and A. K. Chakraborty, 2010, "CD4 and CD8 Binding to MHC Molecules Primarily Acts to Enhance Lck Delivery", *Proceedings of the National Academy of Sciences of the United States of America*, Vol. 107, No. 39, pp. 16916–16921.

Bagchi, S., R. Yuan, and E. G. Engleman, 2021, "Immune Checkpoint Inhibitors for the Treatment of Cancer: Clinical Impact and Mechanisms of Response and Resistance", *Annual Review of Pathology: Mechanisms of Disease*, Vol. 16, No. 1, pp. 223–249.

Barrat, F. J., F. L. Deist, M. Benkerrou, P. Bousso, J. Feldmann, A. Fischer, and G. De Saint Basile, 1999, "Defective CTLA-4 Cycling Pathway in Chediak–Higashi Syndrome: A Possible Mechanism for Deregulation of T Lymphocyte Activation", *Proceedings of the National Academy of Sciences of the United States of America*, Vol. 96, No. 15, pp. 8645–8650.

Chen, L., and D. B. Flies, 2013, "Molecular Mechanisms of T Cell Co-stimulation and Co-inhibition", *Nature Reviews Immunology*, Vol. 13, No. 4, pp. 227–242.

Chuang, E., S. Herschorn, M. S. Robbins, J. M. Duerr, M. Alegre, J. E. Hambor, M. J. Neveu, J. A. Bluestone, and C. B. Thompson, 1999, "Regulation of Cytotoxic T Lymphocyte-Associated Molecule-4 by Src Kinases", *The Journal of Immunology*, Vol. 162, No. 3, pp. 1270–1277.

Chuang, E., T. S. Fisher, R. Morgan, M. S. Robbins, J. M. Duerr, M. G. V. Heiden, J. P. Gardner, J. E. Hambor, M. J. Neveu, and C. B. Thompson, 2000, "The CD28 and

CTLA-4 Receptors Associate with the Serine/Threonine Phosphatase PP2A", *Immunity*, Vol. 13, No. 3, pp. 313–322.

Conner, M. G., K. W. Hance, S. Yadavilli, J. F. Smothers, and J. D. Waight, 2022, "Emergence of the CD226 Axis in Cancer Immunotherapy", *Frontiers in Immunology*, Vol. 13, No. 914406, pp. 1-19.

Courtney, A. H., W. Lo, and A. Weiss, 2018, "TCR Signaling: Mechanisms of Initiation and Propagation", *Trends in Biochemical Sciences*, Vol. 43, No. 2, pp. 108–123.

Cullinane, A. R., A. A. Schäffer, and M. Huizing, 2013, "The BEACH Is Hot: A LYST of Emerging Roles for BEACH-Domain Containing Proteins in Human Disease", *Traffic*, Vol. 14, No. 7, pp. 749–766.

Delage, L., F. Carbone, Q. Riller, J. Zachayus, E. Kerbellec, A. Buzy, M. Stolzenberg, M. Luka, C. De Cevins, G. Kalouche, R. Favier, A. Michel, S. Meynier, A. Corneau, C. Evrard, N. Neveux, S. Roudières, B. P. Pérot, M. Fusaro, C. Lenoir, O. Pellé, M. Parisot, M. Bras, S. Héritier, G. Leverger, A. S. Korganow, C. Picard, S. Latour, B. Collet, A. Fischer, B. Neven, A. Magérus, M. Ménager, B. Pasquier, F. Rieux-Laucat, 2023, "NBEAL2 Deficiency in Humans Leads to Low CTLA-4 Expression in Activated Conventional T Cells", *Nature Communications*, Vol. 14, No. 3728, pp. 1-12.

Fraser, J. F., M. Rincon, K. D. McCoy, and G. L. Gros, 1999, "CTLA4 Ligation Attenuates AP-1, NFAT and NF-κB Activity in Activated T Cells", *European Journal of Immunology*, Vol. 29, No. 3, pp. 838–844.

Gámez-Díaz, L., E. C. Sigmund, V. Reiser, W. Vach, S. Jung, and B. Grimbacher, 2018, "Rapid Flow Cytometry-Based Test for the Diagnosis of Lipopolysaccharide Responsive Beige-Like Anchor (LRBA) Deficiency", *Frontiers in Immunology*, Vol. 9, No. 720, pp. 1-8.

Gebauer, D., J. Li, G. Jogl, Y. Shen, D. G. Myszka, and L. Tong, 2004, "Crystal Structure of the PH−BEACH Domains of Human LRBA/BGL", *Biochemistry*, Vol. 43, No. 47, pp. 14873–14880.

Guntermann, C., and D. R. Alexander, 2002, "CTLA-4 Suppresses Proximal TCR Signaling in Resting Human CD4+ T Cells by Inhibiting ZAP-70 Tyr319 Phosphorylation: A Potential Role for Tyrosine Phosphatases", *The Journal of Immunology*, Vol. 168, No. 9, pp. 4420–4429.

Herrero-Beaumont, G., M. Calatrava, and S. Castaneda, 2012, "Abatacept Mechanism of Action: Concordance with its Clinical Profile", *Reumatologia Clinica*, Vol. 8, No. 2, pp. 78-83.

Hou, T. Z., N. Verma, J. Wanders, A. R. Kennedy, B. Soskic, D. Janman, N. Halliday, B. Rowshanravan, A. Worth, W. Qasim, H. Baxendale, H. J. Stauss, S. L. Seneviratne, O. Neth, P Olbrich., S. Hambleton, P. D. Arkwright, S. O. Burns, L. S. K. Walker, and D. M. Sansom, 2017, "Identifying Functional Defects in Patients with Immune Dysregulation due to LRBA and CTLA-4 Mutations", *Blood*, Vol. 129, No. 11, pp. 1458–1468.

Iida, T., H. Ohno, C. Nakaseko, M. Sakuma, M. Takeda-Ezaki, H. Arase, E. Kominami, T. Fujisawa, and T. Saito, 2000, "Regulation of Cell Surface Expression of CTLA-4 by Secretion of CTLA-4-Containing Lysosomes Upon Activation of CD4+ T Cells", *Journal of Immunology*, Vol. 165, No. 9, pp. 5062–5068.

Janman, D., C. Hinze, A. R. Kennedy, N. Halliday, E. Waters, C. Williams, B. Rowshanravan, T. Z. Hou, S. Minogue, O. S. Qureshi, and D. M. Sansom, 2021, "Regulation of CTLA-4 Recycling by LRBA and Rab11", *Immunology*, Vol. 164, No. 1, pp. 106–119.

Jaramillo, C. M., and C. D. Vargas, 2018, "LRBA in the Endomembrane System", *Colombia Medica*, Vol. 49, No. 3, pp. 236–243.

Jogl, G., Y. Shen, D. Gebauer, J. Li, K. Wiegmann, H. Kashkar, M. Krönke, and L. Tong, 2002, "Crystal Structure of the BEACH Domain Reveals an Unusual Fold and Extensive Association with a Novel PH Domain", *The EMBO Journal*, Vol. 21, No. 18, pp. 4785–4795.

Kim, D., J. M. Paggi, C. H. Park, C. Bennett, and S. L. Salzberg, 2019, "Graph-based Genome Alignment and Genotyping with HISAT2 and HISAT-genotype", *Nature Biotechnology*, Vol. 37, No. 8, pp. 907–915.

Krummel, M. F., and J. P. Allison, 1995, "CD28 and CTLA-4 Have Opposing Effects on the Response of T Cells to Stimulation", *Journal of Experimental Medicine*, Vol. 182, No. 2, pp. 459–465.

Kumar, B. V., T. J. Connors, and D. L. Farber, 2018, "Human T Cell Development, Localization, and Function Throughout Life", *Immunity*, Vol. 48, No. 2, pp. 202–213.

Lafferty, K. J., and A. A. Cunningham, 1975, "A New Analysis of Allogeneic Interactions", *Australian Journal of Experimental Biology and Medical Science*, Vol. 53, No. 1, pp. 27–42.

Lemmon, M. A., 1999, "Structural Basis for High-Affinity Phosphoinositide Binding by Pleckstrin Homology Domains", *Biochemical Society Transactions*, Vol. 27, No. 4, pp. 617–624.

Lo, B., K. Zhang, W. Lu, M. J. Lenardo, Q. Zhang, C. Kanellopoulou, Y. Zhang, Z. Liu, J. M. Fritz, R. A. Marsh, A. Husami, D. Kissell, S. Nortman, V. Chaturvedi, H. Haines, L. R. Young, J. Mo, A. H. Filipovich, J. J. Bleesing, P. Mustillo, M. Stephens, C. M. Rueda, C. A. Chougnet, K. Hoebe, J. McElwee, J. D. Hughes, E. Karakoc-Aydiner, H. F. Matthews, S. Price, H. C. Su, V. K. Rao, M. J. Lenardo, M. B. Jordan, 2015, "Patients with LRBA Deficiency Show CTLA4 Loss and Immune Dysregulation Responsive to Abatacept Therapy", *Science*, Vol. 349, No. 6246, pp. 436–440.

Lo, B., J. M. Fritz, H. C. Su, G. Uzel, M. I. Jordan, and M. J. Lenardo, 2016, "CHAI and LATAIE: New Genetic Diseases of CTLA-4 Checkpoint Insufficiency", *Blood*, Vol. 128, No. 8, pp. 1037–1042.

Lopez-Herrera, G., G. Tampella, Q. Pan-Hammarström, P. Herholz, C. M. Trujillo-Vargas, K. Phadwal, A. Simon, M. Moutschen, A. Etzioni, A. Mory, I. Srugo, D. Melamed, K. Hultenby, C. Liu, M. Baronio, M. Vitali, P. Philippet, V. Dideberg, A. Aghamohammadi, N. Rezaei, V. Enright, L. Du, U. Salzer, H., Eibel, D. Pfeifer, H. Veelken, H. Stauss, V. Lougaris, A. Plebani, E. M. Gertz, A. A. Schaffer, L. Hammarström, B. Grimbacher, 2012, "Deleterious Mutations in LRBA Are Associated with a Syndrome of Immune Deficiency and Autoimmunity", *The American Journal of Human Genetics*, Vol. 90, No. 6, pp. 986–1001.

Love, M. I., W. Huber, and S. Anders, 2014, "Moderated Estimation of Fold Change and Dispersion for RNA-Seq Data with DESeq2", *Genome Biology*, Vol. 15, No. 550, pp. 1-21.

Mi, H., A. Muruganujan, X. Huang, D. Ebert, C. Mills, X. Guo, and P. D. Thomas, 2019, "Protocol Update for Large-scale Genome and Gene Function Analysis with The PANTHER Classification System (v.14.0)", *Nature Protocols*, Vol. 14, No. 3, pp. 703–721.

Murphy, K., and Weaver C., 2017, *Janeway's Immunobiology*, Ninth Edition, Garland Science, New York.

Murter, B., X. Pan, E. Ophir, Z. Alteber, M. Azulay, R. Sen, O. Levy, L. Dassa, I. Vaknin, T. Fridman-Kfir, R. Salomon, A. Ravet, A. J. Tam, D. Levin, Y. Vaknin, E. Tatirovsky, A. Machlenkin, D. M. Pardoll, and S. Ganguly, 2019, "Mouse PVRIG Has CD8+ T Cell–Specific Coinhibitory Functions and Dampens Antitumor Immunity", *Cancer Immunology Research*, Vol. 7, No. 2, pp. 244–256.

Parry, R., J. Chemnitz, K. A. Frauwirth, A. R. Lanfranco, I. Braunstein, S. V. Kobayashi, C. J. Greenbaum, C. B. Thompson, and J. J. Riley, 2005, "CTLA-4 and PD-1 Receptors

Inhibit T-Cell Activation by Distinct Mechanisms", *Molecular and Cellular Biology*, Vol. 25, No. 21, pp. 9543–9553.

Pentcheva-Hoang, T., J. G. Egen, K. Wojnoonski, J. P. Allison, 2004, "B7-1 and B7-2 Selectively Recruit CTLA-4 and CD28 to the Immunological Synapse", *Immunity*, Vol. 21, No. 3, pp. 401–413.

Qureshi, O. S., Y. Zheng, K. Nakamura, K. Attridge, C. N. Manzotti, E. Schmidt, J. L. Baker, L. E. Jeffery, S. Kaur, Z. Briggs, T. Z. Hou, C. E. Futter, G. Anderson, L. S. K. Walker, and D. M. Sansom, 2011, "Trans-Endocytosis of CD80 and CD86: A Molecular Basis for the Cell-Extrinsic Function of CTLA-4", *Science*, Vol. 332, No. 6029, pp. 600–603.

Rensing-Ehl, A., U. Pannicke, S. Zimmermann, M. R. Lorenz, B. Neven, I. Fuchs, U. Salzer, C. Speckmann, A. Strauss, E. Maaβ, B. Collet, A. Enders, R. Favier, M. Alessi, F. Rieux-Laucat, B. Zieger, K. Schwarz, and S. Ehl, 2015, "Gray Platelet Syndrome Can Mimic Autoimmune Lymphoproliferative Syndrome", *Blood*, Vol. 126, No. 16, pp. 1967–1969.

Revel-Vilk, S., U. Fischer, B. Keller, S. Nabhani, L. Gámez-Díaz, A. Rensing-Ehl, M. Gombert, A. Hönscheid, H. Saleh, A. Shaag, A. Borkhardt, B. Grimbacher, K. Warnatz, O. Elpeleg, and P. Stepensky, 2015, "Autoimmune Lymphoproliferative Syndrome-like Disease in Patients with LRBA Mutation", *Clinical Immunology*, Vol. 159, No. 1, pp. 84–92.

Rotte, A., 2019, "Combination of CTLA-4 and PD-1 Blockers for Treatment of Cancer", *Journal of Experimental & Clinical Cancer Research*, Vol. 38, No. 255, pp. 1-12.

Rudd, C. E., A. Taylor, and H. Schneider, 2009, "CD28 and CTLA-4 Coreceptor Expression and Signal Transduction", *Immunological Reviews*, Vol. 229, No. 1, pp. 12–26.

Sambrook, J. and D.W. Russell, 2001, *Molecular Cloning: A Laboratory Manual*, 3rd Edition, Cold Spring Harbor Laboratory Press, New York.

Schneider, H., M. Martin, F. A. Agarraberes, L. Yin, I. Rapoport, T. Kirchhausen, and C. E. Rudd, 1999, "Cytolytic T Lymphocyte-Associated Antigen-4 and the TCRζ/CD3 Complex, But Not CD28, Interact with Clathrin Adaptor Complexes AP-1 and AP-2", *Journal of Immunology*, Vol. 163, No. 4, pp. 1868–1879.

Schubert, D., C. Bode, R. Kenefeck, T. Z. Hou, J. B. Wing, A. R. Kennedy, A. Bulashevska, B. Petersen, A. A. Schäffer, B. Grüning, S. Unger, N. Frede, U. Baumann, T. Witte, R. E. Schmidt, G. Dueckers, T. Niehues, S. L. Seneviratne, M. Kanariou, C. Speckmann, A. Rensing-Ehl, K. Warnatz, M. Rakhmanov, R. Thimme, P. Hasselblatt, F. Emmerich, T. Cathomen, R. Backofen, P. Fisch, M. Seidl, A. May, A. Schmitt-Graeff, S. Ikemizu, U. Salzer, A. Franke, S. Sakaguchi, L. S. K. Walker, D. M. Sansom, and B. Grimbacher, 2014, "Autosomal Dominant Immune Dysregulation Syndrome in Humans with CTLA4 Mutations", *Nature Medicine*, Vol. 20, No. 12, pp. 1410–1416.

Shah, K. J., A. A. Al-Haidari, J. Sun, and L. Rönnstrand, 2021, "T Cell Receptor (TCR) Signaling in Health and Disease", *Signal Transduction and Targeted Therapy*, Vol. 6, No. 1, p. 412.

Shiratori, T., S. Miyatake, H. Ohno, C. Nakaseko, K. Isono, J. S. Bonifacino, and T. Saito, 1997, "Tyrosine Phosphorylation Controls Internalization of CTLA-4 by Regulating Its Interaction with Clathrin-Associated Adaptor Complex AP-2", *Immunity*, Vol. 6, No. 5, pp. 583–589.

Sigismund, S., E. Argenzio, D. Tosoni, E. Cavallaro, S. Polo, and P. P. Di Fiore, 2008, "Clathrin-Mediated Internalization Is Essential for Sustained EGFR Signaling but Dispensable for Degradation", *Developmental Cell*, Vol. 15, No. 2, pp. 209–219.

Verma, N., S. O. Burns, L. S. K. Walker, and D. M. Sansom, 2017, "Immune Deficiency and Autoimmunity in Patients with CTLA-4 (CD152) Mutations", *Clinical and Experimental Immunology*, Vol. 190, No. 1, pp. 1–7.

Wang, J., J. M. Howson, E. M. Haller, and W. R. Kerr, 2001, "Identification of a Novel Lipopolysaccharide-Inducible Gene with Key Features of Both a Kinase Anchor Proteins and Chs1/Beige Proteins", *Journal of Immunology*, Vol. 166, No. 7, pp. 4586–4595.

Wang, J., J. J. Gamsby, S. L. Highfill, L. B. Mora, G. C. Bloom, T. Yeatman, T. Pan, A. Ramne, L. A. Chodosh, W. D. Cress, J. Chen, and W. R. Kerr, 2004, "Deregulated Expression of LRBA Facilitates Cancer Cell Growth", *Oncogene*, Vol. 23, No. 23, pp. 4089–4097.

Waring, P., and A. Müllbacher, 1999, "Cell Death Induced by the Fas/Fas Ligand Pathway and Its Role In Pathology", *Immunology and Cell Biology*, Vol. 77, No. 4, pp. 312–317.

Westbroek, W., D. H. Adams, M. Huizing, A. Koshoffer, H. Dorward, B. Tinloy, J. D. Parkes, A. Helip-Wooley, R. Kleta, E. Tsilou, P. Duvernay, K. B. Digre, D. J. Creel, J. G. White, R. E. Boissy, and W. A. Gahl, 2007, "Cellular Defects in Chediak–Higashi Syndrome Correlate with the Molecular Genotype and Clinical Phenotype", *Journal of Investigative Dermatology*, Vol. 127, No. 11, pp. 2674–2677.

Whelan, S., E. Ophir, M. F. Kotturi, O. Levy, S. Ganguly, L. Y. Leung, I. Vaknin, S. Kumar, L. Dassa, K. R. Hansen, D. Bernados, B. Murter, A. Soni, J. M. Taube, A. N. Fader, T. Wang, I. M. Shih, M. D. White, D. M. Pardoll and S. Liang, 2019, "PVRIG and PVRL2 Are Induced in Cancer and Inhibit CD8+ T-cell Function", *Cancer Immunology Research*, Vol. 7, No. 2, pp. 257–268.

Wickham, H., 2009, *ggplot2: Elegant Graphics for Data Analysis*, Springer-Verlag, New York.

Xu, F., A. Sunderland, Y. Zhou, R. D. Schulick, B. H. Edil, and Y. Zhu, 2017, "Blockade of CD112R and TIGIT Signaling Sensitizes Human Natural Killer Cell Functions", *Cancer Immunology, Immunotherapy*, Vol. 66, No. 10, pp. 1367–1375.

Yablonski, D., T. A. Kadlecek, and A. Weiss, 2001, "Identification of a Phospholipase C-γ1 (PLC-γ1) SH3 Domain-Binding Site in SLP-76 Required for T-Cell Receptor-Mediated Activation of PLC-γ1 and NFAT", *Molecular and Cellular Biology*, Vol. 21, No. 13, pp. 4208–4218.

Yixia, Z., M. Lei, Z. Wang, G. Qiao, T. Yang, and J. Zhang, 2014, "TCR-induced, PKC-θ-Mediated NF-κB Activation is Regulated by a Caspase-8–Caspase-9–Caspase-3 Cascade", *Biochemical and Biophysical Research Communications*, Vol. 450, No. 1, pp. 526–531.

Zahedimaram, P., 2022, *The Identification of the Mechanisms of Lrba Deficiency Dependent Defects in Regulatory T-Cell Function,* Ph.D. Thesis, Sabancı University.

Zaretsky, J. M., A. Garcia-Diaz, D. B. Shin, H. Escuin-Ordinas, W. Hugo, S. Hu-Lieskovan, D. Y. Torrejon, G. Abril-Rodriguez, S. Sandoval, L. Barthly, J. Saco, B. H. Moreno, R. Mezzadra, B. Chmielowski, K. Ruchalski, I. P. Shintaku, P. J. Sanchez, C. Puig-Saus, G. Cherry, E. Seja, X. Kong, J. Pang, B. Berent-Maoz, B. Comin-Anduix, T. G. Graeber, P. C. Tumeh, T. N. M. Schumacher, R.S. Lo, A. Ribas, 2016, "Mutations Associated with Acquired Resistance to PD-1 Blockade in Melanoma", *The New England Journal of Medicine*, Vol. 375, No. 9, pp. 819–829.

Zeng, T., Y. Cao, T. Jin, Y. Tian, C. Dai, and F. Xu, 2021, "The CD112R/CD112 Axis: A Breakthrough in Cancer Immunotherapy", *Journal of Experimental & Clinical Cancer Research*, Vol. 40, No. 1, pp. 1-11.

Zhao, S., L. Zhang, S. Xiang, Y. Hu, Z. Wu, and J. Shen, 2022, "Gnawing Between Cells and Cells in the Immune System: Friend or Foe? A Review of Trogocytosis", *Frontiers in Immunology*, Vol. 13, No. 791006, pp. 1-13.

Zhu, Y., A. Paniccia, A. C. Schulick, W. Chen, M. R. Koenig, J. C. Byers, S. Yao, S. Bevers, and B. H. Edil, 2016, "Identification of CD112R as a Novel Checkpoint for Human T Cells", *Journal of Experimental Medicine*, Vol. 213, No. 2, pp. 167–176.

APPENDIX A: CHEMICALS

Table A.1. Chemicals used in this study.

Chemical	Supplier Company
Acetic Acid	Sigma, USA
Acrylamide/Bis-acrylamide, 30% solution	Sigma, USA
Agar	Millipore, USA
Agarose	Isolab, Germany
Ammonium persulfate	Sigma, USA
Ampicillin Sodium Salt	CellGro, USA
Calcium chloride	Sigma, USA
Chloroquine diphosphate	Applichem, Germany
DMEM	GIBCO, USA
DMSO	Sigma, USA
DPBS	Cytiva, UK
DNA Gel Loading Dye, 6X	NEB, USA
EDTA	Sigma, USA
Ethanol	Isolab, Germany
Ethidium Bromide	Sigma, USA
Fetal Bovine Serum (FBS)	Cytiva, UK
Glass Beads	Sigma, USA
Glycerol	Sigma, USA
Glycine	Sigma, USA
HEPES	Sigma, USA
HCl	Merck, Germany
Isopropanol	Sigma, USA
LB Broth	Sigma, USA
Liquid Nitrogen	Karbogaz, Turkey
MEM Non-essential Amino Acid Solution, 100X	GIBCO, USA

Table A.1. Chemicals used in this study (cont).

Chemical	**Supplier Company**
Methanol	Isolab, Germany
NaCl	Carlo Erba, Italy
Penicillin-Streptomycin	Sigma, USA
PIPES	Sigma, USA
Protease inhibitor cocktail tablets (EDTA-free)	Roche, Germany
RPMI-1640	GIBCO, USA
Skim milk powder	Millipore, USA
Sodium Azide	Amresco, USA
Sodium dodecyl sulfate	Merck, Germany
Tricine	Sigma, USA
Trizma-Base	Sigma, USA
TEMED	Applichem, Germany
Triton-X-100	Promega, USA
Tween-20	Sigma, USA

APPENDIX B: EQUIPMENT

Table B.1. Equipment used in this study.

Equipment	Company
Autoclave	Astell Swiftclave, UK
Adjustable Rocker Shaker	Cole-Parmer, USA
Balance	Sartorius, Germany
Centrifuge	Beckman Coulter, Allegra X-12, USA Beckman Coulter, Allegra X-30R, USA
CO_2 Incubator	Thermo Fisher Scientific, USA
Deepfreeze	-80°C, ThermoForma, USA -20°C, Arçelik, Turkey
Electrophoresis Apparatus	Biorad Inc., USA VWR, USA
Flow Cytometry	BD FACSCalibur Flow Cytometer, USA BD Accuri™ C6 Flow Cytometer, USA
Gel Documentation	Biorad, USA
Heat Block	Eppendorf, Germany
Hemocytometer	Isolab, Germany
Ice Machine	Scotsman Inc., USA
Liquid Nitrogen Tank	International Cryogenics, USA
Microliter Pipettes	Thermo Fisher Scientific, USA
Microcentrifuge	Centrifuge 5415 R, Eppendorf, Germany
Microscope	Zeiss Primovert, Germany
Microwave Oven	Arçelik, Turkey
pH Meter	SevenCompact™, Mettler Toledo, Switzerland
Power Supply	VWR, USA

Table B.1. Equipment used in this study (cont).

Equipment	**Company**
Refrigerator	Arçelik, Turkey
Shaker Incubator	New Brunswick, Innova 44, USA
Spectrophotometer	NanoDrop™ 2000, Thermo Fisher Scientific, USA
Stirrer/Heater	Scilogex, USA
Thermocyler	PTC-200 Peltier Thermal Cycler, MJ Research Inc, CA
Vortex	Velp Scientifica, Italy

APPENDIX C: ADAPTATIONS

Figure 1.1, 1.2, 1.3, 1.4, 1.5 and 5.6 were created using BioRender.com. Figure 1.2 was adapted from “TCR Downstream Signaling”, and Figure 1.4 was adapted from “T-cell Deactivation vs. Activation” on BioRender.com (2023). Figure 1.6 was used from Zahedimaram (2022) with permission from Pegah Zahedimaram.

APPENDIX D: DNA LADDER

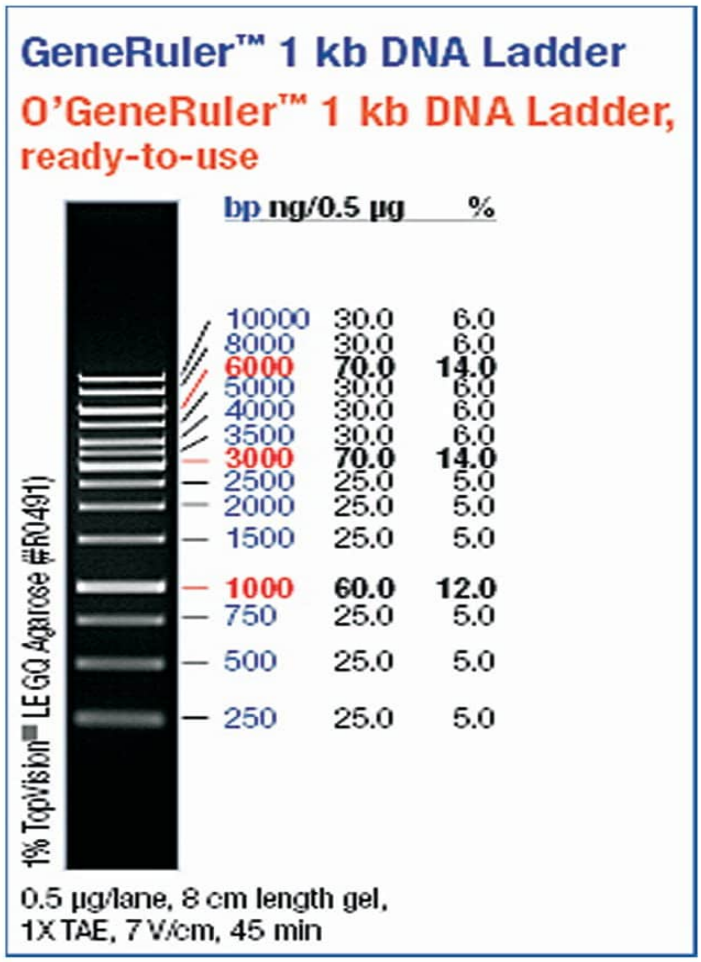

Figure D.1. DNA ladder used in this study.

APPENDIX E: PROTEIN LADDERS

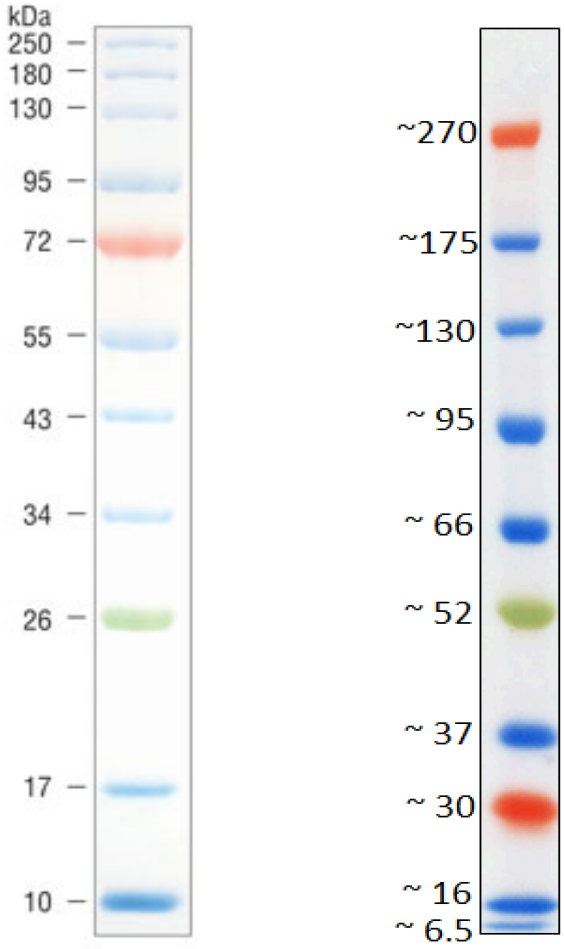

Figure E.1. Protein ladders used in this study.

APPENDIX F: PLASMID MAPS

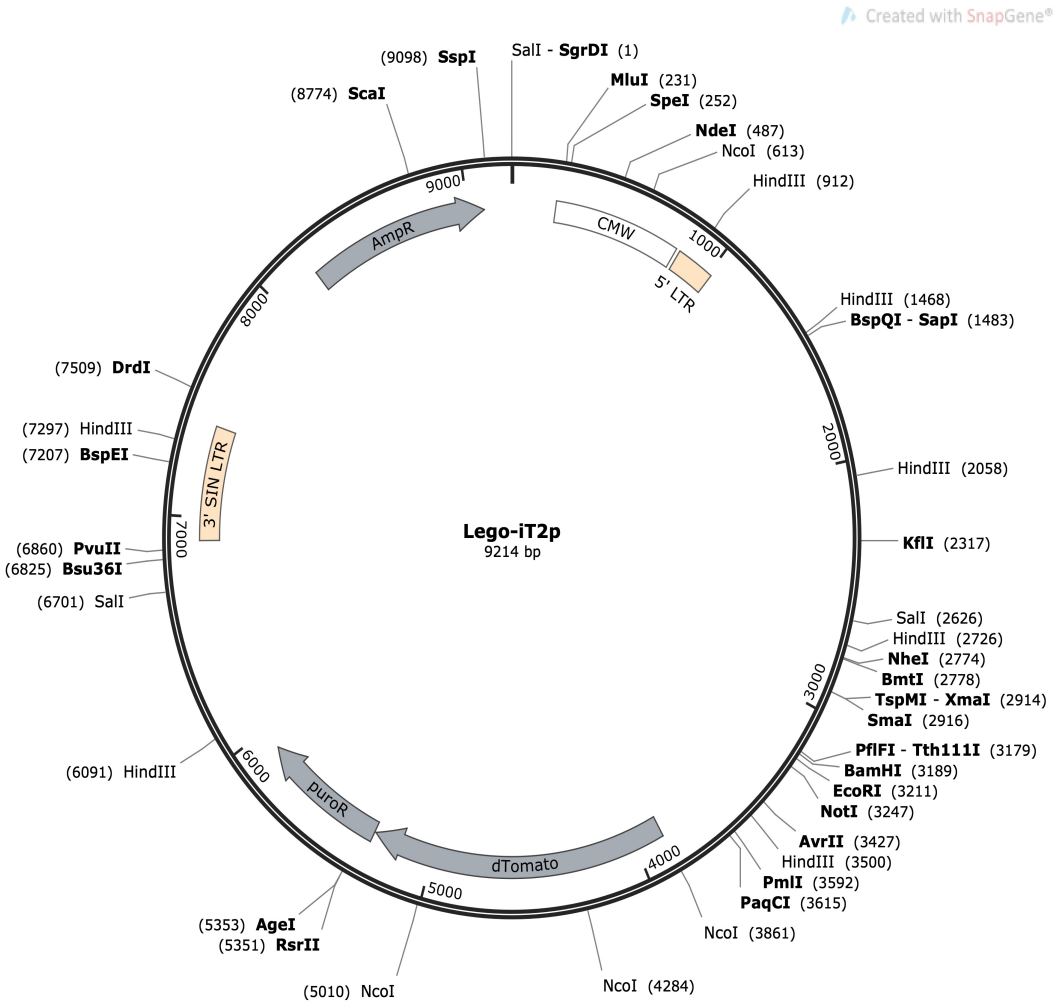

Figure F.1. Plasmid map of pLeGO-iT2p.

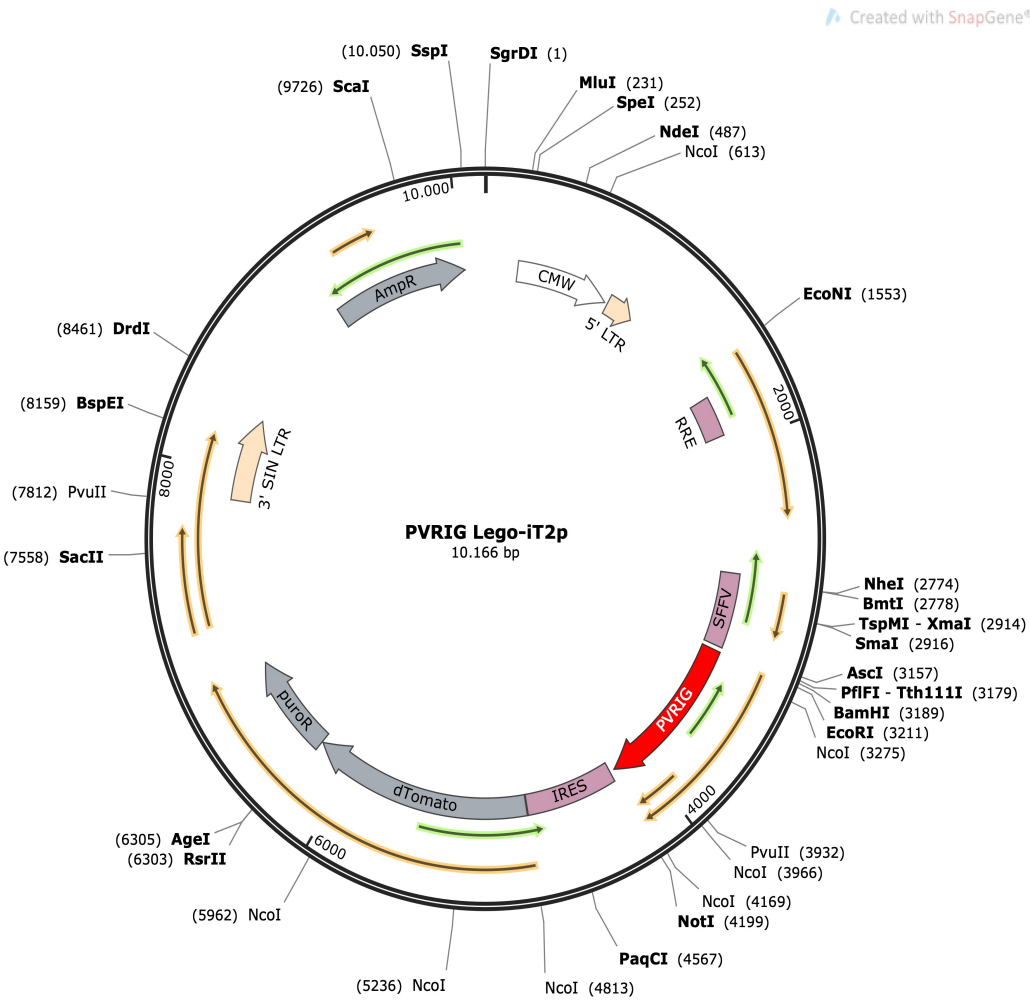

Figure F.2. Plasmid map of pLeGO-iT2p-PVRIG.

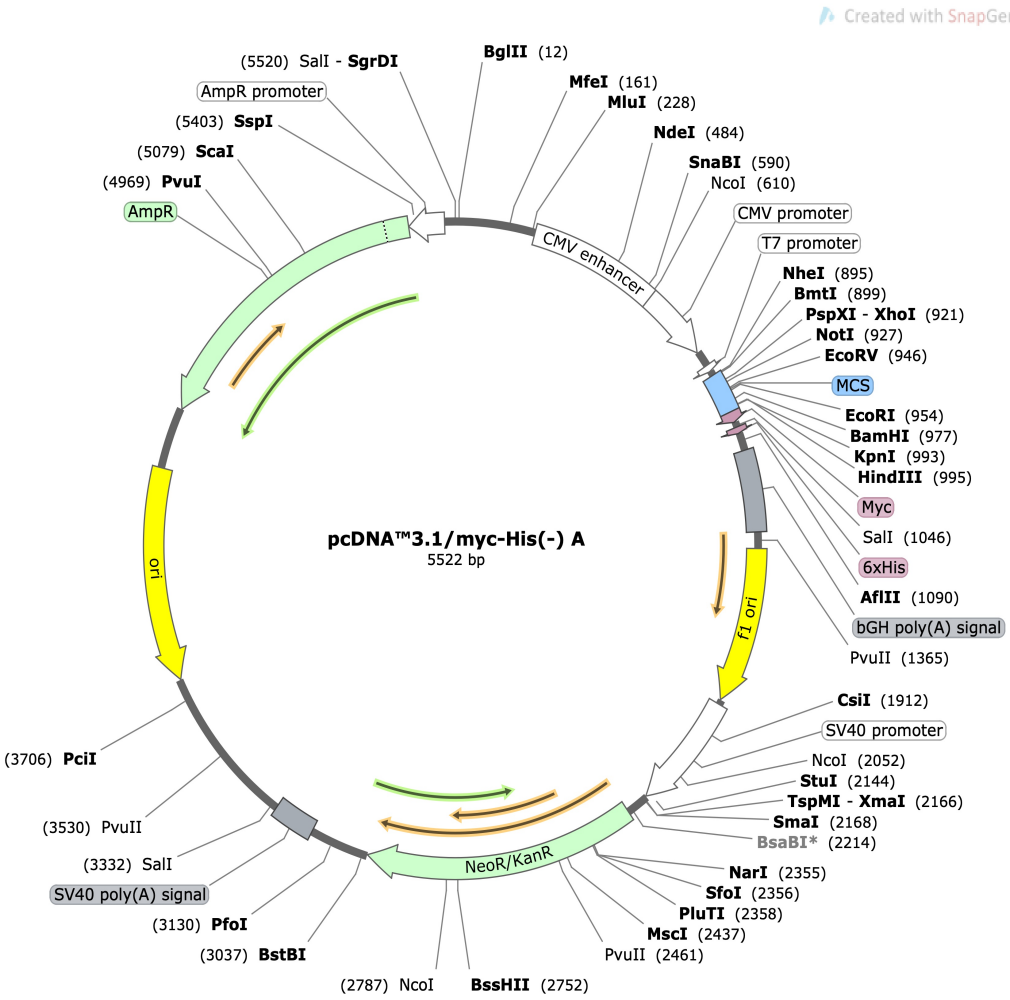

Figure F.3. Plasmid map of pcDNA 3.1 Myc/His (-) A.

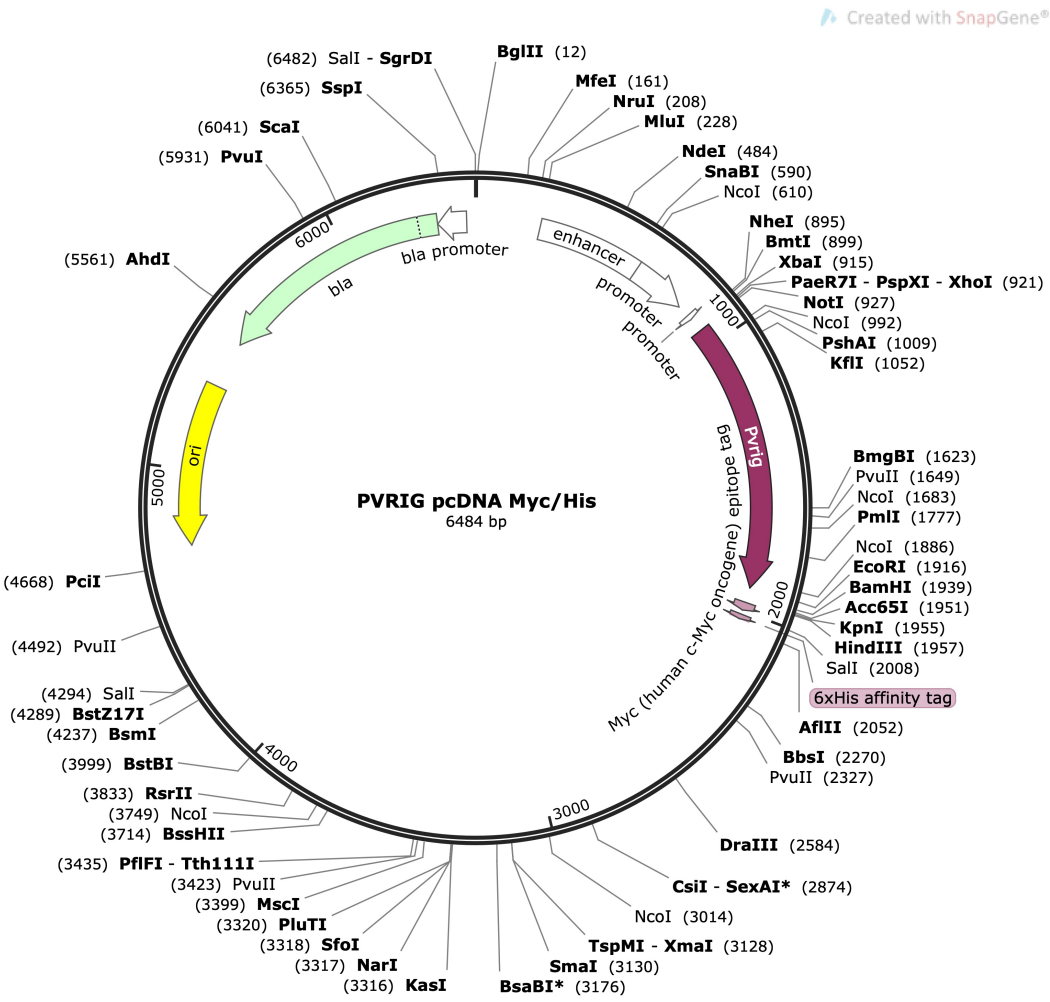

Figure F.4. Plasmid map of PVRIG Myc/His.

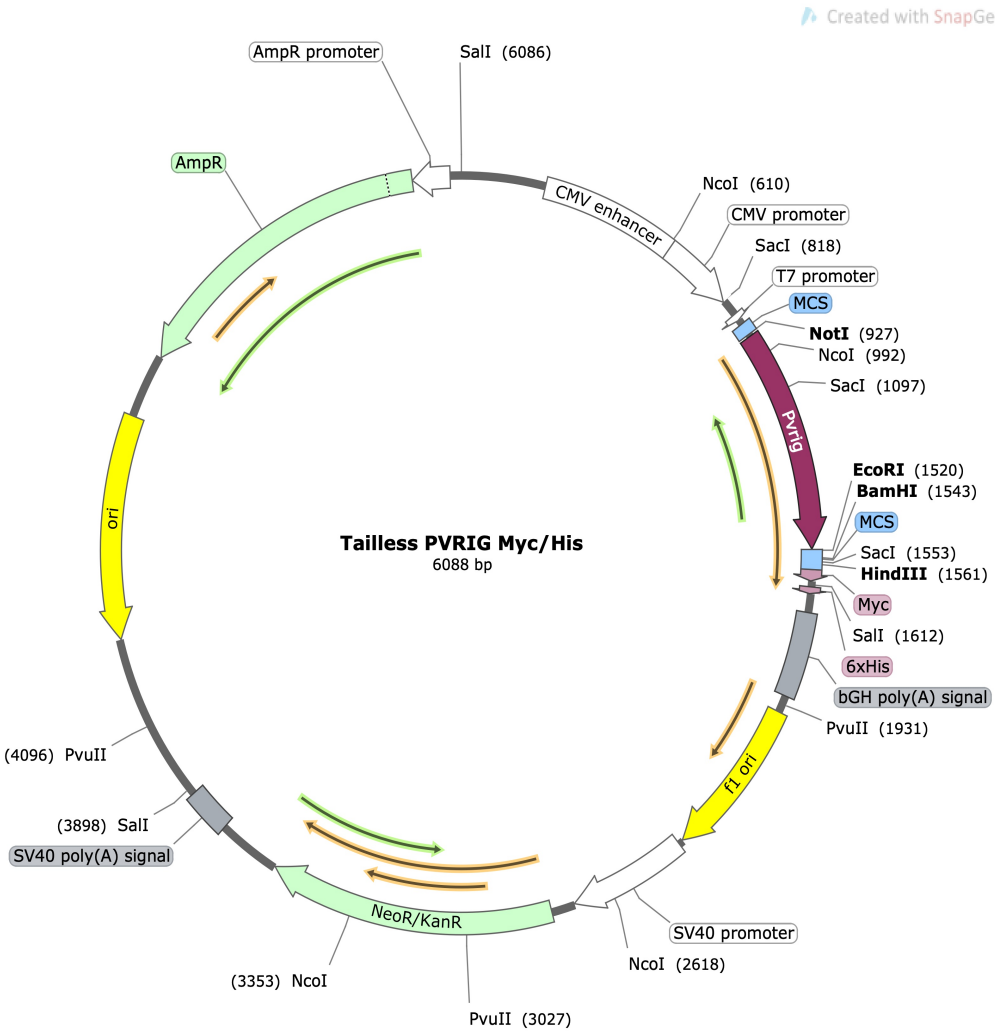

Figure F.5. Plasmid map of Tailless PVRIG Myc/His.

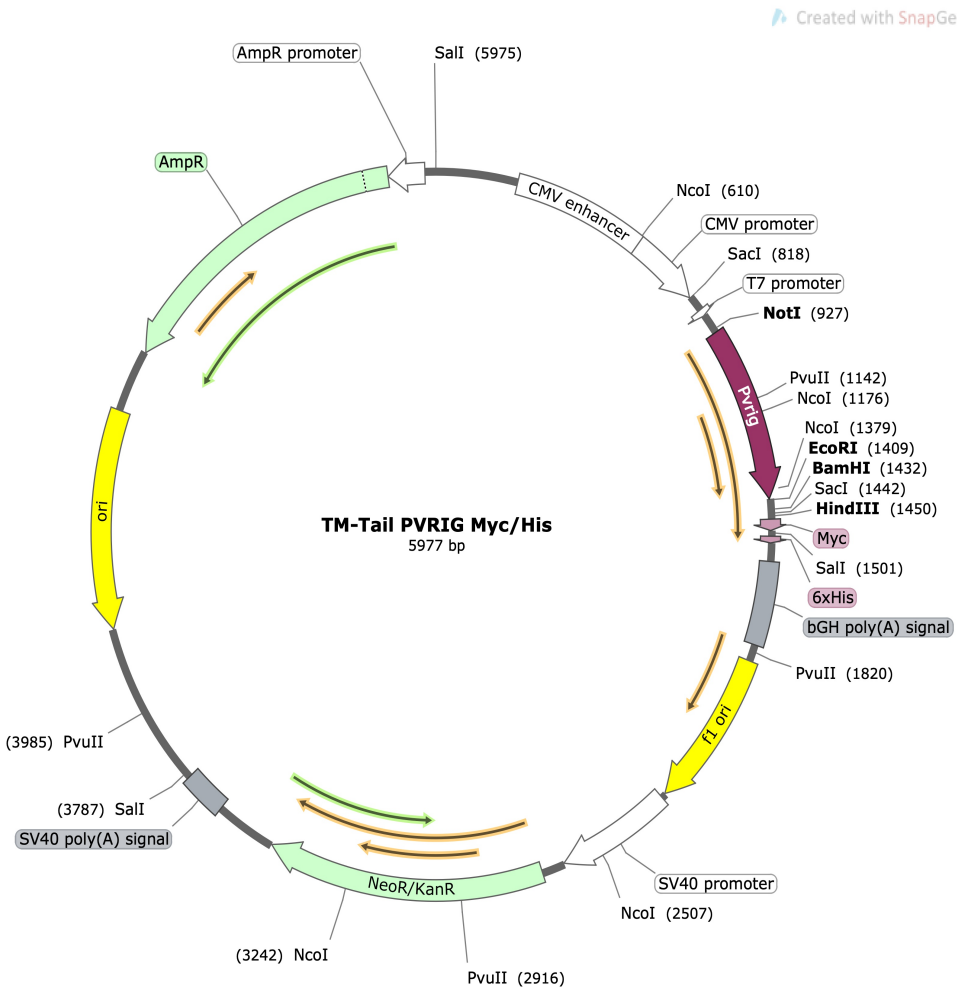

Figure F.6. Plasmid map of TM-Tail PVRIG Myc/His.

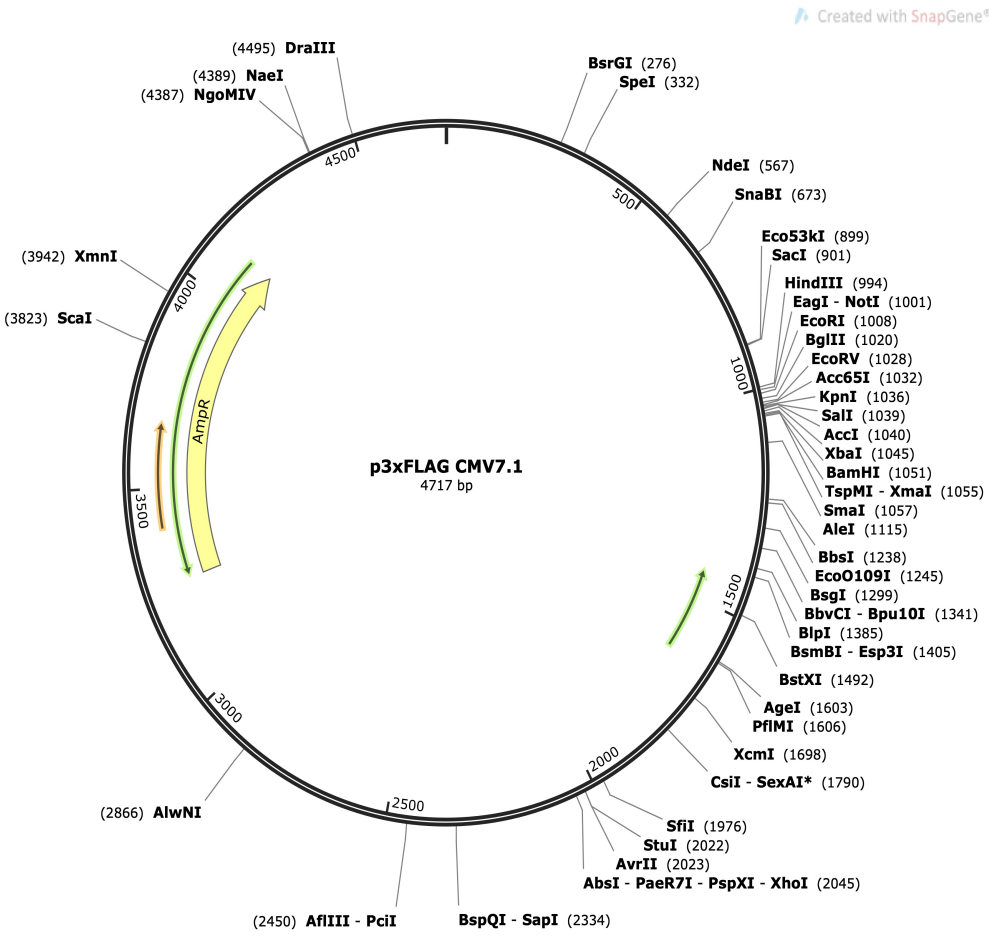

Figure F.7. Plasmid map of p3X Flag CMV 7.1.

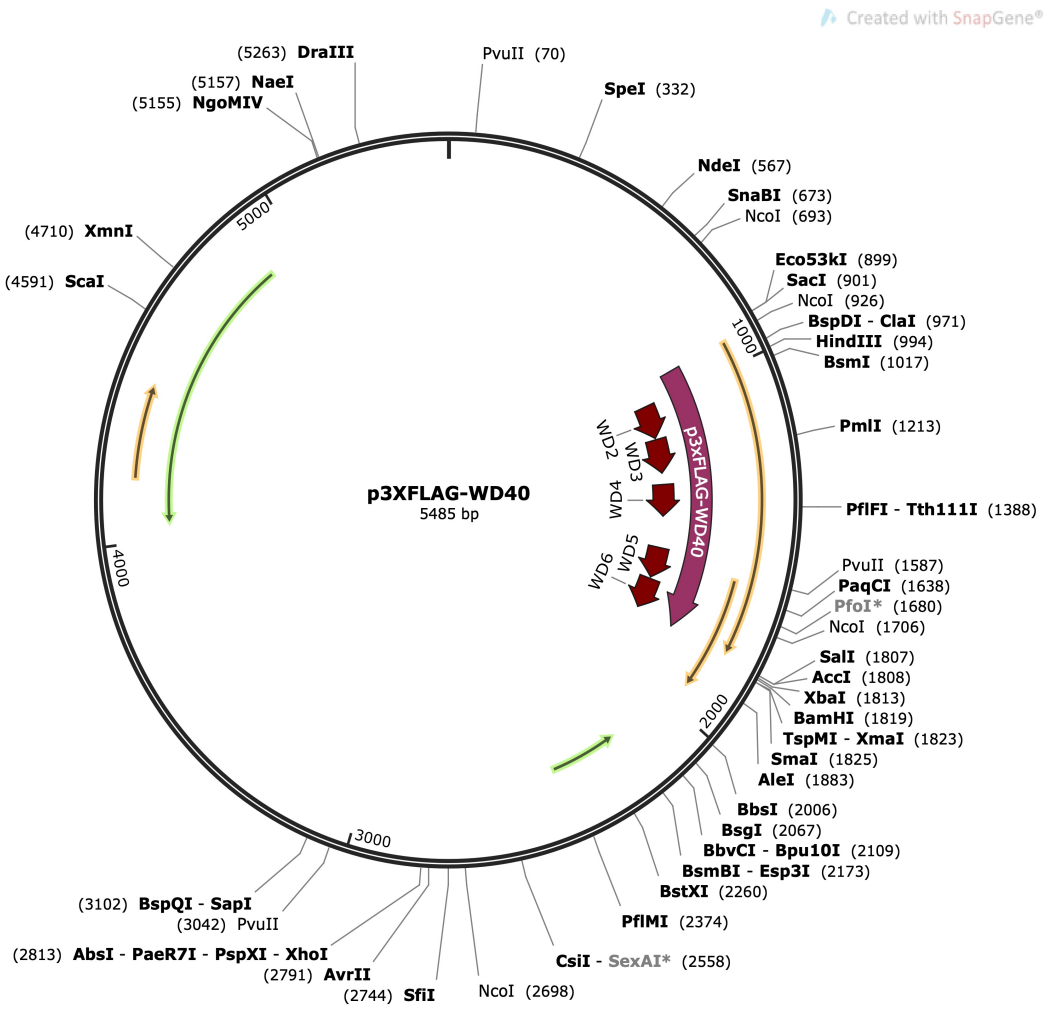

Figure F.8. Plasmid map of p3X Flag-WD40.

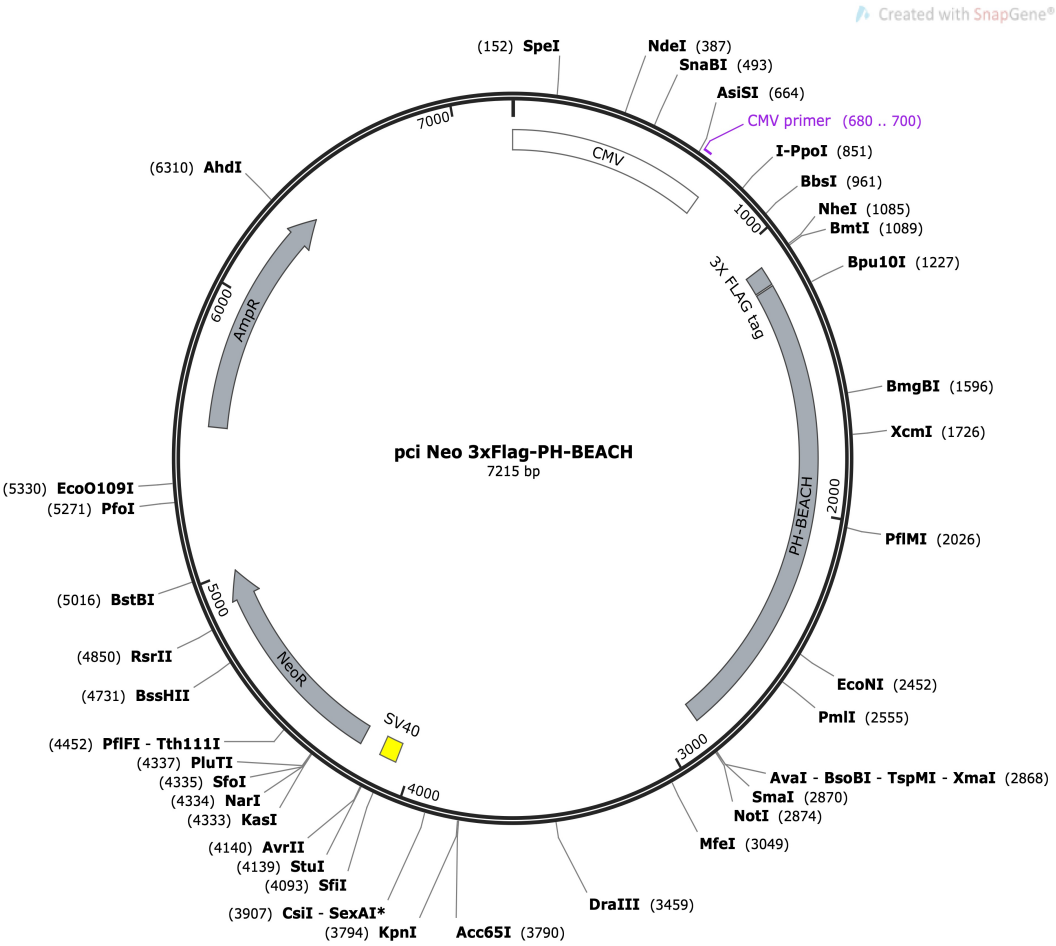

Figure F.9. Plasmid map of pCI-Neo 3xFlag-PH-BEACH.

APPENDIX G: PVRIG WESTERN BLOT GELS FOR STATISTICAL SIGNIFICANCE ANALYSIS

The two additional PVRIG western blot experiments from Jurkat T-cell line that were used to quantify statistical significance (Figure 5.12) are given in Figure G.1.

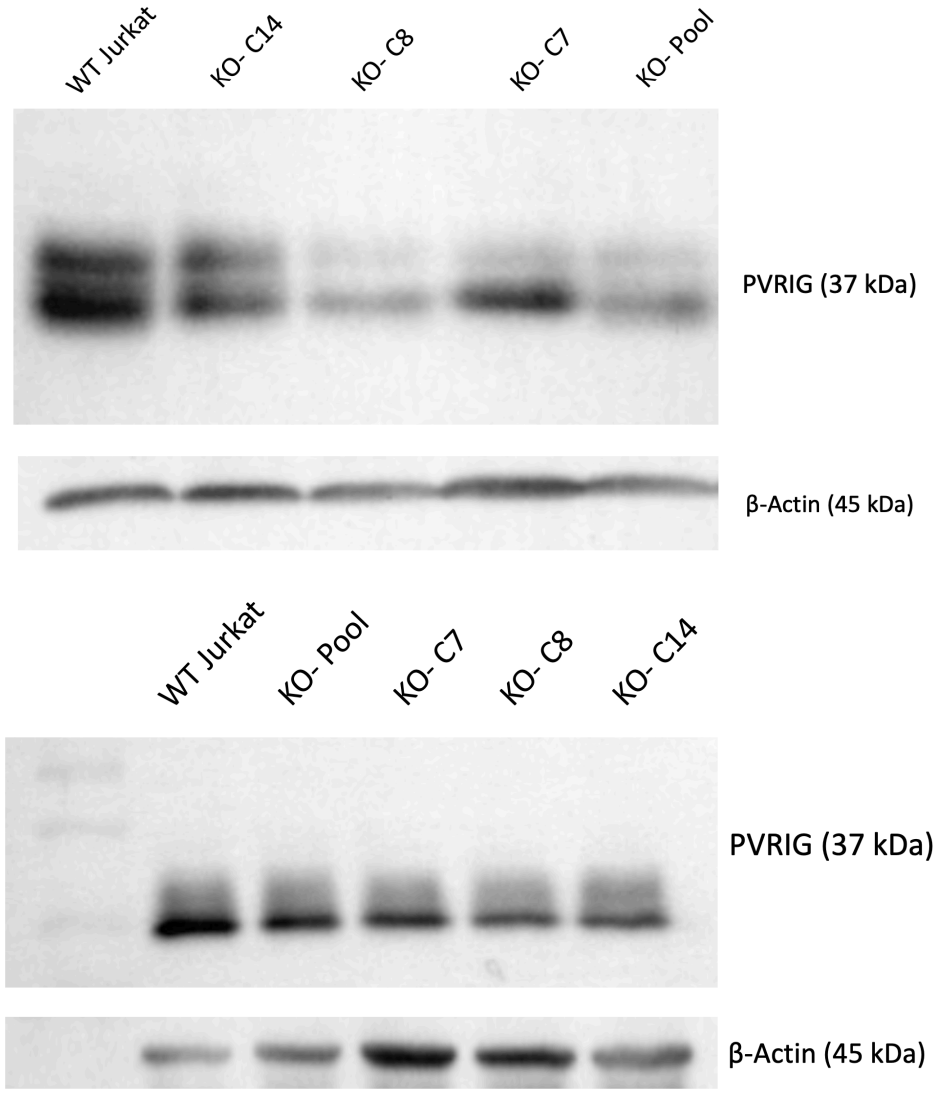

Figure G.1. Additional two PVRIG western blot experiments from Jurkat T-cell line that were used for statistical significance analysis.